THE UNIVERSITY of EDINBURGH

Wave-mean flow interactions: from nanometre to megametre scales

Jin-Han Xie

Doctor of Philosophy
University of Edinburgh
2015

Abstract

Waves, which arise when restoring forces act on small perturbations, are ubiquitous in fluids. Their counterpart, mean flows, capture the remainder of the motion and are often characterised by a slower evolution and larger scale patterns. Waves and mean flows, which are typically separated by time- or space-averaging, interact, and this interaction is central to many fluid-dynamical phenomena. Wave-mean flow interactions can be classified into dissipative interactions and non-dissipative interactions. The former is important for small-scale flows, the latter for large-scale flows. In this thesis these two kinds of interactions are studied in the context of microfluidics and geophysical applications.

Viscous wave-mean flow interactions are studied in two microfluidic problems. Both are motivated by the rapidly increasing number of microfluidic devices that rely on the mean-flow generated by dissipating acoustic waves - acoustic streaming – to drive small-scale flows. The first problem concerns the effect of boundary slip on steady acoustic streaming, which we argue is important because of the high frequencies employed. By applying matched asympototics, we obtain the form of the mean flow as a function of a new non-dimensional parameter measuring the importance of the boundary slip. The second problem examined is the development of a theory applicable to experiments and devices in which rigid particles are manipulated or used as passive tracers in an acoustic wave field. Previous work obtained dynamical equations governing the mean motion of such particles in a largely heuristic way. To obtain a reliable mean dynamical equation for particles, we apply a systematic multiscale approach that captures a broad range of parameter space. Our results clarify the limits of validity of previous work and identify a new parameter regime where the motion of particles and of the surrounding fluid are coupled nonlinearly.

Non-dissipative wave-mean flow interactions are studied in two geophysical fluid problems. (i) Motivated by the open question of mesoscale energy transfer in the ocean, we study the interaction between a mesoscale mean flow and near-inertial waves. By

applying generalized Lagrangian mean theory, Whitham averaging and variational calculus, we obtain a Hamiltonian wave-mean flow model which combines the familiar quasi-geostrophic model with the Young & Ben Jelloul model of near-inertial waves. This research unveils a new mechanism of mesoscale energy dissipation: near-inertial waves extract energy from the mesoscale flow as their horizontal scale is reduced by differential advection and refraction so that their potential energy increases. (ii) We study the interaction between topographic waves and an unidirectional mean flow at an inertial level, that is, at the altitude where the Doppler-shifted frequency of the waves match the Coriolis parameter. This interaction can be described using linear theory, using a combination of WKB and saddle-point methods, leading to explicit expressions for the mean-flow response. These demonstrate, in particular, that this response is switched on asymptotically far downstream from the topography, in contrast to what is often assumed in parameterisation.

Lay summary

When slightly perturbed, fluids tend to recover their original states as a result of some restoring mechanisms. Such restoring mechanisms usually support waves characterised by an oscillatory motion that is often faster and of smaller scale than the rest of the motion. Wave-mean flow interaction theory studies the two-way interaction between such waves and slow, large-scale mean flows.

Observations of wave-mean flow interaction are common in natural fluid systems. In the atmosphere, winds generate inertia-gravity waves when they meet obstacles. This wave generation happens in the troposphere, but the waves can propagate into the stratosphere and higher up still, where they break and generate mean flows. Wave-mean flow interaction mechanisms are also used in artificial devices. With the development of microscale techniques, microfluidics devices are widely used. One of the challenges for these devices is driving fluids in a small confined space. One way to overcome this challenge is to use mean-flow generation by sound waves: when high frequency sound waves are excited in a fluid, they can generate a controllable, directional mean force that drives fluid in microfluid devices.

Mean flows influence waves by advecting and refracting them; at the same time, waves affect mean flows through nonlinear effects. Different mechanisms of wave-mean flow interaction are possible. In geophysical fluids, the characteristic spatial scale of the flows are so large that viscous effects are negligible; therefore, the related wave-mean flow interactions are non-dissipative and controlled by conservation laws such as the conservation of angular momentum. In contrast, in microfluidics applications, viscosity is the dominant effect.

This thesis studies both non-dissipative and viscous wave-mean flow interactions by tackling specific problems in geophysical fluid dynamics and microfluidics. For these problems, we focus on describing the dominant dynamics to provide the theoretical foundations for practical applications.

Declaration

I declare that this thesis was composed by myself and that the work contained therein is my own, except where explicitly stated otherwise in the text.

(*Jin-Han Xie*)

Acknowledgements

Foremost, I would like to express my sincere gratitude to my supervisor Prof. Jacques Vanneste. During my PhD study, he has been patiently teaching me knowledge, methods and the way of scientific thinking; also he helped me a lot in the academic writing. He did not only instruct me by words but also his deed by providing me an example of serious scientist.

I would like to thank the Dr Laura Wisewell Travel Scholarship which made it possible for me to attend the conference "Eddy Mean-Flow Interactions in Fluids" held at the Kavli Institute for Theoretical Physics, University of California, Santa Barbara. In addition, I am grateful for the financial support from Society for Industrial and Applied Mathematics, London Mathematical Society, International Centre for Mathematical Sciences, Maxwell Institute for Mathematical Sciences and School of Mathematics at the University of Edinburgh for funding my academic communication activities. It is only with the scholarship from the School of Mathematics, Edinburgh Global Research program and the Centre for Numerical Analysis and Intelligent Software that my PhD study was made possible.

Thanks must go to people who provide help in my research. Dr. Eric Danioux helped me develop the numerical code for near-inertial waves and provided many comments on this topic. I had discussions with Prof. William Young and Gregory Wagner in UCSD and Prof. David Straub and Stephanne Taylor in McGill on the interaction between near-inertial waves and mean flow. Comments from Prof. Oliver Bühler in Courant Institute were received for the work on topographic waves. Dr. Yue-Kin Tsang taught me a lot on the knowledge of turbulence. Also I thank my fellow postgraduate students for the discussions with and help received from them, especially, Dr. Ke Wei, Dr. Yiming Yan, Hanyi Chen, Sarah Khwaja, Chris Palmer and Feng Qiang.

Last but not least, I would like to thank the support from my parents, Hong-Ming Xie and Gui-Xin Xu, for their love and education.

Contents

Chapter 1

Introduction

Waves, understood broadly to describe propagating oscillatory motions, are one of the most important physical subjects because of their ubiquity. They impact on many phenomena, where different waves arise as a result of different restoring forces. For example, electromagnetic waves, the oscillations of electrical and magnetic fields, rely on electric and magnetic force to transport energy across a large distance. Unsurprisingly, waves have been studied using a rich range of techniques. The simplest and most powerful theory is linear wave theory, which applies to small amplitude perturbations. For example, acoustic waves are governed by the linear hyperbolic equation

$$\partial_{tt}p - c^2\partial_{xx}p = 0, \tag{1.1}$$

where p is the pressure perturbation (or any other wave quantity), t denotes time, x denotes space and c is the sound velocity.

In this thesis, the waves we focus on are the waves propagating in fluids. The nonlinear nature of the fluid model makes the waves and related mechanisms non-trivial: on the one hand, the wave can interact nonlinearly, on the other hand, the nonlinearity leads to the forcing of (non-oscillatory) mean flows through resonant effects. This type of wave-mean flow interaction is the topic of this thesis.

Mathematically, we can illustrate the phenomenon of wave-mean flow interaction in an abstract system expressed as

$$\partial_t u + \mathcal{L}(u) + \mathcal{B}(u, u) = 0, \tag{1.2}$$

where u is some field, $\mathcal{L}$ and $\mathcal{B}$ are linear and bilinear operators respectively. The main assumption, used throughout the thesis, is that the waves have a small amplitude. This

assumption enables us to apply asymptotic expansion methods, which transform the nonlinear problem into a sequence of linear problems. The field is expanded in powers of the small parameter ϵ which characterises the small amplitude:

$$u = u_0 + \epsilon u_1 + \epsilon^2 u_2 + \dots, \tag{1.3}$$

where u_0 is the background flow and the remaining u_i's are perturbations of order $O(\epsilon^i)$. By substituting (1.3) into (1.2) we obtain the multi-level linear system:

$$O(\epsilon^0): \quad \partial_t u_0 + \mathcal{L}(u_0) + \mathcal{B}(u_0, u_0) = 0, \tag{1.4a}$$

$$O(\epsilon^1): \quad \partial_t u_1 + \mathcal{L}(u_1) + \mathcal{B}(u_0, u_1) + \mathcal{B}(u_1, u_0) = 0, \tag{1.4b}$$

$$O(\epsilon^2): \quad \partial_t u_2 + \mathcal{L}(u_2) + \mathcal{B}(u_0, u_2) + \mathcal{B}(u_2, u_0) = -\mathcal{B}(u_1, u_1), \tag{1.4c}$$

$$\dots\dots$$

Here even though the governing equation of the background flow (1.4a) is nonlinear, its solution is regarded as a prescribed field, and around this known field the perturbation is introduced. Based on normal-mode analysis, in order for (1.4b) to support a wave solution, the operator $\mathcal{L} + \mathcal{B}(u_0, \cdot) + \mathcal{B}(\cdot, u_0)$ should have no eigenvalues with negative real part, otherwise the basic state is unstable which this thesis does not consider. [1] We can solve this multi-level linear system level by level: the known background field u_0 can be substituted into (1.4b), which can be solved for the leading order wave u_1, the next order linear equation (1.4c) for u_2 can be solved by substituting background field u_0 and leading order wave u_1, etc. The key point comes from (1.4c), whose solution u_2 can have a non-oscillatory mean component.

Now let us consider an example, that of gravity waves in a shallow-water system. The governing equations are:

$$\partial_t \boldsymbol{u} + \boldsymbol{u}\cdot\nabla\boldsymbol{u} = -g\nabla h, \tag{1.5a}$$

$$\partial_t h + \nabla\cdot(h\boldsymbol{u}) = 0, \tag{1.5b}$$

where $\boldsymbol{u} = (u, v)$ is the two-dimensional velocity and $\nabla = (\partial_x, \partial_y)$, h is the fluid height and the constant coefficient g is the gravity. The governing system (1.5) is a realization of the abstract dynamical equation (1.2), and the (1.5a) and (1.5b) represent the momentum and mass conservations, respectively. We can prescribe the background field

[1] There is a possibility that the normal modes are not complete, therefore, the continuous part of the spectrum must be included to represent arbitrary initial disturbances.

as

$$\boldsymbol{u}_0 = (U,\, 0) \quad \text{and} \quad h_0 = H, \tag{1.6}$$

where U and H are constants. So perturbations about this background field are given by the linear leading-order wave equations

$$\partial_t \boldsymbol{u}_1 + U\partial_x \boldsymbol{u}_1 + g\nabla h_1 = 0, \tag{1.7a}$$

$$\partial_t h_1 + U\partial_x h_1 + \nabla\cdot(H\boldsymbol{u}_1) = 0, \tag{1.7b}$$

corresponding to (1.4b). This leading order wave field can be solved by Fourier transform

$$(u_1,\, v_1,\, h_1) = (\hat{u}_1,\, \hat{v}_1,\, \hat{h}_1)\mathrm{e}^{\mathrm{i}(\boldsymbol{k}\cdot\boldsymbol{x}-\omega t)}, \tag{1.8}$$

where $\boldsymbol{k} = (k, l)$ and $\boldsymbol{x} = (x, y)$. We can obtain from (1.7) that

$$(\omega - kU)^2 - gH|\boldsymbol{k}|^2 = 0 \quad \text{and} \quad \hat{h}_1 = \frac{\omega - kU}{gk}\hat{u}_1 = \frac{\omega - kU}{gl}\hat{v}_1, \tag{1.9}$$

which are the dispersion relation and polarization equation, respectively.

The interesting story happens at the second level (1.4c). If the wavenumber of the wave field has a lower bound, K say, such that $k > K$ and $l > K$, the wave and background flow have a spatial scale separation. We can therefore define an average over an intermediate scale $1/K_*$, such that $0 \ll K_* \ll K$. With this average $\bar{u}_0 = u_0$ and $\bar{\boldsymbol{u}}_1 = \bar{h}_1 = 0$, where "$\bar{\cdot}$" denotes the average. But in (1.4c) these zero-mean waves can force a mean flow through the nonlinear operator $\mathcal{B}$:

$$\partial_t \bar{u}_2 + \mathcal{L}(\bar{u}_2) + \mathcal{B}(u_0, \bar{u}_2) + \mathcal{B}(\bar{u}_2, u_0) = -\overline{\mathcal{B}(u_1, u_1)}. \tag{1.10}$$

In the gravity-wave example (1.10) become

$$\partial_t \bar{\boldsymbol{u}}_2 + U\partial_x \bar{\boldsymbol{u}}_2 + g\nabla \bar{h}_2 = -\overline{\boldsymbol{u}_1\cdot\nabla\boldsymbol{u}_1}, \tag{1.11a}$$

$$\partial_t \bar{h}_2 + H\nabla\cdot\bar{\boldsymbol{u}}_2 = -\nabla\cdot(\overline{h_1\boldsymbol{u}_1}). \tag{1.11b}$$

Hence we can identify the mean flow as

$$\bar{u} = u_0 + \epsilon^2\bar{u}_2 + \ldots, \tag{1.12}$$

which is different from the background flow by the second order wave-induced mean field $\bar{u}_2$. It is possible that $\bar{u}_2$ can increase with time, corresponding to wave-induced $O(1)$

change in the mean flow, which can be captured by more sophisticated asymptotics (e.g. multiscale methods).

After defining waves and mean flow through averaging, we can observe the existence of a two-way coupling between the wave and mean flow – the mean flow modifies the wave field (See (1.4b) and (1.7)), and in the literature different effects are named by advection, dispersion and refraction; and the waves force the mean flow through resonant pairs (See (1.10) and (1.11)).

Wave-mean flow interaction theory can be applied to many problems, especially fluid systems. This adaptability has two reasons. First, the world is multiscale. For example, in the case of the geophysical fluids, like the atmosphere and the ocean, the dynamics has spatial scales ranging from thousands of kilometres, the radius of earth, to several centimetres, the scale of dissipation, and temporal scales ranging from seconds or even smaller, the typical time scale of acoustic waves, to hundreds or even millions of years, the time scale of climate and life of earth. For such multiscale systems, wave-mean flow interaction theory provides a perspective to describe cross scale phenomena via resonance mechanisms. Second, the intrinsic freedom of the wave-mean flow interaction theory – the definition of averaging – enables us to choose convenient averages for different problems. At the same time this freedom brings about the challenge of choosing a suitable average when applying the wave-mean flow interaction theory. The pioneering work by Reynolds [102] uses a temporal average to study the turbulence. Since then, Eulerian averaging has been successfully applied for a long time before the appearance of the generalized Lagrangian mean theory by Soward [114] in magnetohydrodynamics and Andrews and McIntyre [5] in the geophysical fluid context. Here we provide a brief review of generalized Lagrangian mean theory both for its theoretical importance and practical uesfulness. Another geometrical definition of averaging proposed by Soward and Roberts [115] is applied in chapter 4 to study an oceanic problem.

The very distinctive feature of fluid systems is their Eulerian description which reduces one degree of freedom from the Lagrangian description. However, because inviscid fluid systems are Hamiltonian systems whose conservation laws are best described in terms of the canonical Lagrangian variables, the Eulerian averaging, which is defined at fixed positions and therefore mixes different fluid elements, is not a convenient choice to explore the conservation laws. Consequently, the generalized Lagrangian mean theory defines the average following the fluid elements so that the conservation laws are well-expressed after averaging (Ref. [22]). Because of the particle-following average used, naturally, another advantage of a Lagrangian mean is its inheritance of material invariances that is not included in abstract system (1.2), such as the vorticity and potential

vorticity, which are crucial for describing the flows. This averaging is mathematically realized by introducing the disturbance displacement field $\boldsymbol{\xi} = \boldsymbol{\xi}(\boldsymbol{x}, t)$ such that $\boldsymbol{x} + \boldsymbol{\xi}$ is the actual position of a fluid element, whose mean position is $\boldsymbol{x}$. Here, the disturbance has zero mean $\bar{\boldsymbol{\xi}} = 0$, where the average can be chosen to cater for specific problems. The Lagrangian mean of a field ϕ is defined by

$$\bar{\phi}^{\mathrm{L}} = \overline{\phi^{\xi}(\boldsymbol{x}, t)} = \overline{\phi(\boldsymbol{x} + \boldsymbol{\xi}(\boldsymbol{x}, t), t)}, \tag{1.13}$$

where ϕ is an arbitrary field.

For example, the one-dimensional velocity field

$$u = U_0 + u' = U_0 + \epsilon A \cos(kx - \omega t) \tag{1.14}$$

contains the constant Eulerian mean flow U_0 and perturbation $u' = \epsilon A \cos(kx - \omega t)$, which are separated by the temporal or spatial average. The disturbance displacement corresponding to the perturbative velocity field u' is calculated as

$$\xi = \int u' \mathrm{d}t = -\frac{A}{\omega} \sin(kx - \omega t). \tag{1.15}$$

The Lagrangian mean velocity is then calculated perturbatively from the definition (1.13), leading to

$$\begin{aligned} \bar{u}^{\mathrm{L}} &= \overline{u(\boldsymbol{x} + \xi(\boldsymbol{x}, t), t)} \\ &= U_0 + \overline{\xi \partial_x u_1} + O(\epsilon^3) \\ &= U_0 + \frac{kA^2}{2\omega} + O(\epsilon^3). \end{aligned} \tag{1.16}$$

The term $\overline{\xi \partial_x u_1}$ can be recognised as the Stokes drift, which has the general form $\overline{\boldsymbol{\xi} \cdot \nabla \boldsymbol{u}_1}$ in higher spatial dimensions. Hence, for small amplitude waves, we obtain the kinematic relation of general Lagrangian mean theory:

$$\text{Lagrangian mean velocity} = \text{Eulerian mean velocity} + \text{Stokes drift}. \tag{1.17}$$

Because of the advantage of describing the conservation laws effectively the generalized Lagrangian mean theory has been successfully applied, for example, to explain the "non-acceleration" theorem [6], where the Eulerian mean flow change is exactly balanced by Stokes drift. For the details of general Lagrangian mean theory see [5, 22].

In addition to the choice of averaging, another challenge of wave-mean flow interaction theory is a dynamical one: what are the appropriate dependent variables to

formulate in order to obtain simple governing equations? In other words, what dominant balance should be studied? This question is unlikely answered by a single or a class of quantities, since many properties of the wave-mean flow interaction depend on the specific problems under consideration. However, in fluid applications, a sharp distinction can be made between two types of interactions: dissipative and non-dissipative interactions. The distinction stems from the importance of vorticity conservation for a non-dissipative fluid which puts a strong constraint on the interaction.

Dissipative wave-mean flow interaction is studied in the context of microfluidic problems in chapters 2 and 3. The motivation for these microfluidic problems is the rapid development of techniques using acoustic waves for the manipulation of microfluids. Here, microfluidics refers to devices and methods for controlling and manipulating fluid flows with length scales less than a millimeter. They have recently received increasing attention due to the following advances [117]: (i) the availability of methods for generating flow configurations with length scales on the order of tens and hundreds of microns; (ii) the ability to develop biotechnology by detecting small quantities and manipulating small volumes; (iii) the demand for cheap portable devices able to perform simple analytical tasks; (iv) the potential use of microsystems for fundamental studies of physical, chemical, and biological processes.

In chapter 2, we consider boundary streaming, a classic problem in acoustics, with a Navier boundary condition. It differs from the standard no-slip boundary condition in that the velocity at the boundary is proportional to the local shear with a coefficient termed slip length. The existence of slip boundary conditions has been observed in experiments, however, the mechanism of slip (and no-slip) at solid boundaries is still debated [71]. Even so, we can still understand the effect of a slip boundary condition by exploring how it modifies familiar results derived for a no-slip boundary condition. In the boundary streaming problem we consider, we identify a parameter that captures the effect of slip length on the streaming velocity and express the streaming velocity as an explicit function of this parameter. Considering the simplicity of our setup and the relative easiness of measuring streaming velocity in the regions that are not close to the boundary, experiments can be carried out to detect the impact of slip.

In chapter 3, we study the mean motion of a spherical particle in an acoustic wave field. When a particle is placed in an acoustic field, it has both a fast oscillatory motion at the frequency of the surrounding acoustic wave, and a slow, secular motion. We concentrate on this mean motion because it is the motion that is important for most microfluidic applications. For instance, spherical particles are used as tracers to visualise flow, or when particles are manipulated by acoustic waves. In chapter 3, we

derive governing equations that control a particle's mean motion in different parameter regimes. Besides clarifying the range of validity of several classical models, we discover a distinguished regime where a novel model is derived.

Non-dissipative wave-mean flow interaction is studied in the context of two geophysical fluid problems. The large characteristic spatial scales in these problems means that dissipative effects can be safely ignored. The first geophysical fluid problem – the interaction between near-inertial waves and mean flow in the ocean – is studied in chapter 4. Near-inertial waves have a frequency close to the Coriolis frequency, while the mean flow possesses relatively slow dynamics. The separation between two time scales is characterized by a small Rossby number. Therefore, to capture the slow dynamics including the near-inertial waves' influence, direct numerical simulations are inevitably expensive because of the small time step required to resolve fast near-inertial waves. In this work, by taking advantage of the time scale separation, we apply a fast time average to derive a coupled model that only depends on the slow time scale: the slow near-inertial wave dynamics is represented by the modulation of a wave amplitude. The model we obtain possesses a Hamiltonian structure which ensures conservation laws, such as energy conservation and momentum conservation. Based on them, we propose a novel mechanism – stimulated wave generation – that provides a candidate for the dissipation of mesoscale mean flow required for the closure of the oceanic energy budget. The closure remains one of the main problems in dynamical oceanography.

In chapter 5, we study the interaction between steady topographic waves and a shear flow in the limit of zero viscosity. In the setup that we consider, a distinctive feature is that the waves have a singular structure. As a result, the limiting situation of zero viscosity is different from the inviscid situation because of the existence of a non-vanishing wave absorption. Due to momentum conservation, this wave absorption forces a mean flow. However, in our zero-viscosity limit setup, viscosity is only important for the waves, so that the wave-mean flow interaction remains an inviscid process. The novelties of the work are the multiple spatial-scale setup and the inclusion of the Coriolis effect. The waves are generated from a multi-scale topography, which enables us to calculate the large spatial structure by applying small-scale averaging. Our results predicate different mean-flow scales from the ones obtained from earlier works ignoring the Coriolis force: the interaction location is far away downstream, and the interaction region is much larger than the envelope scale of topography

In chapter 6, we summarise our results and discuss some general lessons learned from our researches on specific wave-mean flow problems.

Throughout this thesis, we apply techniques such as asymptotic expansion and av-

eraging to obtain reduced models where the waves' influences on the mean flow are parameterized. Even though the fluid governing equations are known, this process is necessary for the following reasons: (i) computational constraints limit numerical simulations of the primitive equations to resolutions that are insufficient to capture all temporal and spatial scales of dynamical relevance; (ii) because of the complexity of fluid systems, where many mechanisms are intertwined, numerical results alone provide us with a limited understanding.

Chapter 2

Boundary streaming with Navier boundary condition

In this chapter the first microfluidic problem – acoustic boundary streaming with slip boundary condition – is examined. Here, the waves are high-frequency acoustic waves, which are widely used in micrometre-scale devices to generate mean flow. A natural use of the acoustic-generated mean flow is to transport fluid in microfluid devices [51, 3], which is a challenge due to the failure of classical methods: for example, it is very hard to build a turbine that is small enough to fit microfluid devices. Moreover, in many experiments related to biology and chemistry it is important to ensure that the fluid remain unpolluted. A cheap way to overcome these obstacles is to use acoustic streaming, which has lead to the creation of a fast-developing field, acoustic microfluidics [49, 136]. An example of a device is shown in figure 2.1, with figure 2.2 shows the generated flow, from the experiments of microfluid mixing in a channel designed by Tan et al. [119].

The distinctive mechanism of the wave-mean flow interaction in a microfluid is con-

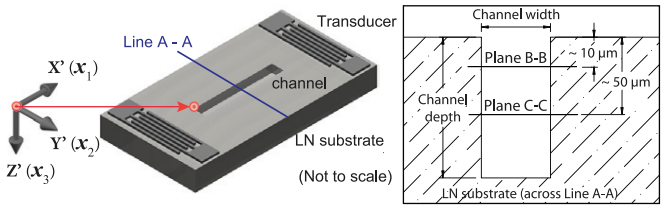

Figure 2.1: Device for microfluid mixing developed by Tan et al. [119]. Two transducers generate acoustic waves which propagate into the channel to induce a mean flow.

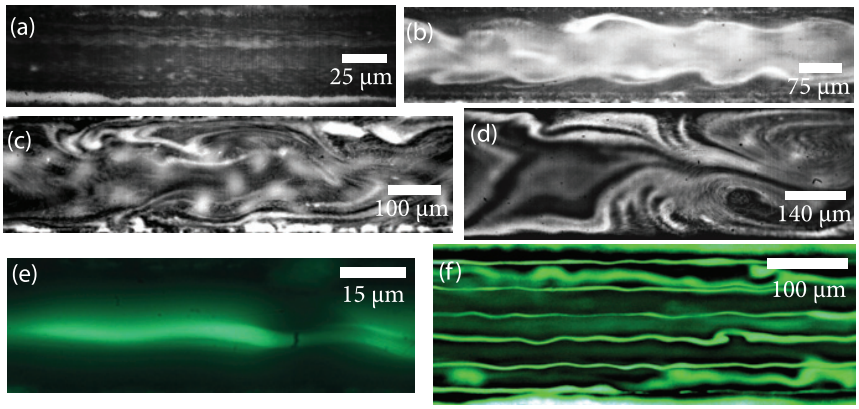

Figure 2.2: Mean flow generated by acoustic waves in the microfluid mixing experiment of Tan et al. [119]. The lengths in the panels show the half-width of the channel. The fluid is driven by 20 MHz surface acoustic waves.

trolled by viscosity, which is a consequence of a typical small spatial scale. In the momentum equation of the Navier-Stokes equations

$$\partial_t \boldsymbol{u} + \boldsymbol{u}\cdot\nabla\boldsymbol{u} = -\frac{1}{\rho}\nabla p + \nu\nabla^2\boldsymbol{u}, \tag{2.1}$$

where $\boldsymbol{u}$ is the velocity, ρ is the density, p is the pressure and ν is the fluid kinematic viscosity, the relative importance of the viscosity increases as the scale of the flow decreases due to the highest order spatial derivative in the last viscous term. Generally, the fluid kinetic viscosity is so small that only in the region with strong shear that the viscosity effect is important, which motivates boundary-layer theory. In boundary-layer theory the boundary layer is the thin layer adjacent to the boundary, and it is important by connecting the no-slip boundary condition with the outer, predominantly inviscid flow. The thickness of the boundary layer depends on the viscosity, and it can be estimated from dimensional analysis as

$$\delta \sim \sqrt{\nu T}, \tag{2.2}$$

where T is the characteristic time scale of the flow. For example, the Stokes boundary layer thickness generated by boundary oscillations is defined as $\delta = \sqrt{2\nu/\omega}$, where ω is the oscillation frequency; similarly the thickness of laminar boundary layer on a flat plane, which is also known as Blasius boundary layer [14], is expressed by $\delta = \sqrt{2\nu x/U}$ with U the flow velocity and x the distance from the edge.

In this specific acoustic streaming problem the acoustic wave is generated by the

vibrating solid boundary, hence the Stokes boundary layer thickness is the relevant one. This work is motivated by microfluidic applications involving high-frequency acoustic waves over a solid boundary, where the Stokes boundary-layer thickness δ is so small that some non-negligible slip may occur at the fluid-solid interface. In this chapter we assess the impact of this slip by revisiting the classical problem of steady acoustic streaming over a flat boundary [12], replacing the no-slip boundary condition with the Navier boundary condition $u|_{y=0} = L_s \partial_y u|_{y=0}$, where u is the velocity tangent to the boundary $y = 0$, and the parameter L_s is the slip length. By applying matched asymptotics, a general expression is obtained for the streaming velocity across the boundary layer as a function of the dimensionless parameter L_s/δ. The limit outside the boundary layer provides an effective slip velocity satisfied by the interior mean flow. Particularising to travelling and standing waves shows that the boundary slip respectively increases and decreases the streaming velocity.

This chapter is mainly based on the published paper [132].

2.1 Introduction

Among the many techniques devised to manipulate fluids at microscales [e.g. 116, 118], the use of high-frequency acoustic waves appears particularly promising. As a result, the field of what Friend and Yeo [49] term acoustic microfluidics is rapidly expanding; see Ref. 49, 136 for reviews of the experimental and theoretical state of the art in this field.

One of the main ingredients in the techniques developed is streaming—the generation of mean flow by dissipating acoustic waves. Two forms of streaming can be distinguished [74, 104]: (i) interior streaming, induced by wave attenuation in the fluid interior [44, 127, 96, 97]; and (ii) boundary streaming [101] which is confined near solid boundaries but influences the interior mean flow by modifying its effective boundary condition [see also 76, 18]. Both types of streaming share the remarkable property of non-vanishing mean motion in the limit of vanishing viscosity [97, 74]; both contribute to the interior mean flow, although the boundary contribution is small when the acoustic wavelengths are small compared to the flow scales [125].

A feature of many experiments in acoustic microfluidics [e.g. 51, 106, 3, 82, 36] is the high frequencies employed. A consequence is that the Stokes boundary-layer thickness is very small. This thickness estimates the size of the near-boundary region where viscous effects dominate and is given by $\delta = \sqrt{2\nu/\omega}$, where ν is the fluid's kinematic shear viscosity and ω is the wave's angular frequency. In water, and for typical frequencies in

the range 1 MHz to 1 GHz, δ is in the range 500 nm to 10 nm. This implies large stresses at the fluid-solid interface and, as a result, suggests that the no-slip boundary condition that is traditionally used for the study of boundary streaming may not be appropriate [71].

Motivated by this observation, we assess the effect that the possible slip of the fluid along the boundary has on boundary streaming. We do so by revisiting the classical model of boundary streaming over a flat plate, replacing the no-slip boundary condition by the more accurate Navier boundary condition [93]

$$u|_{y=0} = L_\mathrm{s}\, \partial_y u|_{y=0}\,, \tag{2.3}$$

where $y = 0$ defines the boundary, u is the velocity tangent to the boundary, and L_s is the so-called slip length, a property of the fluid-solid interactions [e.g. 71, 118]. The key dimensionless parameter in the problem is the ratio

$$\beta = L_\mathrm{s}/\delta \tag{2.4}$$

of the slip length to the Stokes boundary-layer thickness. With typical values for L_s of 10 to 100 nm (see e.g. Ref. 71), this parameter can take a broad range of values.

We examine the streaming induced on a motionless flat boundary by a plane acoustic wave in the far field. This is a simple problem, which we solve explicitly using a matched asymptotics technique relying on the small parameter δk, where k denotes the acoustic wavenumber. The solution is instructive, however, since the effect of slip, $\beta \neq 0$, on the streaming velocity is not obvious a priori: on the one hand, the slip reduces the shear and hence the Reynolds stress associated with the wave field; on the other hand, by weakening the constraint at the wall, it can increase the mean flow response to a given wave forcing. The non-trivial impact of the slip is illustrated by the fact that travelling and standing waves—two particular cases of our more general set-up—have different responses, respectively an increase and a decrease of the streaming velocity outside the boundary layer as β increases from zero.

2.2 Wave field

We consider a plane acoustic wave with velocity

$$\mathbf{U}_1 = \mathrm{Re}\,\left(U(x)\mathrm{e}^{-\mathrm{i}\omega t}\mathbf{e}_x\right), \tag{2.5}$$

propagating over a horizontal plate located at $y = 0$. Here $U(x)$ is an arbitrary complex function, ω is the (angular) frequency and $\mathbf{e}_x$ the unit vector in the x direction. Note that the form (2.5) includes both travelling waves (for which $U(x) \propto \mathrm{e}^{\mathrm{i}kx}$) and standing waves (for which $U(x)$ is real).

The dynamics is governed by the compressible Navier–Stokes equations

$$\begin{aligned} &\partial_t \rho + \nabla \cdot (\rho \mathbf{u}) = 0, \\ &\rho \partial_t \mathbf{u} + \rho \mathbf{u} \cdot \nabla \mathbf{u} = -\nabla p + \mu \nabla^2 \mathbf{u} + (\mu^{\mathrm{b}} + \mu/3) \nabla \nabla \cdot \mathbf{u}, \end{aligned} \tag{2.6}$$

where μ and μ^{b} are the shear and bulk viscosities, supplemented by an equation of state $p = p(\rho)$. Assuming that $U(x)$ is small compared with the sound speed c_0, we introduce the expansions

$$\mathbf{u} = \mathbf{u}_1 + \mathbf{u}_2 + \dots, \tag{2.7}$$

$$p - p_0 = p_1 + p_2 + \dots, \tag{2.8}$$

$$\rho - \rho_0 = \rho_1 + \rho_2 + \dots, \tag{2.9}$$

where the subscripts indicate the order in U/c_0. We are seeking a perturbative solution of (2.6) with $\mathbf{u}_1$ matching the far-field form (2.5) away from the boundary and satisfying the Navier boundary condition (2.3) at $y = 0$. We consider the case of a small viscosity, characterised by $k\delta \ll 1$, with $k = \omega/c_0$ the wavenumber; in this case, the effect of viscosity is confined to a layer of thickness δ above the boundary. The solution in this boundary layer is best written in terms of the rescaled coordinate $Y = y/\delta$. This yields the order-one equations in the boundary layer,

$$\partial_t \rho_1 + \rho_0 \left(\partial_x u_1 + \delta^{-1} \partial_Y v_1 \right) = 0, \tag{2.10}$$

which indicates that $v_1/u_1 = O(k\delta)$,

$$\rho_0 \partial_t u_1 = -\partial_x p_1 + \mu \delta^{-2} \partial_{YY}^2 u_1 \quad \text{and} \quad \partial_Y p_1 = 0, \tag{2.11}$$

where we have neglected terms of relative size $O(k\delta)$. Away from the boundary layer, in the outer region, the flow is irrotational and viscous terms are negligible, so $R_1 = \lim_{Y\to\infty} \rho_1$, $\mathbf{U}_1 = \lim_{Y\to\infty} \mathbf{u}_1$ and $P_1 = \lim_{Y\to\infty} p_1$ satisfy

$$\partial_t R_1 + \rho_0 \partial_x U_1 = 0, \tag{2.12}$$

$$\rho_0 \partial_t \mathbf{U}_1 = -\nabla P_1. \tag{2.13}$$

For consistency with (2.5), $V_1 = \lim_{Y\to\infty} v_1 = 0$.

It follows from (2.10) and (2.11) that p_1 is independent of Y, such that $p_1 = P_1$, leading to

$$\partial_t u_1 = \partial_t U_1 + \omega \partial^2_{YY} u_1/2. \tag{2.14}$$

Solving (2.14) with the boundary conditions $u_1 \to U$ as $Y \to \infty$ and $u_1 = \beta \partial u_1/\partial Y$ at $Y = 0$, we obtain

$$u_1 = \mathrm{Re}\left(U \mathrm{e}^{-\mathrm{i}\omega t} \left(1 - \frac{\mathrm{e}^{-(1-\mathrm{i})Y}}{1 + (1-\mathrm{i})\beta} \right) \right) \tag{2.15}$$

to leading order in $k\delta$. The equation of state implies that $p_1 = c_0^2 \rho_1$ and, using (2.11), that ρ_1 is independent of Y: $\rho_1 = R_1$. Subtracting (2.12) from (2.10), integrating and imposing v_1 bounded as $Y \to \infty$ then gives

$$v_1 = \delta \mathrm{Re}\left(U' \mathrm{e}^{-\mathrm{i}\omega t} \frac{(1+\mathrm{i})}{2(1+(1-\mathrm{i})\beta)} \left(1 - \mathrm{e}^{-(1-\mathrm{i})Y} \right) \right), \tag{2.16}$$

also to leading order in $k\delta$. The two components (u_1, v_1) of the wave velocity in the boundary layer for different values of β are displayed in Figure 2.3. We only show the result of the travelling wave, and the response to a standing wave is the same up to phase differences. The figure indicates that the amplitude of the component u_1 of the wave velocity parallel to the wall is almost constant as β varies while the perpendicular component v_1 decreases as β increases.

2.3 Mean flow

Using the form (2.15)–(2.16) for the wave field, we can calculate the Reynolds stress and solve the mean-flow equation which, in the boundary layer, takes the form

$$\omega \partial^2_{YY} \overline{u}_2/2 = \delta^{-1} \left(\partial_Y \overline{u_1 v_1} - \partial_Y \overline{u_1 v_1}|_\infty \right) + \partial_x \overline{u_1^2} - \partial_x \overline{u_1^2}\Big|_\infty, \tag{2.17}$$

where the subscripts ∞ indicate the limit $Y \to \infty$ and the overbars indicate averaging over a wave period. This expression is obtained by averaging (2.6), retaining only leading-order terms in $k\delta$, and subtracting from the inner equation its limit as $Y \to \infty$ to eliminate the Y-independent pressure term in exactly the same manner as employed for the wave equations.

It is convenient to consider the effect of $\partial_Y \overline{u_1 v_1}$ and $\partial_x \overline{u_1 u_1}$ separately, taking advantage of the linearity of Eq. (2.17) for $\overline{u}_2$. First we calculate the effect of $\partial_Y \overline{u_1 v_1}$. A

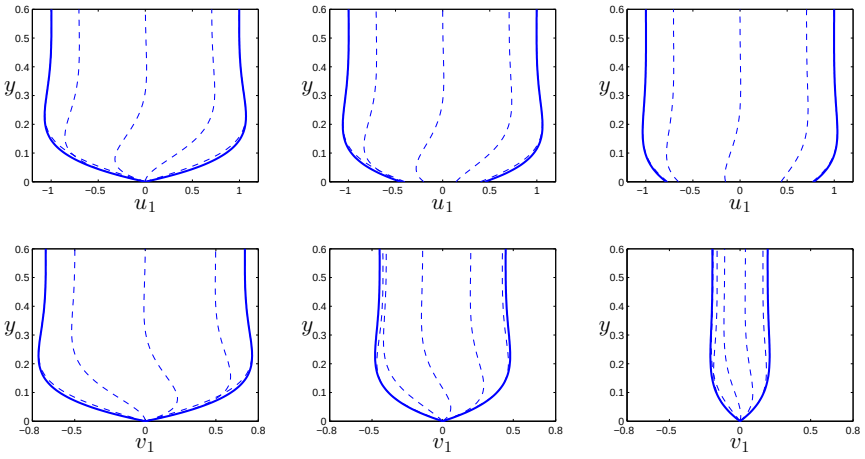

Figure 2.3: Wave field in the boundary layer. The solid lines show the amplitude of the velocities $|u_1/U|$ (top row) and $|v_1/U'|$ (bottom row) for $\beta = 0$ (left), 0.5 (middle) and 2 (right). The time evolution is illustrated by the dashed lines showing $u_1/|U|$ and $v_1/|U'|$ at $x = 0$ with assumption of a travelling wave $U \propto \mathrm{e}^{\mathrm{i}kx}$ and for the phases $\omega t = 0,\ \pi/4,\ \pi/2,\ 3\pi/4,\ \pi$ (from right to left).

short computation leads to

$$\begin{aligned}\overline{u_1 v_1} = \frac{1}{8}\frac{\delta U U'^*}{(1+\beta)^2+\beta^2}\Big(&1-\mathrm{i}(1+2\beta)-(1-\mathrm{i})\mathrm{e}^{-(1-\mathrm{i})Y}\\ &-(1-\mathrm{i}(1+2\beta))\mathrm{e}^{-(1+\mathrm{i})Y}+(1-\mathrm{i})\mathrm{e}^{-2Y}\Big)+\text{c.c.},\end{aligned} \tag{2.18}$$

where c.c. denotes the complex conjugate of the preceding term. Since $\partial_Y \overline{u_1 v_1}|_\infty = 0$, the Y-dependent terms immediately give the contribution to the shear $\omega \partial_Y \overline{u}_2/2$. Integrating these terms and using the averaged Navier boundary condition $\overline{u}_2 = \beta \partial_Y \overline{u}_2$ at $Y = 0$ finally gives the first contribution to the mean velocity

$$\begin{aligned}\overline{u}_2^{(\mathrm{i})} = \frac{1}{4\omega}\frac{U U'^*}{(1+\beta)^2+\beta^2}\Big(&\mathrm{e}^{-(1-\mathrm{i})Y}-1+\frac{(1-\mathrm{i}(1+2\beta))}{1+\mathrm{i}}(\mathrm{e}^{-(1+\mathrm{i})Y}-1)\\ &-\frac{(1-\mathrm{i})}{2}(\mathrm{e}^{-2Y}-1)+\beta(-1+\mathrm{i}(1+2\beta))\Big)+\text{c.c.}.\end{aligned} \tag{2.19}$$

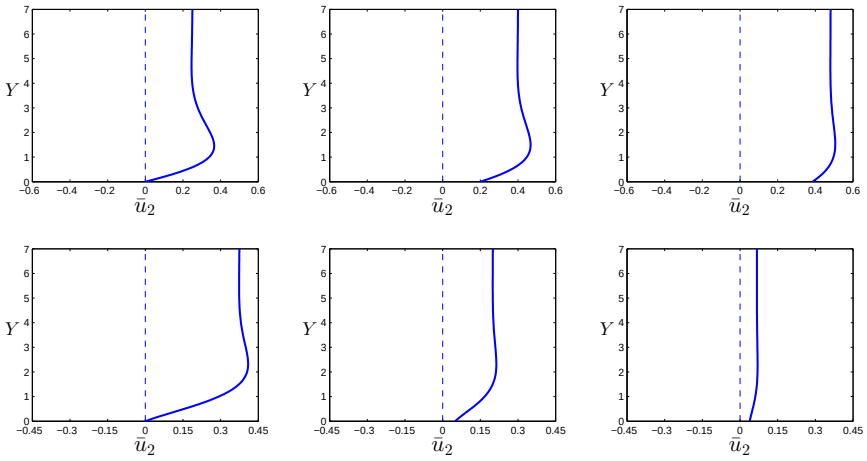

Figure 2.4: Mean velocity profiles for the travelling wave $U(x) = A\mathrm{e}^{\mathrm{i}kx}$ (top) and the standing wave $U(x) = A\cos(kx)$ (bottom) for $\beta = 0$ (left), 0.1 (middle) and 2 (right). The profiles are normalized by A^2/c_0 (travelling wave) and $\sin(2kx)A^2/c_0$ (standing wave).

Next we calculate the effect of $\partial_x \overline{u_1^2}$: starting with

$$\omega \partial_{YY}^2 \overline{u}_2/2 = \partial_x \left(\overline{u_1^2} - \overline{u_1^2}\Big|_\infty \right) = -\frac{(|U|^2)'}{4} \left(\frac{2}{1+\beta-\mathrm{i}\beta} \mathrm{e}^{-(1-\mathrm{i})Y} - \frac{\mathrm{e}^{-2Y}}{(1+\beta)^2+\beta^2} \right) + \text{c.c.}, \tag{2.20}$$

integrating twice and applying the boundary conditions $\partial_Y \overline{u}_2 \to 0$ as $Y \to \infty$ and $\overline{u}_2 = \beta \partial_Y \overline{u}_2$ at $Y = 0$ yields

$$\overline{u}_2^{(\mathrm{ii})} = \frac{1}{2\omega} \frac{(|U|^2)'}{(1+\beta)^2+\beta^2} \left((\beta - \mathrm{i}(1+\beta)) \mathrm{e}^{-(1-\mathrm{i})Y} + \frac{\mathrm{e}^{-2Y}}{4} - \frac{1}{4} - \frac{\beta}{2} \right) + \text{c.c.}. \tag{2.21}$$

Combining (2.19) and (2.21) leads to the mean profile $\overline{u}_2 = \overline{u}_2^{(\mathrm{i})} + \overline{u}_2^{(\mathrm{ii})}$. This is illustrated in Figure 2.4 for a travelling wave with $U(x) = A\exp(\mathrm{i}kx)$, and for a standing wave with $U(x) = A\cos(kx)$. As β increases, the amplitude of $\overline{u}_2$ increases for the travelling wave and decreases for the standing wave; we comment on the physical mechanism underlying this dependence in Sec. 2.4.

Letting $Y \to \infty$ in $\overline{u}_2$, we obtain the total steady streaming velocity outside the boundary layer as

$$\overline{U}_2 = -\gamma^{\mathrm{s}}(|U|^2)'/\omega - \gamma^{\mathrm{t}}\mathrm{i}(U^*U' - U(U')^*)/\omega, \tag{2.22}$$

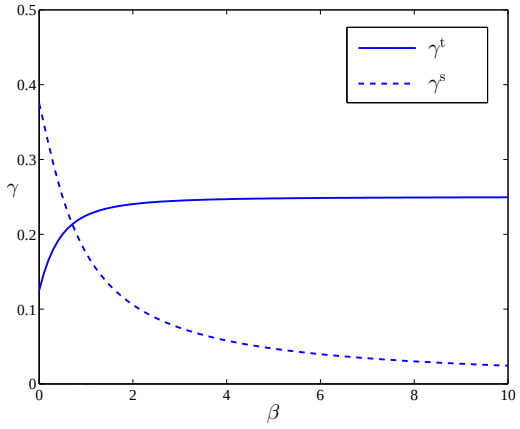

Figure 2.5: Coefficients γ^{t} and γ^{s} in expression (2.22) for the streaming velocity as a function of the slip parameter β.

where

$$\gamma^{\mathrm{s}} = \frac{3+4\beta}{8\left((1+\beta)^2+\beta^2\right)} \quad \text{and} \quad \gamma^{\mathrm{t}} = \frac{1+4\beta+4\beta^2}{8\left((1+\beta)^2+\beta^2\right)}.$$

This expression provides an effective slip condition for the flow in the interior. It generalises to the Navier condition results obtained by Nyborg [97] and Lighthill [74, 75] in the no-slip case $\beta = 0$. Note that $(|U|^2)' = 2\,\mathrm{Re}\,(U^*U')$ and $\mathrm{i}(U^*U' - U(U')^*) = -2\,\mathrm{Im}\,(U^*U')$ can be thought of as measuring the standing- and travelling-wave components of more general wave fields.

We emphasise that (2.22) gives the Eulerian mean flow: results of this type can alternatively be formulated in terms of the Lagrangian mean slip velocity, as in Ref. [125]. The difference between the two mean velocities is the Stokes drift, given outside the boundary layer by

$$\overline{U}_2^{\mathrm{Sto}} = -\mathrm{i}(U^*U' - U(U')^*)/(4\omega), \tag{2.23}$$

leading to the Lagrangian mean slip velocity

$$\overline{U}_2^{\mathrm{L}} = \overline{U}_2 + \overline{U}_2^{\mathrm{Sto}} = -\gamma^{\mathrm{s}}(|U|^2)'/\omega - \left(\gamma^{\mathrm{t}} + 1/4\right)\mathrm{i}(U^*U' - U(U')^*)/\omega \tag{2.24}$$

which may be more easily accessible in observations.

From (2.22) we can compute the steady streaming by travelling and standing waves, with $U = \hat{U}\exp(\mathrm{i}kx)$ and $U(x)$ real, respectively, to find

$$\overline{U}_2^{\mathrm{t}} = 2\gamma^{\mathrm{t}}|\hat{U}|^2/c_0 \quad \text{and} \quad \overline{U}_2^{\mathrm{s}} = -2\gamma^{\mathrm{s}}UU'/\omega. \tag{2.25}$$

These expressions, which provide an interpretation for the coefficients γ^{t} and γ^{s}, reduce to well-known expressions [97, Eq. (61)] and [74, Eq. (94)], including Rayleigh's result for standing waves [101], when $\beta = 0$. The dependence of γ^{t} and γ^{s} on β is illustrated in Figure 2.5. One (not necessarily intuitive) conclusion is that slip at the boundary increases the streaming velocity away from the boundary for travelling waves while it decreases the streaming velocity for standing waves. More specifically, in the limit of large slip $\beta \to \infty$, the streaming velocity for travelling waves is increased by a factor 2 for travelling waves but reduced to zero for standing waves.

2.4 Discussion

This chapter derives the general expression (2.22) for the streaming velocity induced by acoustic waves over a flat boundary with Navier boundary condition. This expression can be used as an effective boundary condition for the mean flow in the interior when both interior and boundary streaming are important. Naturally, it reduces to well-known results in the no-slip case $\beta = 0$.

In the opposite limit $\beta \to \infty$, the two parameters γ^{t} and γ^{s} that appear in (2.22) and are associated, respectively, with travelling and standing waves, behave very differently, with $\gamma^{\mathrm{t}} \to 1/4$ while $\gamma^{\mathrm{s}} \to 0$. Physically, the travelling wave contribution γ^{t} stems from $\partial_Y \overline{u_1 v_1}$, the divergence of the y-component of the flux of x-momentum, while the standing wave component contribution γ^{s} also stems from $\partial_x \overline{u_1 u_1}$, the divergence of the x-component of this flux. Only u_1 appears in $\partial_x \overline{u_1 u_1}$; as u_1 becomes unaffected by the wall in the limit $\beta \to \infty$, $\partial_x \overline{u_1 u_1}$ clearly tends to 0. The contribution of $\partial_Y \overline{u_1 v_1}$ in the limit of $\beta \to \infty$, which involves the y-components of the wave fields, is more complex. Because the outer flow is fixed and the wave velocity is bounded, the wave shear, Reynolds stress and hence mean-flow forcing decrease as the slip length increases. However, for a given mean-flow forcing, the mean velocity at the boundary and indeed across the boundary layer increases as the slip length increases (because the constraint imposed by the boundary condition weakens). The competition between the two effects leads to a balance as $\beta \to \infty$. Importantly, this shows the limit $\beta \to \infty$ to be singular, with the Navier condition yielding a different solution to a completely stress-free condition at the wall. The small but non-zero velocity perpendicular to the wall, $v_1 = O(\beta^{-1})$, imposed by mass conservation, leads to a non-zero mean momentum flux which in turns affects the mean flow in boundary layer at $O(1)$. This can be seen directly by combining the Navier boundary condition with the mean momentum equation to obtain $\overline{u}_2|_0 = L_{\mathrm{s}}\, \partial_y \overline{u}_2|_0 = -\,(L_{\mathrm{s}}/\nu)\overline{u_1 v_1}|_\infty = -(L_{\mathrm{s}}/\nu)\overline{U_1 V_1}$, neglecting the contribution of $\partial_x \overline{u_1^2}$

which is $O(\beta^{-1})$. In the outer region, $U_1 = \mathrm{Re}\left(U\mathrm{e}^{-\mathrm{i}\omega t}\right)$ and $V_1 = \mathrm{Re}\left(\mathrm{i}\delta U'\mathrm{e}^{-\mathrm{i}\omega t}/(2\beta)\right)$ as $\beta \to \infty$ (see (2.15)–(2.16)); furthermore, $\overline{U}_2 \sim \overline{u}_2|_0$ (since $\overline{u}_2$ becomes independent of Y as expected in the stress-free limit) so that $\overline{U}_2 \sim -\mathrm{i}(U^*U' - U(U')^*)/(4\omega)$, consistent with (2.22). It is only for standing waves, for which U and U' are in phase, that this vanishes.

We conclude with two remarks. First, different wave frequencies lead to very different mean velocity profiles because of the dependence of the boundary-layer thickness on the frequency. One can therefore propose that acoustic waves with a rich, variable wave spectrum may provide a method for controlling the mean-velocity profile near a solid boundary. Second, the dependence of the mean velocity on the slip length suggests that acoustic streaming could be used for the (notoriously difficult) estimation of the slip lengths of various fluid-solid combinations. An experiment estimating the Lagrangian slip velocity $\overline{U}_2^{\mathrm{L}}$ by measuring the mean speed of tracer particles would make it possible to infer β from (2.24) and, since $L_\mathrm{s} = \beta\sqrt{2\nu/\omega}$, the slip length. Carrying out such an experiment over a range of frequencies would ensure a good accuracy. The frequencies ω should be chosen with β of order one so that it depends substantially on ω. For instance, in water, if $L_\mathrm{s} \sim 100$ nm, β varies from 1 to 3 as ω varies from about 0.1 to 1 GHz. One difficulty may be to ensure that the tracer particles provide an accurate estimate of the Lagrangian slip velocity: their motion may be affected by interior streaming [e.g. 125] if they are not confined sufficiently close to the wall, and by radiation pressure [e.g. 39].

Chapter 3

Dynamics of a spherical particle in an acoustic field

From chapter 2 we know that the acoustic waves in microfluid devices can generate mean flow through the nonlinear terms in the Navier-stokes equations. This chapter focuses on the applications of acoustic waves and the mean flow they generate, specifically, on the mean dynamics of spherical particles in an acoustic field.

In addition to the fluid transportation mentioned in chapter 2, the focus of some other applications is not on the fluid but on its use to manipulate matter within it. Such applications include particle collection or separation [112, 64, 73, 98, 106, 10, 59], and acoustic levitation [122]. For example, Figure 3.1 shows particle collection experiments in a droplet by standing acoustic waves performed by Oberti et al. [98].

These applications – fluid transportation and matter manipulation – involve the motion of small, typically spherical particles, either simply as tracers used to visualise the flow, or as objects to be manipulated. In an acoustic field, spherical particles have both an oscillatory motion with the period of the acoustic wave field, and a mean motion on a longer time scale. The mean motion is the key for microfluidic applications. Motivated by these applications, in this chapter, we study the dynamics of such particles in acoustic fields theoretically, concentrating on the mean dynamics that results from averaging over many wave periods.

Particles are influenced by many mean effects. Since the particles do not deform like the fluid under the same pressure, however small they are, these particles are distinctive from fluid elements. So particles immersed in a fluid are forced by the integrated effect of pressure over their surfaces. In the context of acoustic waves, the mean effect of this force is termed acoustic pressure (e.g. [68, 57]). As mentioned, another effect of

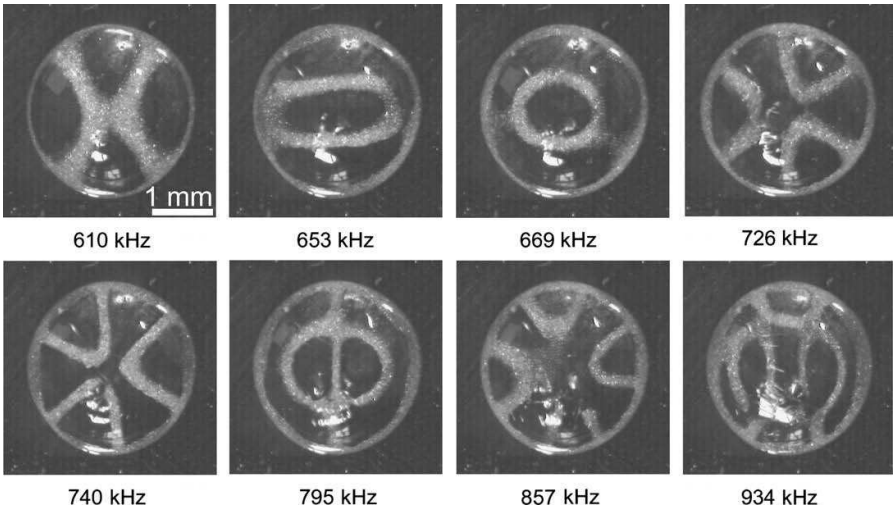

Figure 3.1: Patterns of particle collection in a droplet with different standing waves, from Oberti et al. [98].

acoustic waves is acoustic streaming [97, 74, 104], which is the nonlinear generation of mean flow by the acoustic waves. Streaming acts even in the absence of particles and is the main mechanism exploited in acoustic microfluidics; it clearly affects the dynamics of particles, though in a way that is sometimes difficult to distinguish from acoustic radiation. In addition, because of the small characteristic spatial scales in microfluidics, viscous effects are important. They influence particles explicitly through viscous drag, which is similar with that in classic fluid scenarios such as Stokes flows; they also affect particles implicitly through modifications of the acoustic pressure and streaming. Finally, because the particles are forced, their inertia needs to be taken into account.

For this particle-fluid coupled problem, the complete governing equations are not hard to write down. However, the cost of solving these complete equations, even numerically, is large. Furthermore, because they are very complex, these complete equations are not very helpful in guiding experiments, for which an important question is how can we choose suitable parameters – frequency of the acoustic wave, size and density of the particles, etc. – to fulfil aims such as flow visualization. In this chapter we systematically explore the parameter regimes defined by combinations of these physical parameters and make approximations to obtain different dominant mean dynamics for rigid spherical particles in an acoustic-wave field. This chapter is largely based on the published paper [133].

3.1 Introduction

High-frequency acoustic waves are increasingly used to actuate and manipulate fluids at microscales. As a result, the field of acoustic microfluidics is in rapid development [49, 136]. In these applications, spherical particles, whose dynamics is controlled by acoustic pressure, streaming, viscous drag and inertia, are used as passive tracers or the objects to manipulate. The relative role of these four effects is the main theme of this chapter. Specifically, we explore how, depending on the parameters of the problems, the mean dynamics of a single spherical rigid particle can be controlled by different balances among these effects, and we derive the corresponding mean equations of motion. We do so by applying a systematic multiscale approach: taking the standard linear acoustics hypothesis of small-amplitude waves, characterised by an acoustic Mach number $\epsilon \ll 1$, we consider possible distinguished scalings of the other parameters in the problem, primarily viscosity measured by the ratio δ/a of the Stokes boundary-layer thickness to the sphere radius. We apply multiscale and matched-asymptotics methods to obtain asymptotic equations governing the motion over long time scales. Crucially, this requires (i) to consider the fully coupled fluid-particle system, recognising that a reduction to an ordinary differential equation for the particle alone is possible only in certain parameter regimes; and (ii) to take into account explicitly the mean displacements of the particle. This is in contrast with much of previous work which, as mentioned, concentrates on acoustic pressure and typically assumes that the mean particle position can be taken as frozen.

In the classic work by King [68] and Gor'kov [57] on acoustically-driven particles in inviscid fluids (with assumptions of, respectively, axisymmetry and long wavelength $ka \ll 1$, with k the wavelength), explicit expressions are derived for the acoustic pressure in this way; the effect of the fluid motion is subsequently taken into account in a somewhat ad hoc manner by including an added mass effect in Newton's second law for the particle. Our treatment shows this to be valid for sufficiently small viscosity and makes precise how small the viscosity needs to be. The case of a viscous fluid has been considered in many papers,[126, 28, 29] culminating in the work of Doinikov [37, 38, 39] who provides complete expressions for the acoustic pressure in an axisymmetric field for arbitrary viscosity and wavelength. Simplified expressions valid for $ka \ll 1$ and arbitrary wave fields have recently been obtained by Settnes and Bruus [110] (see also Ref. 30 and references therein). In this viscous case, a closed equation of motion for the sphere can be inferred from the acoustic force by assuming that the inertia of the particle and surrounding fluid is negligible. Again, our treatment shows this to be a valid

approximation under conditions that we make explicit. More importantly, our analysis reveals a new regime (termed Regime II below) in which the fluid motion driven by the particle is both crucial for the particle dynamics and determined by the full (viscous) Navier–Stokes equations instead of the simple potential solution relevant in the purely inviscid approximation. In this regime, the particle and fluid motion are completely coupled, and no reduction to a single ordinary differential equation is possible.

Much of the earlier work on acoustic pressure was motivated by applications very different from those arising today from developments in acoustic microfluidics. The focus of this chapter reflects these developments: in particular, we pay attention to the case of particles with the same density as the fluid. While this case is 'of no interest for practice' [39] when dealing with, say, dust particles or water drops in air, it is highly relevant in microfluidics applications where the particle density is often selected to avoid buoyancy effects. We examine the conditions that need to be satisfied for such particles to follow fluid elements and hence act as genuinely passive tracers. This is important in view of the widespread use of particles for this purpose in acoustic microfluidics.

The chapter is structured as follows. Section 3.2 introduces the governing equations and relevant non-dimensional parameters. Based on this, and under the assumption $ka = O(1)$ (which includes $ka \ll 1$), it gives a heuristic argument for the existence of two distinguished asymptotic regimes in which three of the four physical effects affecting particle motion balance. These two regimes are considered in detail in sections 3.3 and 3.4. There we apply systematically multiscale asymptotics to derive the equations governing the mean dynamics in each regime. These equations can be further simplified in several intermediate regimes in which only two of the four physical effects come into play. These regimes are of great practical importance; the relevant equations are derived in section 3.5. The chapter concludes in section 3.6 with a brief summary, a discussion of the relevance of the results to examples of acoustic microfluidics experiments, and pointers to further work, including on the case $ka \gg 1$. Throughout, we emphasise the systematic derivation of mean equations of motion over specific expressions for the acoustic-pressure terms. We refer the reader to earlier work for these and point out the approximations that can be made consistently in each of the regimes we analyse. We note that complete expressions for the acoustic pressure have been obtained for axisymmetric wave fields (Ref. 39 and references therein) and for general wave fields provided that $ka \ll 1$ (Refs. 30, 110 and references therein). Our results have the same range of validity.

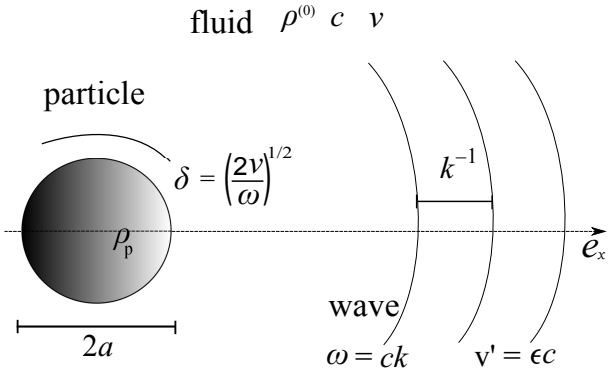

Figure 3.2: Parameters controlling the motion of a spherical particle in an acoustic field.

3.2 Formulation

3.2.1 Dimensionless parameters and scaling

We study the mean dynamics of a rigid sphere in an axisymmetric acoustic wave field. For simplicity we neglect the effect of heat conduction [41, 42]. The problem is then characterised by eight parameters: the fluid properties determine the equilibrium density $\rho^{(0)}$, sound speed c and shear and bulk viscosities η and ξ; the particle is characterised by its density ρ_p and radius a; the incident wave by a frequency ω and a velocity amplitude v'. See Figure 3.2 for an illustration. The π-theorem of dimensional analysis yields five dimensionless parameters: η/ξ, $\lambda = \rho^{(0)}/\rho_\mathrm{p}$, $\epsilon = v'/c$, δ/a, where $\delta = \sqrt{2\eta/(\rho^{(0)}\omega)}$ is the Stokes boundary-layer thickness (e.g., Ref. 12, section 5.13), and ka, where $k = \omega/c$ is a wavenumber.

Since we are dealing with acoustic waves, we naturally assume that the acoustic Mach number ϵ is small: $\epsilon \ll 1$. Different dynamical regimes then emerge depending on the size of the other dimensionless parameters relative to ϵ. We assume that both η/ξ and λ are $O(1)$ as is relevant to most applications. This leaves the two parameters δ/a and ka which we relate to ϵ according to

$$\delta/a = O(\epsilon^\alpha) \quad \text{and} \quad ka = O(\epsilon^\gamma). \tag{3.1}$$

The exponents α and γ introduced in (3.1) control the nature of the dynamics. Their physical interpretation is clear: increasing α decreases the strength of the viscous effects, while increasing γ increases the wavelength.

The problem at hand involves two distinct time scales: the wave time scale ω^{-1} and a slower time scale characterising the mean motion of the sphere. To capture this, we

introduce a slow time variable T, related to the fast (wave) time t by

$$T = \epsilon^{\beta} t. \tag{3.2}$$

To apply systematic asymptotic methods, the exponent β should be related to α and γ. This requires to consider the balance of terms in the equations governing the dynamics of the coupled fluid-particle system.

3.2.2 Basic equations

The fluid is governed by the compressible Navier–Stokes equations

$$\frac{\partial}{\partial t}(\rho \boldsymbol{v}) = \nabla \cdot (\sigma - \rho \boldsymbol{v} \otimes \boldsymbol{v}), \tag{3.3a}$$

$$\frac{\partial \rho}{\partial t} + \nabla \cdot (\rho \boldsymbol{v}) = 0, \tag{3.3b}$$

$$\text{with} \quad \sigma_{ij} = -p\delta_{ij} + \eta \left(\frac{\partial v_i}{\partial x_j} + \frac{\partial v_j}{\partial x_i} - \frac{2}{3} \frac{\partial v_k}{\partial x_k} \delta_{ij} \right) + \xi \frac{\partial v_k}{\partial x_k} \delta_{ij}, \tag{3.3c}$$

where ρ is the fluid density, $\boldsymbol{v}$ its velocity, σ is the stress tensor, and p is the pressure. Subscripts denote components and Einstein's summation convention is used. Eqs. (3.3) are supplemented by an equation of state $p = p(\rho)$, from which the sound velocity is defined, by the no-slip boundary condition at the surface of the particle

$$\boldsymbol{v}(\boldsymbol{x}, t) = \frac{\mathrm{d}\boldsymbol{X}}{\mathrm{d}t} \quad \text{for} \quad \boldsymbol{x} \in S_{\boldsymbol{X}}, \tag{3.4}$$

where $\boldsymbol{x}$ is the position vector, $\boldsymbol{X}$ the position of the centre of the particle, and $S_{\boldsymbol{X}}$ denotes the sphere of radius a centred at $\boldsymbol{X}$, and by a prescribed incident acoustic field at infinity

$$\boldsymbol{v}(\boldsymbol{x}, t) \sim \boldsymbol{v}_{\text{incident}} \quad \text{as} \quad \boldsymbol{x} \to \infty. \tag{3.5}$$

The motion of the particle is governed by Newton's second law written as

$$M \frac{\mathrm{d}^2 \boldsymbol{X}}{\mathrm{d}t^2} = \boldsymbol{F} = \int_{S_{\boldsymbol{X}}} \sigma \cdot \boldsymbol{n} \, \mathrm{d}s, \tag{3.6}$$

where $M = 4\pi\rho_{\mathrm{p}} a^3/3$ is the mass of the particle and $\boldsymbol{n}$ denotes the outer normal. Since the sphere is symmetric and placed in an axisymmetric wave field, its motion is one dimensional along the axis of symmetry of the wave field; we choose this direction to be the x-axis, with unit vector $\boldsymbol{e}_x$, so that $\boldsymbol{X} = X\boldsymbol{e}_x$. Note that the assumption of an

axisymmetric wave can be relaxed when $ka \ll 1$ since an arbitrary wave field is can then be regarded as locally planar. In view of the practical importance of this approximation, satisfied in the majority of applications, we write our results, whenever possible, in a vector form that can be employed for general wave fields when $ka \ll 1$.

3.2.3 Regimes

Our focus is on the mean motion of the particle, driven by the force on the right-hand side of (3.6) averaged over a wave period. We denote this average by $\langle\cdot\rangle$, so that $\langle\partial_t\cdot\rangle = 0$. Considering an expansion of all the variables in the form

$$\boldsymbol{v} = \epsilon\boldsymbol{v}^{(1)} + \epsilon^2\boldsymbol{v}^{(2)} + \cdots, \tag{3.7a}$$

$$\boldsymbol{x} = \boldsymbol{X}^{(0)} + \epsilon\boldsymbol{X}^{(1)} + \epsilon^2\boldsymbol{X}^{(2)} + \cdots, \tag{3.7b}$$

$$p = p^{(0)} + \epsilon p^{(1)} + \epsilon^2 p^{(2)} + \cdots, \tag{3.7c}$$

where $\boldsymbol{X}^{(0)}$ captures the mean motion of the particle, we write the averaged force as

$$\langle\boldsymbol{F}\rangle = \int_{S_{\boldsymbol{X}^{(0)}}} \left\langle\sigma^{(2)}\right\rangle \cdot \boldsymbol{n}\,\mathrm{d}s - \int_{S_{\boldsymbol{X}^{(0)}}} \rho^{(0)} \left\langle\boldsymbol{v}^{(1)} \otimes \boldsymbol{v}^{(1)}\right\rangle \cdot \boldsymbol{n}\,\mathrm{d}s + O(\epsilon^3). \tag{3.8}$$

Note that the integrations are over the surface of the sphere centred at $\boldsymbol{X}^{(0)}$ which moves only over the slow time scale. The second term on the right-hand side, however, arises from the integration of $\sigma^{(1)}$ over the rapidly moving surface $S_{\boldsymbol{X}^{(0)}+\epsilon\boldsymbol{X}^{(1)}}$ (see, e.g., Ref. 39 for a derivation).

The force in (3.8) contains two distinct physical effects. The first is a viscous drag which relaxes the particle's velocity to the velocity of the surrounding fluid. It is not obvious what the relevant fluid velocity is but it certainly includes the streaming velocity that is generated by dissipation and nonlinearity even in the absence of a particle [126, 96, 104]. The second effect is the radiation pressure associated with the scattered wave. With this in mind, we can postulate a heuristic form for the equation governing the mean motion of the particle, estimate the order of magnitudes of its terms, and find the combinations of α, β and γ that lead to distinguished limits as $\epsilon \to 0$. These limits are crucial since the corresponding regimes include all the physical mechanisms that can possibly have a leading-order effect simultaneously. Our aim is to derive mean equations that apply to these regimes; simpler models, valid in intermediate regimes, can then be deduced straightforwardly by neglecting certain terms.

Heuristically, we can expect the mean motion of the particle to be governed by an

equation of the form

$$\begin{array}{lccccc} & \tilde{M}\ddot{\boldsymbol{X}}^{(0)} & +6\pi a\eta(\dot{\boldsymbol{X}}^{(0)} & - & \tilde{\boldsymbol{v}}) & = & \boldsymbol{F}_{\mathrm{ap}}, \\ \text{relative order:} & \epsilon^{2\beta} & \epsilon^{2\alpha+\beta} & & \epsilon^{2\alpha+2} & & \epsilon^{2} \end{array} \tag{3.9}$$

where $\tilde{M}$ is a mass, expected to be the mass of the particle plus a possible added mass stemming from fluid motion, $\tilde{\boldsymbol{v}}$ is a streaming velocity, and $\boldsymbol{F}_{\mathrm{ap}}$ is the acoustic-pressure force. Here and henceforth, the overdot denotes the time derivative with respect to the slow time T. Below each term in (3.9) we indicate its relative order of magnitude, based on the dimensional estimates $\rho_{\mathrm{p}}a^3k^{-1}T^{-2}$, $a\eta k^{-1}T^{-1}$, $a\eta v'^2c^{-1}$ and $\rho^{(0)}ka^3v'^2$. These assume: typical particle displacements $\boldsymbol{X}^{(0)}$ of size $O(k^{-1})$; a streaming velocity $\tilde{\boldsymbol{v}} = O(v'^2/c)$, which holds provided that the amplitude of the waves varies on an 'outer scale' that is not too dissimilar to k^{-1} (e.g., Refs. 96, 125); and the scaling $ka^3v'^2$ for the surface integrals in (3.8). The latter scaling follows from applying the divergence theorem and the assumption that $ka = O(1)$, i.e., $\gamma \geq 0$ so that the spatial derivatives scale like k rather than a^{-1}; it is confirmed by explicit computations of the acoustic radiation force, e.g. in Ref. 57. For now, we focus on the case $\gamma \geq 0$ and leave a brief analysis of the case $\gamma < 0$ for the Discussion.

Distinguished limits are obtained by selecting α and β to balance as many of the four terms in (3.9) as possible. It is easy to see that three terms at most can be involved in any dominant balance. This yields four possibilities:

1. The particle's inertia is negligible, leading to the condition $2\alpha + \beta = 2\alpha + 2 = 2$, that is $\alpha = 0$ and $\beta = 2$, for the balance of the remaining terms. We refer to the corresponding regime as Regime I.

2. The streaming velocity $\tilde{\boldsymbol{v}}$ is negligible, leading to $2\beta = 2\alpha + \beta = 2$, that is, $\alpha = 1/2$ and $\beta = 1$. We refer to this as Regime II.

3. The particle's viscous drag is negligible. Balancing the remaining terms leads to $\alpha = 0$ and $\beta = 1$ but also to an $O(\epsilon)$ viscous drag, thus much larger than the other terms, inconsistent with our assumption. There is, therefore, no distinguished limit in which the viscous drag is negligible.

4. Acoustic pressure is negligible. This leads to $\alpha = 1$ and $\beta = 2$ and again to an inconsistency: there is no distinguished limit with negligible acoustic pressure.

We derive the average equations holding in Regimes I and II in sections 3.3 and 3.4. Intermediate regimes, in which only two of the terms in (3.9) enter the dominant balance,

are examined in section 3.5. We emphasise that these intermediate regimes, though they may formally correspond to values of α and β different from those in Regimes I and II, can be deduced as limiting cases. For instance, a balance between the particle's inertia and the acoustic pressure, obtained for $\beta = 1$ and any value $\alpha > 1/2$, is deduced from Regime II by neglecting viscous drag.

3.3 Regime I

We first consider the distinguished limit in which the particle's inertia is negligible, corresponding to $\alpha = 0$ and $\beta = 2$. Because viscosity is an $O(1)$ effect in this case, the averaged force (3.8) is given by the complete expression computed by Doinikov [39]. Although he assumed that the particle does not have a slow motion, including this motion requires only a straightforward modification of his calculation because of the large time-scale separation implied by $\beta = 2$; the present section is therefore largely a brief review of Ref. 39 to which the reader is referred for details.

3.3.1 Wave dynamics

All dynamical variables are expanded in powers of ϵ according to (3.7) and regarded as functions of both times t and T, except for the constant $\rho^{(0)}$ and the t-independent $\boldsymbol{X}^{(0)}$. We assume that $\boldsymbol{X}^{(0)}$ captures the entirety of the slow motion so that $\langle \boldsymbol{X}^{(j)} \rangle = 0$ for $j \geq 1$. Introducing the expansion into the governing equations (3.3)–(3.6) yields linear viscous wave equations for $\boldsymbol{v}^{(1)}$, $p^{(1)}$ and $\rho^{(1)}$ coupled with the equations

$$\boldsymbol{v}^{(1)} = \partial_t \boldsymbol{X}^{(1)} \quad \text{for} \quad \boldsymbol{x} \in S_{\boldsymbol{X}^{(0)}} \quad \text{and} \quad M \partial_{tt} \boldsymbol{X}^{(1)} = \int_{S_{\boldsymbol{X}^{(0)}}} \sigma^{(1)} \cdot \boldsymbol{n} \, \mathrm{d}s \tag{3.10}$$

governing the particle motion and its interaction with the fluid. The solution for an axisymmetric flow is best written using spherical polar coordinates centred at $\boldsymbol{X}^{(0)}$. With θ denoting the angle about the axis $\boldsymbol{e}_x$, the potential of the incident part of the wave field can be written as

$$\phi_{\mathrm{i}} = \mathrm{e}^{-\mathrm{i}\omega t} \sum_{n=0}^{\infty} A_n(\boldsymbol{X}^{(0)}) j_n(kr) P_n(\cos\theta), \tag{3.11}$$

where $r = |\boldsymbol{x} - \boldsymbol{X}^{(0)}|$, j_n denotes the spherical Bessel function of order n, P_n the Legendre polynomial of degree n,

$$k = \omega/(c^2 - \mathrm{i}\omega(\xi + 4\eta/3)/\rho^{(0)})^{1/2} \tag{3.12}$$

is the wavenumber, and the real part is implied. The amplitudes A_n are determined by the prescription of the incident wave as $r \to \infty$. The scattered part of the wave field is determined by a potential ϕ_s and streamfunction ψ_s such that $\boldsymbol{v}_\mathrm{s}^{(1)} = \nabla\phi_\mathrm{s} + \nabla\times(\boldsymbol{e}_\varphi\psi_\mathrm{s})$, with $\boldsymbol{e}_\varphi$ the azimuthal unit vector of the spherical coordinate system; these are given by

$$\phi_\mathrm{s} = \mathrm{e}^{-\mathrm{i}\omega t}\sum_{n=0}^{\infty}\alpha_n A_n(\boldsymbol{X}^{(0)})h_n(kr)P_n(\cos\theta) \tag{3.13}$$

$$\text{and}\quad \psi_\mathrm{s} = \mathrm{e}^{-\mathrm{i}\omega t}\sum_{n=0}^{\infty}\beta_n A_n(\boldsymbol{X}^{(0)})h_n((1+\mathrm{i})r/\delta)P_n^1(\cos\theta), \tag{3.14}$$

where h_n is the spherical Hankel function and P_n^1 the associated Legendre polynomial. Doinikov [39] gives explicit expressions for the constants α_n and β_n:

$$\alpha_0 = -j_1(kr)/h_1(kr), \quad \beta_0 = 0, \tag{3.15a}$$

$$\alpha_1 = -\left[\mu_1\mu_2 + 2(1-\lambda)^2 j_1(kr)h_1((1+\mathrm{i})r/\delta)\right]/\mu_4, \tag{3.15b}$$

$$\beta_1 = (1-\lambda)\left[\mu_1 h_1(kr) - \mu_2 j_1(kr)\right]/\mu_4 \tag{3.15c}$$

where

$$\mu_1 = \lambda j_1(kr) - kr j_1'(kr), \tag{3.16a}$$

$$\mu_2 = \lambda h_1(kr) - kr h_1'(kr), \tag{3.16b}$$

$$\mu_3 = (1-2\lambda)h_1((1+\mathrm{i})r/\delta) - (1+\mathrm{i})r h_1'((1+\mathrm{i})r/\delta)/\delta, \tag{3.16c}$$

$$\mu_4 = \mu_2\mu_3 + 2(1-\lambda)^2 h_1(kr)h_1((1+\mathrm{i})r/\delta), \tag{3.16d}$$

with the prime denotes differentiation and for $n > 1$

$$\alpha_n = \left[n(n+1)j_n(kr)h_n((1+\mathrm{i})r/\delta) - kr\gamma_n j_n'(kr)\right]/\xi_n, \tag{3.17a}$$

$$\beta_n = \left[kr j_n'(kr)h_n(kr) - kr j_n(kr)h_n'(kr)\right]/\xi_n, \tag{3.17b}$$

$$\gamma_n = h_n((1+\mathrm{i})r/\delta) + (1+\mathrm{i})r/\delta h_n'((1+\mathrm{i})r/\delta), \tag{3.17c}$$

$$\xi_n = kr h_n'(kr)\gamma_n - n(n+1)h_n(kr)h_n((1+\mathrm{i})r/\delta). \tag{3.17d}$$

3.3.2 Mean dynamics

Continuing the expansion of (3.3) to $O(\epsilon^2)$ leads to the equations

$$\rho^{(0)}\partial_t \boldsymbol{v}^{(2)} + \partial_t\left(\rho^{(1)}\boldsymbol{v}^{(1)}\right) = \nabla\cdot\left(\sigma^{(2)} - \rho^{(0)}\boldsymbol{v}^{(1)}\otimes\boldsymbol{v}^{(1)}\right), \tag{3.18a}$$

$$\partial_t\rho^{(2)} = -\nabla\cdot\left(\rho^{(0)}\boldsymbol{v}^{(2)} + \rho^{(1)}\boldsymbol{v}^{(1)}\right), \tag{3.18b}$$

which become

$$\nabla\cdot\left\langle\sigma^{(2)}\right\rangle = \rho^{(0)}\nabla\cdot\left\langle\boldsymbol{v}^{(1)}\otimes\boldsymbol{v}^{(1)}\right\rangle, \tag{3.19a}$$

$$\rho^{(0)}\nabla\cdot\left\langle\boldsymbol{v}^{(2)}\right\rangle = -\nabla\cdot\left\langle\rho^{(1)}\boldsymbol{v}^{(1)}\right\rangle, \tag{3.19b}$$

upon averaging. Averaging the boundary condition (3.4) gives

$$\left\langle\boldsymbol{v}^{(2)}\right\rangle + \left\langle\boldsymbol{X}^{(1)}\cdot\nabla\boldsymbol{v}^{(1)}\right\rangle = \dot{\boldsymbol{X}}^{(0)} \quad \text{for} \quad \boldsymbol{x}\in S_{\boldsymbol{X}^{(0)}}. \tag{3.20}$$

The left-hand side of (3.20) can be recognised as a Lagrangian mean velocity summing Eulerian mean velocity and Stokes drift [e.g. 22]: indeed, in view of (3.10), $\boldsymbol{X}^{(1)}$ is both the particle and fluid displacement. The final equation for the mean flow is provided by the average of (3.6) to order $O(\epsilon^2)$ i. With $\beta = 2$, the slow acceleration of the particle is $\epsilon^4\ddot{\boldsymbol{X}}^{(0)}$ and does not appear at this order, leaving the dominant balance

$$\int_{S_{\boldsymbol{X}^{(0)}}}\left\langle\sigma^{(2)}\right\rangle\cdot\boldsymbol{n}\,\mathrm{d}s - \int_{S_{\boldsymbol{X}^{(0)}}}\rho^{(0)}\left\langle\boldsymbol{v}^{(1)}\otimes\boldsymbol{v}^{(1)}\right\rangle\cdot\boldsymbol{n}\,\mathrm{d}s = 0. \tag{3.21}$$

The linear problem (3.19)–(3.20) for $\langle\boldsymbol{v}^{(2)}\rangle$ and $\langle p^{(2)}\rangle$ was solved explicitly by Doinikov [39] with a vanishing right-hand side for (3.20); the difference is minor and the effect of the extra term is easy to track down. Introducing the result into (3.21) leads to the final equation for the particle motion

$$6\pi\eta a\left(\dot{\boldsymbol{X}}^{(0)} - \tilde{\boldsymbol{v}}\right) = \boldsymbol{F}_{\mathrm{ap}}, \tag{3.22}$$

which has the form expected in our discussion of distinguished regimes in section 3.2 (cf. (3.9)). The velocity $\tilde{\boldsymbol{v}}$ in (3.22) is given by

$$\tilde{\boldsymbol{v}} = \frac{1}{4\pi a^2}\int_{S_{\boldsymbol{X}^{(0)}}}\left(\left\langle\boldsymbol{v}_{\mathrm{i}}^{(2)}\right\rangle + \left\langle X_r^{(1)}\frac{\partial\boldsymbol{v}^{(1)}}{\partial r}\right\rangle\right)\mathrm{d}s, \tag{3.23}$$

and can be interpreted as a form of Lagrangian velocity averaged over the surface of the particle. Here, we have used axisymmetry to express the Stokes drift in terms of the r-component of the particle displacement $X_r^{(1)} = X^{(1)}\cos\theta$. Note that while the second term in (3.23) is the Stokes drift of fluid particles lying on the sphere, the first only includes the Eulerian-mean velocity associated with the incident part of the wave; as a result, $\tilde{\boldsymbol{v}}$ differs from the full Lagrangian velocity of these fluid particles.

The acoustic pressure in (3.22) is given by

$$\boldsymbol{F}_{\mathrm{ap}} = -\frac{3\pi\rho^{(0)}}{2}\sum_{n=0}^{\infty}\frac{n+1}{(2n+1)(2n+3)}\left(E_nA_nA_{n+1}^{*}+E_n^{*}A_n^{*}A_{n+1}\right)\boldsymbol{e}_x. \tag{3.24}$$

It depends on the wave amplitudes A_n and on the coefficients E_n, which are slight modifications of the D_n computed by Doinikov [39] (his Eq. (5.6)). Specifically, our E_n are deduced from the D_n by setting the coefficients S_{9n} to zero and omitting the terms proportional to the functions $G_n^{(l)}$, $L_n^{(l)}$, $K_n^{(l)}$ from the coefficients S_{1n} to S_{8n}. This modification is made to include the Stokes-drift term in the velocity $\tilde{\boldsymbol{v}}$ whereas Doinikov [39] includes it in his acoustic force (see also Ref. 30). We find our choice convenient for two reasons: (i) all the terms in $\boldsymbol{F}_{\mathrm{ap}}$ depend on the scattered wave in the sense that $\boldsymbol{F}_{\mathrm{ap}} \to 0$ as α_n, $\beta_n \to 0$; and (ii) $\eta\tilde{\boldsymbol{v}}$ and $\boldsymbol{F}_{\mathrm{ap}}$ have different behaviours in the limits of large and small viscosity. We discuss (ii) further in section 3.5.1.

To summarise, the dynamics of the sphere in Regime I is controlled by a balance between a Stokes drag towards the streaming velocity $\tilde{\boldsymbol{v}}$ and the acoustic pressure. We next illustrate the transient dynamics with the familiar example of a plane standing wave.

3.3.3 Standing wave

For a plane standing wave, the potential of the incident wave can be expressed as

$$\phi_{\mathrm{i}} = A\cos(kr\cos\theta + kX^{(0)})\mathrm{e}^{-\mathrm{i}\omega t} = \mathrm{e}^{-\mathrm{i}\omega t}\sum_{n=0}^{\infty}A_nj_n(kr)P_n(\cos(\theta)), \tag{3.25}$$

where $A_n = \frac{1}{2}A(2n+1)i^n[\mathrm{e}^{\mathrm{i}kX^{(0)}} + (-1)^n\mathrm{e}^{-\mathrm{i}kX^{(0)}}]$. Note that the dependence of the A_n on $X^{(0)}$ couples the wave field on the particle to the mean position $X^{(0)}$ of the particle. For simplicity, we consider the particle motion in the particular case $\lambda = 1$ and in the long wavelength limit $|ka| \ll 1$, $|k\delta| \ll 1$. In this limit, it can be shown using the asymptotics of Bessel functions [1] that the coefficients E_n in (3.24) satisfy

$E_0 = 2(ka)^3/9 \gg E_n$, $n \geq 1$. As a result, the acoustic pressure reduces to

$$\boldsymbol{F}_{\mathrm{ap}} = -\frac{\pi\rho^{(0)}|A|^2(ka)^3}{3}\sin(2kX^{(0)})\,\boldsymbol{e}_x. \tag{3.26}$$

Similarly, $\tilde{\boldsymbol{v}}$ reduces to the Lagrangian-mean velocity of the incident wave (see section 3.5.4), which vanishes for standing waves. The position of the sphere therefore obeys the equation

$$\dot{X}^{(0)} = -\frac{\rho^{(0)}|A|^2\sin(2kX^{(0)})(ka)^3}{18\eta a}, \tag{3.27}$$

with solution

$$X^{(0)} = k^{-1}\tan^{-1}\left(C\mathrm{e}^{-t/\tau}\right), \quad \text{where} \quad \tau = \frac{9\eta}{\rho^{(0)}|A|^2k^4a^2} \tag{3.28}$$

and C is determined by the initial condition. This shows that the sphere converges exponentially towards the nodes of the standing waves over a time scale τ.

3.4 Regime II

Regime II is characterised by $\alpha = 1/2$, corresponding to a weaker dissipation than in Regime I, with $\delta/a = O(\epsilon^{1/2})$ rather than $O(1)$. As a result, the acoustic pressure on the particle is balanced by a combination of viscous drag and inertia, while the streaming velocity $\tilde{\boldsymbol{v}}$ is negligible. The mean time scale is short compared to that in Regime I, $O(\epsilon^{-1})$ rather $O(\epsilon^{-2})$; crucially, this leads to mean velocities, both of the particle and of the surrounding fluid, that are comparable to the wave velocities.

These large mean velocities, and hence mean displacements necessitate to introduce coordinates that follow the motion of the particle. Defining $\boldsymbol{r} = \boldsymbol{x} - \boldsymbol{X}$, we rewrite the Navier–Stokes equations (3.3b)–(3.3c) in these coordinates, noting that $\nabla \mapsto \nabla_{\boldsymbol{r}}$ and $\partial_t \mapsto \partial_t - \dot{\boldsymbol{X}}\cdot\nabla_{\boldsymbol{r}}$ to obtain

$$\frac{\partial}{\partial t}(\rho\boldsymbol{v}) - \dot{\boldsymbol{X}}\cdot\nabla(\rho\boldsymbol{v}) + \nabla\cdot(\rho\boldsymbol{v}\otimes\boldsymbol{v}) = -\nabla p + \eta(\nabla^2\boldsymbol{v} + \frac{1}{3}\nabla\nabla\cdot\boldsymbol{v}) + \xi\nabla\nabla\cdot\boldsymbol{v}, \tag{3.29a}$$

$$\frac{\partial\rho}{\partial t} - \dot{\boldsymbol{X}}\cdot\nabla\rho + \nabla\cdot(\rho\boldsymbol{v}) = 0, \tag{3.29b}$$

where we have omitted the subscripts $\boldsymbol{r}$ from $\nabla_{\boldsymbol{r}}$ for convenience.

The weak viscosity of Regime II makes it possible to use a boundary-layer approach for both the wave and mean part of the dynamics. The boundary-layer thickness is

$\delta = O(\epsilon^{1/2}a)$ so that all fields need to be expanded in powers of $\epsilon^{1/2}$ according to

$$\boldsymbol{v} = \epsilon\boldsymbol{v}^{(1)} + \epsilon^{3/2}\boldsymbol{v}^{(3/2)} + \epsilon^2\boldsymbol{v}^{(2)} + \cdots, \tag{3.30a}$$

$$\rho = \rho^{(0)} + \epsilon\rho^{(1)} + \epsilon^{3/2}\rho^{(3/2)} + \epsilon^2\rho^{(2)} + \cdots, \tag{3.30b}$$

$$p = p^{(0)} + \epsilon p^{(1)} + \epsilon^{3/2}p^{(3/2)} + \epsilon^2 p^{(2)} + \cdots, \tag{3.30c}$$

$$\boldsymbol{X} = \boldsymbol{X}^{(0)} + \epsilon\boldsymbol{X}^{(1)} + \epsilon^{3/2}\boldsymbol{X}^{(3/2)} + \epsilon^2\boldsymbol{X}^{(2)} + \cdots, \tag{3.30d}$$

where $\rho^{(0)}$ and $p^{(0)}$ are constants. We anticipate that $\boldsymbol{X}^{(0)}$ depends on the slow time $T = \epsilon t$ only, but all the other variables depend on both t and T. We emphasise that $\boldsymbol{v}^{(1)}$, $\rho^{(1)}$ and $p^{(1)}$ have both oscillatory and mean contributions: we separate these two contributions using the notation

$$\boldsymbol{v}^{(1)} = \bar{\boldsymbol{v}}^{(1)} + \boldsymbol{v}'^{(1)}, \quad \text{with} \quad \left\langle \boldsymbol{v}'^{(1)} \right\rangle = 0.$$

3.4.1 Wave dynamics

We now obtain the form of the leading-order wave fields. Substituting (3.30) into (3.29) and the equation of state, and subtracting the mean contribution, we find the leading-order wave equations

$$\rho^{(0)}\frac{\partial \boldsymbol{v}'^{(1)}}{\partial t} = -\nabla p'^{(1)}, \tag{3.31a}$$

$$\frac{\partial \rho'^{(1)}}{\partial t} = -\rho^{(0)}\nabla\cdot\boldsymbol{v}'^{(1)}, \tag{3.31b}$$

$$p'^{(1)} = c^2\rho'^{(1)}, \tag{3.31c}$$

with boundary conditions

$$\boldsymbol{v}'^{(1)} = \partial_t \boldsymbol{X}'^{(1)} \quad \text{for} \quad \boldsymbol{r} \in S_0, \tag{3.32a}$$

$$\boldsymbol{v}'^{(1)} \sim \boldsymbol{v}_{\text{incident}} \quad \text{as} \quad \boldsymbol{r} \to \infty, \tag{3.32b}$$

where S_0 denotes the sphere centred at origin. The equation for the sphere becomes

$$M\partial_{tt}\boldsymbol{X}'^{(1)} = -\int_{S_0} p'^{(1)}\boldsymbol{n}\,\mathrm{d}s. \tag{3.33}$$

Eqs. (3.31) are the familiar equations for inviscid acoustic waves which can be solved in terms of a potential. As is standard, these equations are solved by imposing only

the normal component of the boundary condition (3.32a). The potential solution so obtained is valid to leading order for $|r-a| \gg \delta$ only. Viscous effects are important in a boundary layer of thickness δ in which the velocity has a rotational contribution. The resulting velocity tangential to the sphere varies rapidly so as to both match the potential solution and satisfy the no-slip condition. It turns out that the details of the solution in the boundary layer are unimportant for the leading-order dynamics of the sphere in Regime II; in particular, the effect of boundary streaming is $O(\epsilon^2)$ like that of interior streaming [97] and both contribute to the streaming velocity $\tilde{\boldsymbol{v}}$ whose drag is $O(\epsilon^{5/2})$ hence negligible.

The solution for $|r-a| \gg \delta$ is given, as in Regime I, by the sum $\phi_\mathrm{i}+\phi_\mathrm{s}$ of the incident and scattered wave, with

$$\phi_\mathrm{i} = \mathrm{e}^{-\mathrm{i}\omega t} \sum_{n=0}^{\infty} A_n j_n(k_0 r) P_n(\cos\theta). \tag{3.34}$$

In this expression, the functions $A_n(\boldsymbol{X})$ which appear in the far-field condition (3.32b) when this is written in terms of $\boldsymbol{r}$ are approximated as $A_n(\boldsymbol{X}^{(0)})$. The correction involving $\boldsymbol{X}^{(1)} \cdot \nabla A(\boldsymbol{X}^{(0)})$ is $O(\epsilon^2)$ and negligible. Note that the wavenumber can be taken as the inviscid approximation $k_0 = \omega/c$, assuming implicitly that the far-field condition is imposed for some $\boldsymbol{r}$ not so large that the viscous decay (on scales given by $(\operatorname{Im} k)^{-1} \sim k_0^{-1}(k_0\delta)^2 = O(k_0^{-1}\epsilon^{-1})$ for $k_0\delta \ll 1$, see (3.12)) matter. This damping introduces an outer scale that can modify the streaming, which is further discussed in §3.6. The potential of the scattered wave is given by

$$\phi_\mathrm{s} = \mathrm{e}^{-\mathrm{i}\omega t} \sum_{n=0}^{\infty} \alpha_n A_n h_n(kr) P_n(\cos\theta), \tag{3.35}$$

where the coefficients are obtained from (3.31)–(3.33) as

$$\alpha_0 = -\frac{j_1(\kappa)}{h_1(\kappa)}, \quad \alpha_1 = \frac{\lambda j_1(\kappa) - \kappa j_1'(\kappa)}{\kappa h_1'(\kappa) - \lambda h_1(\kappa)}, \quad \alpha_n = -\frac{j_n'(\kappa)}{h_n'(\kappa)} \quad \text{for} \quad n > 1, \tag{3.36}$$

with $\kappa = k_0 a$. This result was first obtained by King [68].

3.4.2 Mean dynamics

We now turn to the mean dynamics. Time averaging the transformed Navier–Stokes equations (3.29), we obtain

$$\epsilon\left\langle\frac{\partial\rho\boldsymbol{v}}{\partial T}\right\rangle-\left\langle\frac{d\boldsymbol{X}}{dt}\cdot\nabla(\rho\boldsymbol{v})\right\rangle+\nabla\cdot\langle\rho\boldsymbol{v}\otimes\boldsymbol{v}\rangle$$
$$=-\nabla\bar{p}+\eta\left(\nabla^2\bar{\boldsymbol{v}}+\frac{1}{3}\nabla(\nabla\cdot\bar{\boldsymbol{v}})\right)+\xi\nabla(\nabla\cdot\bar{\boldsymbol{v}}),\tag{3.37a}$$
$$\epsilon\frac{\partial\bar{\rho}}{\partial T}-\left\langle\frac{d\boldsymbol{X}}{dt}\cdot\nabla\rho\right\rangle+\nabla\cdot\langle\rho\boldsymbol{v}\rangle=0,\tag{3.37b}$$

where $d/dt=\partial_t+\epsilon\partial_T$. The boundary condition is given by

$$\bar{\boldsymbol{v}}=\dot{\boldsymbol{X}}^{(0)}\text{ for }\boldsymbol{r}\in S_0,\tag{3.38}$$

and an prescribed outer boundary condition depending on the specific application.

Corresponding to the wave solution, the mean flow has a boundary layer of thickness δ around the particle. We therefore analyse the mean equations (3.37) separately in an outer region with $r-a\gg\delta$ and in a boundary layer with $r-a=O(\delta)$.

Outer region

Substituting (3.30) into the mean mass-conservation equation (3.37b) gives

$$O(\epsilon):\qquad\nabla\cdot\bar{\boldsymbol{v}}^{(1)}=0,\tag{3.39a}$$
$$O(\epsilon^{3/2}):\quad\nabla\cdot\bar{\boldsymbol{v}}^{(3/2)}=0,\tag{3.39b}$$

which imply that both $\bar{\boldsymbol{v}}^{(1)}$ and $\bar{\boldsymbol{v}}^{(3/2)}$ are incompressible.

Similarly, the mean momentum equation (3.37a) gives

$$O(\epsilon):\quad 0=-\nabla\bar{p}^{(1)},\tag{3.40a}$$
$$O(\epsilon^{3/2}):\quad 0=-\nabla\bar{p}^{(3/2)},\tag{3.40b}$$
$$O(\epsilon^2):\quad\rho^{(0)}\frac{\partial\bar{\boldsymbol{v}}^{(1)}}{\partial T}-\rho^{(0)}\dot{\boldsymbol{X}}^{(0)}\cdot\nabla\bar{\boldsymbol{v}}^{(1)}-\rho^{(0)}\left\langle\frac{\partial\boldsymbol{X}'^{(1)}}{\partial t}\cdot\nabla\boldsymbol{v}'^{(1)}\right\rangle$$
$$+\nabla\cdot\left\langle\rho^{(0)}\boldsymbol{v}'^{(1)}\otimes\boldsymbol{v}'^{(1)}\right\rangle+\nabla\cdot\left(\rho^{(0)}\bar{\boldsymbol{v}}^{(1)}\otimes\bar{\boldsymbol{v}}^{(1)}\right)=-\nabla\bar{p}^{(2)}+\hat{\eta}\nabla^2\bar{\boldsymbol{v}}^{(1)},\tag{3.40c}$$

where (3.39a) is used and we have defined $\hat{\eta}=\eta/\epsilon=O(1)$ consistent with the assumption that $\delta=O(\epsilon^{1/2})$. Assuming that $\bar{p}^{(1)}$ and $\bar{p}^{(3/2)}$ tend to constants as $|\boldsymbol{r}|\to\infty$, we

conclude that $\bar{p}^{(1)}$ and $\bar{p}^{(3/2)}$ are constant in the outer region. The key equation is (3.40c) which describes the mean dynamics in the outer region; its boundary conditions are obtained by considering the boundary layer.

Boundary layer

This region is defined by $R = (r-a)/\delta = O(1)$. Denoting the dependent variables regarded as functions of R and θ by capital letters, we obtain from the mass conservation (3.37b) that

$$O(\epsilon^{1/2}): \quad \rho^{(0)} \frac{\partial \bar{V}_r^{(1)}}{\partial R} = 0, \tag{3.41a}$$

$$O(\epsilon): \quad 2\bar{V}_r^{(1)} + \frac{1}{\sin\theta}\frac{\partial}{\partial\theta}(\sin\theta\, \bar{V}_\theta^{(1)}) + \frac{\partial \bar{V}_r^{(3/2)}}{\partial R} = 0. \tag{3.41b}$$

Eq. (3.41a) indicates that $\bar{V}_r^{(1)}$ is independent of R across the boundary layer: $\bar{V}_r^{(1)}(R,\theta) = \bar{v_r}^{(1)}(r=a,\theta)$. The mean momentum conservation (3.37a) gives

$$O(\epsilon^{1/2}): \quad 0 = -\frac{\partial \bar{P}^{(1)}}{\partial R}, \tag{3.42a}$$

$$O(\epsilon): \quad 0 = -\frac{\partial \bar{P}^{(3/2)}}{\partial R}, \tag{3.42b}$$

$$0 = -\frac{1}{a}\frac{\partial \bar{P}^{(1)}}{\partial \theta} + \frac{\hat{\eta}}{a^2}\frac{\partial^2 \bar{V}_\theta^{(1)}}{\partial R^2}, \tag{3.42c}$$

when (3.41a) is used. We conclude from (3.42a) and (3.42b) that $\bar{P}^{(1)}$ and $\bar{P}^{(3/2)}$ are constant across the boundary layer, so that $\bar{p}^{(1)}$ and $\bar{p}^{(3/2)}$ are constant throughout the fluid. It then follows from (3.42c) that $\partial^2 \bar{V}_\theta^{(1)}/\partial R^2 = 0$, hence

$$\bar{V}_\theta^{(1)} = f_1(\theta) R + f_2(\theta), \tag{3.43}$$

where the functions f_1 and f_2 remain to be determined. Matching with the outer solution gives that $f_1 = a\partial_r \bar{\boldsymbol{v}}^{(1/2)}(r=a,\theta) = 0$ (since $\bar{\boldsymbol{v}} = O(\epsilon)$), and $f_2 = \bar{v}_\theta^{(1)}(r=a,\theta)$. This implies that $\bar{\boldsymbol{V}}^{(1)}$ is independent of R across the boundary layer. As a result, the outer velocity satisfies the simple boundary condition

$$\bar{\boldsymbol{v}}^{(1)}(r=a,\theta) = \bar{\boldsymbol{V}}^{(1)}(r=a,\theta) = \dot{\boldsymbol{X}}^{(0)}. \tag{3.44}$$

The momentum equation obtained at the next order, $O(\epsilon^{3/2})$, can be reduced using

(3.41a) and (3.41b) to

$$\frac{\rho^{(0)}}{a}\left\langle (V_r'^{(1)\phi} - \frac{\partial X'^{(1)}}{\partial t}\cos\theta)\frac{\partial V_\theta'^{(1)\psi}}{\partial R}\right\rangle + \frac{\rho^{(0)}}{a}\left(\bar{V}_r^{(1)} - \dot{X}^{(0)}\cos\theta\right)\frac{\partial \bar{V}_\theta^{(1)}}{\partial R}$$
$$= -\frac{1}{a}\frac{\partial \bar{P}^{(3/2)}}{\partial\theta} + \frac{\hat{\eta}}{a^2}\frac{\partial^2 \bar{V}_\theta^{(3/2)}}{\partial R^2} + \frac{2\hat{\eta}}{a^2}\frac{\partial \bar{V}_\theta^{(1)}}{\partial R}, \tag{3.45a}$$
$$0 = -\frac{1}{a}\frac{\partial \bar{P}^{(2)}}{\partial R} + \frac{\hat{\eta}}{a^2}\frac{\partial^2 \bar{V}_r^{(3/2)}}{\partial R^2} + \frac{2\hat{\eta}}{a^2}\frac{\partial \bar{V}_r^{(1)}}{\partial R}, \tag{3.45b}$$

where the mass conservation (3.41) and wave solutions have been used. Here $V_r'^{(1)\phi}$ and $V_\theta'^{(1)\psi}$ denote potential and rotational contributions to the wave velocity $\boldsymbol{V}'^{(1)}$. Since, as discussed above, the potential part satisfies the no-normal flow condition, the term involving these contributions vanishes. Using the constancy of $P^{(3/2)}$ and (3.44) reduces (3.45) to

$$0 = \hat{\eta}\frac{\partial^2 \bar{V}_\theta^{(3/2)}}{\partial R^2}, \tag{3.46a}$$
$$0 = -\frac{1}{a}\frac{\partial \bar{P}^{(2)}}{\partial R} + \frac{\hat{\eta}}{a^2}\frac{\partial^2 \bar{V}_r^{(3/2)}}{\partial R^2}. \tag{3.46b}$$

Therefore, $\bar{V}_\theta^{(3/2)} = f_3(\theta)R + f_4(\theta)$, where f_3 and f_4 are obtained by matching as $f_3 = a\partial_r \bar{v}_\theta^{(1)}(r=a,\theta)$ and $f_4 = \bar{v}_\theta^{(3/2)}(r=a,\theta)$. Taking the R derivative of (3.41b) yields $\partial^2 \bar{V}_r^{(3/2)}/\partial R^2 = 0$, which implies $\bar{V}_r^{(3/2)} = a\partial_r \bar{v}_r^{(1)}(r=a,\theta)R + \bar{v}_r^{(3/2)}(r=a,\theta)$ after matching. Therefore, (3.46b) reduces to $\partial \bar{P}^{(2)}/\partial R = 0$ so that $\bar{p}^{(2)}$ is R-independent in the boundary layer.

The above calculation provides us with two important pieces of information: (i) the $O(\epsilon)$ velocity and $O(\epsilon^2)$ pressure are R-independent; and (ii) the $O(\epsilon^{3/2})$ velocity depends linearly on R. From this, we conclude that the stress is constant across the boundary layer up to $o(\epsilon^2)$ corrections. As a result, the leading-order particle motion, which depends only on the $O(\epsilon^2)$ stress, can be computed from the outer solution alone.

Governing equations

From previous two sections it can be concluded that the mean dynamics is controlled by the incompressible-fluid momentum equation (3.40c) and the mean particle equation

$$M\ddot{\boldsymbol{X}}^{(0)} = -\int_{S_0} \bar{p}^{(2)}\boldsymbol{n}\,\mathrm{d}s + \int_{S_0} \bar{\tau}^{(2)}\cdot\boldsymbol{n}\,\mathrm{d}s, \tag{3.47}$$

that arises when (3.30) is introduced into (3.6). These two equations are coupled through the mean stress tensor $\bar{\tau}$, defined by

$$\begin{aligned}
\bar{\tau}^{(2)}_{rr} &= -2\hat{\eta}\frac{\partial \bar{v}^{(1)}_r}{\partial r}, \\
\bar{\tau}^{(2)}_{\theta\theta} &= -2\hat{\eta}\left(\frac{1}{r}\frac{\partial \bar{v}^{(1)}_\theta}{\partial \theta} + \frac{\bar{v}^{(1)}_r}{r}\right), \\
\bar{\tau}^{(2)}_{r\theta} = \bar{\tau}^{(2)}_{\theta r} &= -\hat{\eta}\left(r\frac{\partial}{\partial r}\left(\frac{\bar{v}^{(1)}_\theta}{r}\right) + \frac{1}{r}\frac{\partial \bar{v}^{(1)}_r}{\partial \theta}\right),
\end{aligned} \tag{3.48}$$

and through the no-slip condition (3.44) satisfied by $\bar{\boldsymbol{v}}^{(1)}$. We now recast these equations in a simpler form and discuss the physical mechanism they describe.

The effect of the waves on the particle is implicit in (3.47): it arises through changes in $\bar{p}^{(2)}$ and $\bar{\boldsymbol{v}}^{(1)}$ that are induced by the presence of wave terms in the momentum equation (3.40c). We can make the effect of the waves explicit in (3.47) by writing these terms using the wave potential in the outer region [57] to obtain

$$\nabla \cdot \left\langle \boldsymbol{v}'^{(1)} \otimes \boldsymbol{v}'^{(1)} \right\rangle = \nabla \left\langle \frac{1}{2}\left(\nabla \phi'^{(1)}\right)^2 - \frac{1}{2c^2}\left(\frac{\partial \phi'^{(1)}}{\partial t}\right)^2 \right\rangle, \tag{3.49a}$$

$$\left\langle \frac{\partial \boldsymbol{X}'^{(1)}}{\partial t} \cdot \nabla \mathbf{v}'^{(1)} \right\rangle = \nabla \left\langle \frac{\partial \boldsymbol{X}'^{(1)}}{\partial t} \cdot \nabla \phi'^{(1)} \right\rangle. \tag{3.49b}$$

It is therefore natural to redefine pressure as

$$\tilde{p}^{(2)} = \bar{p}^{(2)} + \rho^{(0)}\left\langle \frac{1}{2}\left(\nabla \phi'^{(1)}\right)^2 - \frac{1}{2c^2}\left(\frac{\partial \phi'^{(1)}}{\partial t}\right)^2 \right\rangle - \rho^{(0)}\left\langle \frac{\partial \boldsymbol{X}'^{(1)}}{\partial t} \cdot \nabla \phi'^{(1)} \right\rangle, \tag{3.50}$$

leading to the simpler momentum equation

$$\rho^{(0)}\frac{\partial \bar{\boldsymbol{v}}^{(1)}}{\partial T} - \rho^{(0)}\dot{\boldsymbol{X}}^{(0)} \cdot \nabla \bar{\boldsymbol{v}}^{(1)} + \rho^{(0)}\nabla \cdot \left(\bar{\boldsymbol{v}}^{(1)} \otimes \bar{\boldsymbol{v}}^{(1)}\right) = -\nabla \tilde{p}^{(2)} + \hat{\eta}\nabla^2 \bar{\boldsymbol{v}}^{(1)}. \tag{3.51}$$

The advection term $\rho^{(0)}\dot{\boldsymbol{X}}^{(0)} \cdot \nabla \bar{\boldsymbol{v}}^{(1)}$ in the above equation can be eliminated by using the spatial coordinates

$$\tilde{\boldsymbol{x}} = \boldsymbol{r} + \boldsymbol{X}^{(0)} = \boldsymbol{x} + O(\epsilon), \tag{3.52}$$

which can be identified with the original, fixed-frame coordinates $\boldsymbol{x}$, as the second equal-

ity indicates. This reduces (3.51) to

$$\rho^{(0)}\frac{\partial\bar{\boldsymbol{v}}^{(1)}}{\partial T}+\rho^{(0)}\nabla\cdot\left(\bar{\boldsymbol{v}}^{(1)}\otimes\bar{\boldsymbol{v}}^{(1)}\right)=-\nabla\tilde{p}^{(2)}+\hat{\eta}\nabla^2\bar{\boldsymbol{v}}^{(1)}, \tag{3.53}$$

where the spatial derivatives are with respect to $\tilde{\boldsymbol{x}}$. Eq. (3.53), together with the incompressibility condition

$$\nabla\cdot\bar{\boldsymbol{v}}^{(1)}=0, \tag{3.54}$$

are the usual incompressible Navier–Stokes equations. At the same time, equation (3.47) for the sphere becomes

$$M\ddot{\boldsymbol{X}}^{(0)}=-\int\limits_{S_{\boldsymbol{X}^{(0)}}}\tilde{p}^{(2)}\boldsymbol{n}\,\mathrm{d}s+\int\limits_{S_{\boldsymbol{X}^{(0)}}}\bar{\tau}\cdot\boldsymbol{n}\,\mathrm{d}s+\boldsymbol{F}_{\mathrm{inv}}, \tag{3.55}$$

where

$$\boldsymbol{F}_{\mathrm{inv}}=\rho^{(0)}\int\limits_{S_{\boldsymbol{X}^{(0)}}}\left\{\left\langle\frac{1}{2}\left|\nabla\phi'^{(1)}\right|^2-\frac{1}{2c^2}\left(\frac{\partial\phi'^{(1)}}{\partial t}\right)^2\right\rangle-\left\langle\frac{\partial\boldsymbol{X}'^{(1)}}{\partial t}\cdot\nabla\phi'^{(1)}\right\rangle\right\}\boldsymbol{n}\,\mathrm{d}s \tag{3.56}$$

is the inviscid acoustic pressure. The boundary conditions for (3.53) become

$$\bar{\boldsymbol{v}}^{(1)}=\dot{\boldsymbol{X}}^{(0)}\quad\text{for}\quad\tilde{\boldsymbol{x}}\in S_{\boldsymbol{X}^{(0)}}, \tag{3.57}$$

together with a condition on the outer of the fluid region, at infinity for instance. The latter boundary condition is naturally expressed in terms of the Lagrangian-mean velocity which, in particular, vanishes on the surface of oscillating wavemakers [18]. This velocity can be identified with $\bar{\boldsymbol{v}}^{(1)}$, however, since the Stokes drift is $O(\epsilon^2)$ hence negligible.

The force in (3.68) is that obtained for a purely inviscid fluid and used, e.g., by Gor'kov [57]. Explicit expressions for this force in terms of the coefficients A_n in the expansion (3.34) of the incident wave are given in Refs. 68, 39 and, in the long-wave limit $ka\ll 1$, in Ref. 57. Note that Gor'kov uses an integration over a large sphere rather than over the particle itself, replacing $\partial_t\boldsymbol{X}'^{(1)}$ by $\nabla\phi'^{(1)}$ for inviscid waves and taking advantage of the divergence-free property of the mean inviscid stress tensor (the integrand). In our case, because the mean flow is affected by viscosity and acts on the particle through the first two terms on the right-hand side of (3.55), this technique is not as useful.

To summarise, in Regime II, the slow, averaged dynamics is controlled by the coupled system (3.53)–(3.57), where the unknown pressure is solved by a Possion equation with the help of incompressibility. In this system, viscosity enters only in the Navier–Stokes equation governing the fluid motion and not in the acoustic pressure. This is a complex, nonlinear system involving a moving boundary, but a classical one, describing the motion of an externally forced spherical particle in incompressible viscous fluid. It has been studied extensively, both theoretically (e.g., to find approximate solutions [11, 84]) and numerically [66, 105, 35]. The specificity of our problem is the form of the external force, namely the inviscid acoustic pressure which can be obtained solely from the potential wave solution.

3.4.3 Example: plane standing wave

To illustrate the difference between Regimes I and II, we consider again a standing wave in the limit $|ka| \ll 1$, $|k\delta| \ll 1$ for $\lambda = 1$. The acoustic pressure is then

$$\boldsymbol{F}_{\text{inv}} = -\frac{\pi\rho^{(0)}|A|^2(ka)^3}{3}\sin(2kX^{(0)})\,\boldsymbol{e}_x \tag{3.58}$$

and identical to that of Regime I [e.g. 68, 39]. To obtain a simple closed-form solution, we restrict our attention to the Basset limit [11] where $\dot{\boldsymbol{X}}^{(0)}$ is small enough that the advection terms can be treated perturbatively. This reduces (3.53)–(3.57) to the single equation

$$(M+M')\ddot{X}^{(0)} = -DX^{(0)} - K\dot{X}^{(0)} - B\int_0^T \ddot{X}^{(0)}(T-\tau)\,\tau^{-1/2}d\tau, \tag{3.59}$$

where we have linearised the acoustic pressure (3.58) using that $X^{(0)} \ll 1$. The coefficients

$$M' = \frac{2\pi}{3}a^3\rho^{(0)},\ D = \frac{2}{3}\pi\rho^{(0)}|A|^2k_0^4a^3,\ K = 6\pi\hat{\eta}a,\ B = 6a^2(\pi\rho^{(0)}\hat{\eta})^{1/2} \tag{3.60}$$

can be associated with distinct physical effects: added mass, acoustic pressure, Stokes drag, and the (history-dependent) Basset force.

We solve (3.59) with $X^{(0)}(0) = X$ and $\dot{X}^{(0)} = 0$ using Laplace transform (see Appendix A for details). The solution is the sum of exponentially damped oscillations and

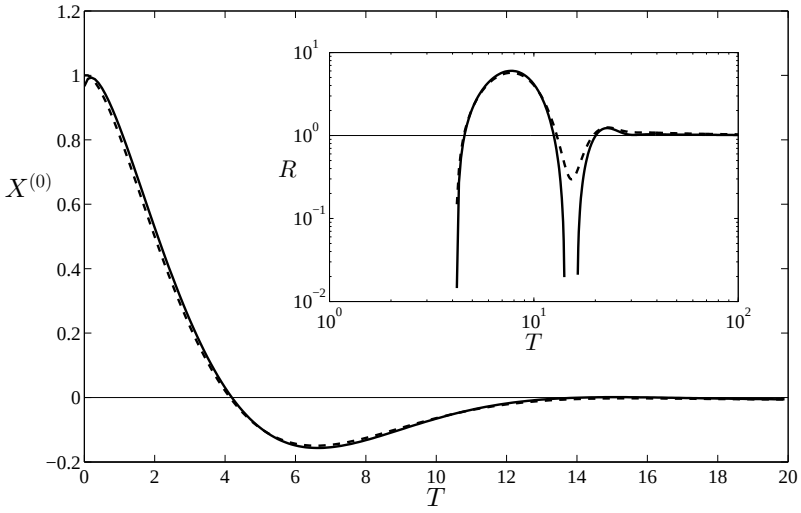

Figure 3.3: Particle position $X^{(0)}$ as a function of T for a standing wave in the Basset limit of Regime II obtained by solving (3.59) analytically (solid line, see Appendix A) and numerically (dashed line). The long-time asymptotics is confirmed in the log-log coordinate inset which displays R, the ratio of the exact solution to (3.61). The parameters are chosen as $M = 1$, $B = 1$, $K = 1$ and $D = 1$.

a continuous-spectrum contribution. This controls the $T \gg 1$ asymptotics, given by

$$X^{(0)} \sim -\frac{BX}{2D} T^{-3/2}. \tag{3.61}$$

As in Regime I, the particle tends to its equilibrium position at the node $X^{(0)}(0) = 0$ of the standing wave. The differences are that the process is not monotonic, with the particle oscillating around the node, and is much slower than in Regime I, with a $T^{-3/2}$ decay of the distance to the node rather than the exponential decay of Regime I. This is illustrated in Figure 3.3.

3.5 Intermediate regimes

Regimes I and II are distinguished regimes characterised by specific scaling relations between the parameters δ/a and ϵ. We now briefly consider intermediate regimes which can be regarded as sublimits of Regimes I and II; these apply over broad regions of the $(\delta/a, \epsilon)$–space and yield much simplified governing equations. These intermediate

Regime	Parameter range	α
Large-viscosity regime	$\delta/a \gg 1$	$\alpha < 0$
Regime I	$\delta/a = O(1)$	$\alpha = 0$
Transition regime	$\epsilon^{1/2} \ll \delta/a \ll 1$	$0 < \alpha < 1/2$
Regime II	$\delta/a = O(\epsilon^{1/2})$	$\alpha = 1/2$
Inviscid regime	$\delta/a \ll \epsilon^{1/2}$	$\alpha > 1/2$

Table 3.1: The asymptotic regimes considered in this chapter are characterised by relations between δ/a and $\epsilon \ll 1$ or, equivalently, by α such that $\delta/a = \epsilon^{\alpha}$.

regimes are listed in Table 3.1 together with the asymptotic inequalities that define them. A particularly important regime from the theoretical viewpoint is defined by $\epsilon^{1/2} \ll \delta/a \ll 1$ and marks the transition between Regimes I and II. By showing that the mean equation in this transition regime is the limit of those in both Regime I and Regime II, we confirm that our heuristic arguments in section 2 identify all possible distinguished regimes.

3.5.1 Large-viscosity regime

This regime corresponds to a large viscosity and is deduced from Regime I by letting $\eta \to \infty$. It can be shown that the coefficients E_n in the acoustic pressure (3.24) remain bounded in this limit so $\boldsymbol{F}_{\text{ap}}$ is negligible. This motivated our separation between $6\pi\eta\tilde{\boldsymbol{v}}$ and $\boldsymbol{F}_{\text{ap}}$ in (3.24). Physically, these terms describe two very different effects. The first is a linear (Stokes) drag controlled by the moving boundary; the second is controlled by the average wave momentum flux and pressure which are bounded as $\eta \to \infty$. As a result, (3.22) reduces to

$$\dot{\boldsymbol{X}}^{(0)} = \tilde{\boldsymbol{v}}. \tag{3.62}$$

This simple balance is important for practical purpose since it allows for the possibility of particles following fluid elements as is required when using tracer particles; we this discuss this point further in section 3.5.4.

3.5.2 Transition regime

We now show that the Regimes I and II overlap: specifically, the small-viscosity limit of Regime I matches the large-viscosity limit of Regime II in a transition regime where both streaming velocity and particle acceleration are negligible.

Starting from Regime I, we let $\eta \to 0$ in (3.22): the acoustic pressure then reduces to its inviscid form, while the viscous drag term $\eta\tilde{\boldsymbol{v}}$ becomes negligible, leading to the balance

$$6\pi\eta a\dot{\boldsymbol{X}}^{(0)} = \boldsymbol{F}_{\mathrm{inv}}. \tag{3.63}$$

Conversely, letting $\hat{\eta} \to \infty$ in the mean momentum equation of Regime II, (3.53), reduces this to the Stokes equation

$$0 = -\nabla\tilde{p}^{(2)} + \hat{\eta}\nabla^2\bar{\boldsymbol{v}}^{(1)}. \tag{3.64}$$

Since $\nabla\cdot\bar{\boldsymbol{v}}^{(1)} = 0$, $\bar{\boldsymbol{v}}^{(1)}$ is a Stokes flow around the spherical particle and the associated stress (first two terms on the right-hand side of (3.55)) is the familiar linear Stokes drag. Since, furthermore, the particle's acceleration is negligible, (3.63) is recovered.

3.5.3 Inviscid regime

We now consider the limit where viscosity is so small as to be negligible in both the acoustic pressure and flow equation. Letting $\hat{\eta} \to 0$ in (3.53) yields the Euler equation

$$\rho^{(0)}\frac{\partial\bar{\boldsymbol{v}}^{(1)}}{\partial T} + \rho^{(0)}\bar{\boldsymbol{v}}^{(1)}\cdot\nabla\bar{\boldsymbol{v}}^{(1)} = -\nabla\tilde{p}^{(2)}. \tag{3.65}$$

Assuming a potential mean flow $\bar{\boldsymbol{v}}^{(1)} = \nabla\bar{\phi}^{(1)}$, the pressure is expressed as

$$\tilde{p}^{(2)} = \rho^{(0)}\frac{\partial\bar{\phi}^{(1)}}{\partial T} + \rho^{(0)}\frac{|\nabla\bar{\phi}^{(1)}|^2}{2}. \tag{3.66}$$

The force on the particle associated with this pressure (first term on the right-hand side of (3.55)) is the well-known added-mass effect (e.g. Ref. 12). This reduces (3.55) to

$$(M + M')\ddot{\boldsymbol{X}}^{(0)} = \boldsymbol{F}_{\mathrm{inv}}, \tag{3.67}$$

where the added mass $M' = 2\pi a^3 \rho^{(0)}/3$ and $\boldsymbol{F}_{\text{inv}}$ is the inviscid acoustic pressure:

$$\boldsymbol{F}_{\text{inv}} = \rho^{(0)} \int_{S_{\boldsymbol{X}^{(0)}}} \left\{ \left\langle \frac{1}{2} \left| \nabla \phi'^{(1)} \right|^2 - \frac{1}{2c^2} \left(\frac{\partial \phi'^{(1)}}{\partial t} \right)^2 \right\rangle - \left\langle \frac{\partial \boldsymbol{X}'^{(1)}}{\partial t} \cdot \nabla \phi'^{(1)} \right\rangle \right\} \boldsymbol{n} \, \mathrm{d}s \quad (3.68)$$

This provides a consistent derivation of the added-mass effect incorporated by King [68] in an ad hoc manner.

3.5.4 When do spherical particles follow fluid elements?

Rigid spherical particles are often used in experiments as passive tracers to visualise and quantify fluid motion. It is therefore important to find conditions that ensure the spherical particles follow closely the motion of the fluid elements they are meant to trace, without being disturbed by the scattering induced by the rigid particle itself. In the presence of acoustic waves, fluid elements move (on average) with the Lagrangian mean velocity, so the conditions should ensure that $\dot{\boldsymbol{X}}^{(0)} = \left\langle \boldsymbol{v}_{\text{i}}^{(2)} + \boldsymbol{\xi}_{\text{i}}^{(1)} \cdot \nabla \boldsymbol{v}_{\text{i}}^{(1)} \right\rangle$ up to negligible errors. Here $\boldsymbol{\xi}_{\text{i}}^{(1)}$ is the displacement of fluid elements associated with the incident wave only. We now show that sufficient conditions for this are that

$$\delta/a \gg 1, \ |ka| \ll 1 \quad \text{and} \quad \lambda = 1. \quad (3.69)$$

The first condition places the dynamics in the large-viscosity regime discussed in section 3.5.1 in which the acoustic pressure is negligible so that $\dot{\boldsymbol{X}}^{(\mathbf{0})} = \tilde{\boldsymbol{v}}$. The second condition ensures that the average over the sphere in (3.23) is a good approximation to the value of the integrand at the centre of the sphere. It remains to show that $X_r^{(1)} \partial_r \boldsymbol{v}^{(1)} \approx \xi_{\text{i}r}^{(1)} \partial_r \boldsymbol{v}_{\text{i}}^{(1)}$ to ensure that the second term in (3.23) approximates the Stokes drift associated with the incident wave.

To show this, we consider the leading-order particle velocity

$$u = \frac{\lambda A_1 \boldsymbol{e}_x}{ka} \left[j_1(ka) + \alpha_1 h_1(ka) + 2\beta_1 h_1((1+\mathrm{i})\delta/a) \right] \mathrm{e}^{-i\omega t}, \quad (3.70)$$

with coefficients α_1 and β_1 given explicitly by Doinikov [38]. It can be checked that $\lambda = 1$ leads to $\beta_1 = 0$ and, using the asymptotics of spherical Bessel functions [e.g., 1], that $|ka| \ll 1$ leads to $\alpha_1 = o(|ka|)$. Therefore the velocity of the sphere reduces to $u = A_1 \boldsymbol{e}_x \mathrm{e}^{-\mathrm{i}\omega t} + o(|ka| A_1)$. To leading order, this coincides with the radial velocity of the incident wave: indeed, for $|ka| \ll 1$ this velocity is dominated by the mode $n = 1$ in the expansion (3.11) while the scattered wave is negligible, again because $\alpha_1 = o(|ka|)$

and $\beta_1 = 0$. It follows that $X_r^{(1)} = \xi_{\mathrm{i}r}$. Similarly, the wave velocity around the sphere is dominated by the incident component, hence $\partial_r \boldsymbol{v}^{(1)} = \partial_r \boldsymbol{v}_{\mathrm{i}}^{(1)}$.

3.6 Discussion

In this chapter, we examine the dynamics of a spherical particle in an axisymmetric acoustic field and derive simplified models governing the mean motion of the particle. This is controlled by the complex interaction of the particle with both the wave and the surrounding fluid. Specifically, four physical effects come into play: inertia (of the particle and of the fluid it entrains), viscous drag, acoustic streaming, and acoustic pressure. Under the assumption $ka = O(1)$, or more accurately $ka = O(\epsilon^\gamma)$ for $\gamma \geq 0$, of a particle that is of the same order as or smaller than the acoustic wavelength, our analysis shows that these four effects are never concurrent. Depending on the strength of viscosity (measured by the parameter δ/a) relative to the wave amplitude, several regimes, characterised by the balance between two or three of these effects, are possible. These are listed in Table 3.1 and we briefly summarise their main features below.

Fixing the radius of the particle, the relevant regime is determined by the value of viscosity. For large viscosity, the particle is driven by a viscous response to the streaming velocity, with negligible acoustic pressure and inertia, leading to (3.62). As viscosity decreases, the drag effect decreases and acoustic pressure becomes significant, leading to the three-term balance between drag, streaming and acoustic pressure of Regime I and the more complex model (3.22) for $\delta/a = O(1)$. For smaller viscosity still, the streaming effect becomes negligible so that viscous drag balances acoustic pressure, yielding Eq. (3.63). Importantly, in this 'transition regime' viscosity is weak enough for the acoustic pressure to be well approximated by its inviscid form. When viscosity is such that $\delta/a = O(\epsilon^{1/2})$, particle inertia comes into play. This is Regime II, where inertia, fluid stress (associated with both pressure and viscosity) and (inviscid) acoustic pressure balance. This is a rather complex regime in which the mean dynamics of the particle and of the fluid are fully coupled and the Navier–Stokes equations need to be solved to determine the fluid stress acting on the particle. The mean equations of motion are then (3.53)–(3.57). Finally, for very weak viscosity, the fluid motion is governed by the Euler equation and, under the assumption of a potential flow, its impact reduces to the familiar added-mass effect, leading to (3.67). Regimes I and II are of particular importance because they correspond to distinguished, three-term balances, and encompass the other regimes as specific sublimits.

It is interesting to note that various acoustic microfluidic experiments span a range

of parameters and hence a range of regimes. We have estimated the parameters used in several experiments that employ particles for a variety of purposes in order to assess which dynamical regime is relevant to each. The experiments of Frommelt et al. [51] use spherical particles to trace the mixing flow generated by time-dependent acoustic streaming. The key non-dimensional parameters are approximately $\delta/a \approx 0.13$ and $\epsilon^{1/2} \approx 0.03$. This places these experiments in the transition regime and indicates that acoustic pressure could affect the particle and cause their trajectories to depart from those of fluid elements. However, for these experiments, the streaming velocity is substantially larger than our estimate, $O(\epsilon^2)$ non-dimensionally or v'^2/c dimensionally: as discussed in Ref. 125 (for $k\delta \ll 1$) in problems where the wave amplitudes vary over an outer scale ℓ that differs from k (e.g., for weakly damped travelling wave), the streaming velocity is $O((k\ell)^2\epsilon^2)$. In such cases, the viscous drag can dominate the acoustic pressure even though δ/a is not large. In the particle collection experiments of Li et al. [73], Oberti et al. [98] and Tan et al. [119], the values of δ/a are $O(1)$ (1.28, 0.19–0.33 and 0.52–0.64, respectively), placing the experiments in Regime I. Interestingly, Li et al. [73] observe concentration times proportional to a^{-2}, consistent with (3.28). In another set of particle collection experiments, Rogers et al. [106] use a broader range of particle diameter, such that $\delta/a \in [0.017, 0.9]$. Estimating their wave amplitudes be in the range $\epsilon \in [9.5\times10^{-5}, 2.9\times10^{-4}]$, we conclude that the experiments span both Regimes I and II.

While this chapter concentrates on spherical particles that are of the same order as or smaller than the wavelength, we can sketch how the analysis could be extended to larger particles, with $ka = O(\epsilon^\gamma)$ for $\gamma < 0$. The main difference for the balance of terms in the equation governing the particle motion is the order of magnitude of the acoustic pressure. Recall that in the heuristic model (3.9), this was taken to be $O(\epsilon^2)$, corresponding to the dimensional estimate $ka^3v'^2$ and to the assumption that the length scale for the change of momentum flux over the sphere is proportional to k^{-1}. For $\gamma < 0$, this scale is instead controlled by the size of the particle itself, leading to the estimates $a^2v'^2$ and $\epsilon^{2-\gamma}$ for the dimensional and non-dimensional acoustic pressure. Revisiting the arguments of section 3.2.3 about the balance of terms in (3.9) with this new estimate for the acoustic pressure gives the following. A distinguished regime involving all the four terms in (3.9) is possible and corresponds to $\alpha = 1$, $\beta = 2$ and $\gamma = -2$. This is the most general regime from which sublimits can be deduced. In particular, for $\gamma = -2\alpha$ and $\beta = 2$, the dominant balance is between viscous drag, streaming and acoustic pressure, and our Regime I is recovered. Similarly, for $\gamma = -2\alpha$, the balance is between the particle inertia, viscous drag and radiation pressure, analogous to our

Regime II. Detailed calculations would however be necessary to evaluate the acoustic pressure and assess whether the models we derive for $\gamma \geq 0$ remain unchanged for $\gamma < 0$.

Other extensions of the present work could include the effects of particle compressibility, heat conduction (both of which have already been accounted for in calculations of acoustic pressure [29, 40, 41, 42, 30, 110]) and slip boundary conditions [132]. The impact of an outer scale ℓ of variation of the wave amplitude that differs substantially from the wavelength is relevant to many applications and also deserves consideration. The parameter $k\ell$ measuring this scale discrepancy would need to be included in an extension of the heuristic model (3.9) used to assess possible distinguished regimes. Depending on its size relative to ϵ, new regimes, including a regime involving a four-term balance, will appear. We leave the analysis of these regimes for future work.

Chapter 4

Near-inertial wave–mean flow interaction

In the last two chapters 2 and 3, we studied dissipative wave-mean flow interactions with two microfluidics examples. In this chapter, our attention moves to geophysical fluid problems. Because of the large scales involved, dissipation mechanisms are irrelevant and the mechanisms of wave-mean flow interaction take a very different form from those encountered in the previous chapters. In this section we study the interaction between near-inertial waves (NIWs) and a mesoscale mean flow.

To illustrate the effect of NIWs, we show in Figure 4.1 the trajectories of drifters in the mixed layer in the North Pacific as measured by D'Asaro et al. [33]. Here the mixed layer is the top layer of the ocean, extending about 50 m down from the sea surface where winds play an important role and the density stratification is very weak. In the figure we can observe that the drifters have an oscillatory motion and a drift caused by the large-scale flow. The oscillatory motion results from the NIWs so named because they are controlled by a balance between inertia and Coriolis force. The large-scale flow is in fact a mesoscale flow as usually modelled by quasi-geostrophic approximation.

On the f-plane and in the hydrostatic-Boussinesq approximation fluid, with no background flow, the dispersion relation of inertia-gravity waves (IGWs) reads

$$\omega = \pm\sqrt{f_0^2 + \frac{N^2|\boldsymbol{k}|^2}{m^2}}, \tag{4.1}$$

where f_0 is the Coriolis frequency, N is the Brunt–Väisälä frequency, and $\boldsymbol{k}$ and m are horizontal and vertical wavenumbers, respectively. When the second term on the r.h.s of (4.1) is small compared to f_0^2, i.e. the aspect ratio $|\boldsymbol{k}|/m \ll f_0/N$, we obtain

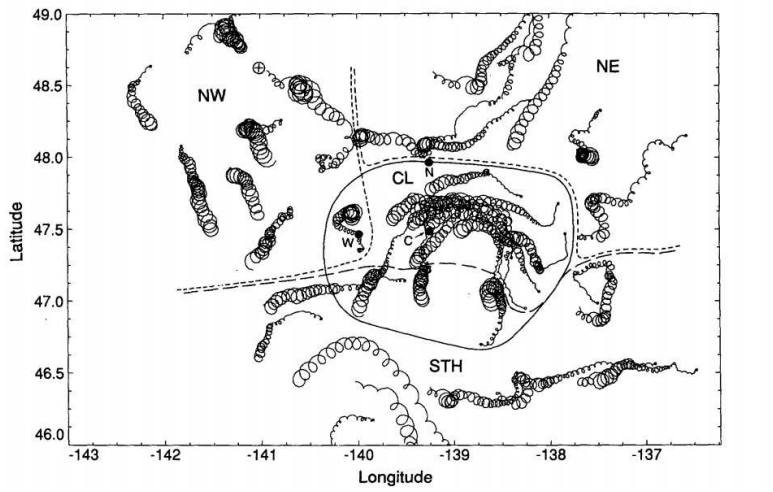

Figure 4.1: Tracks of drifters in the observations by D'Asaro et al. [33]. Different curves show the paths of different drifters, whose motion contains both an oscillatory part and a drift part.

NIWs whose leading order frequency equals the Coriolis frequency (inertial frequency). One specificity of NIWs is their large energy in the ocean: the frequency spectrum of oceanic inertia-gravity wave is sharply peaked near the local Coriolis frequency (see figure 4.2), and the corresponding NIWs contain around 50% of the total oceanic wave energy [33]. The reasons for this large energy are as follows: the NIWs are generated by the low frequency winds in the mixed layer, the inertial frequency is the lowest frequency in the inertia-gravity wave spectrum hence they are easily excited by the winds; and through parametric subharmonic instability mechanism the M_2 tides can force NIWs [138]. Further discussion on the properties of the NIW band can be found in [54]. Because

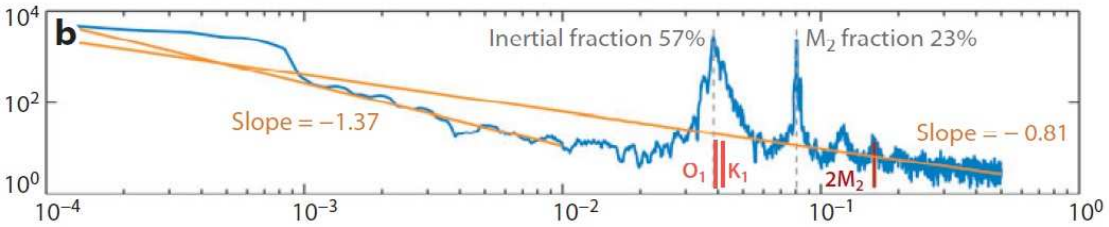

Figure 4.2: Kinetic energy spectrum (cm^2m^{-2}/cycles per hour) vs. frequency (cycles per hour) at 27° with depth 1500 m in the ocean [53]. The dashed line (close to the O_1 and K_1 bars) corresponds to the Coriolis frequency $\omega = f_0$, where a large proposition of wave energy concentrates. The bulk on the left (frequency less than 0.001) corresponds to the mesoscale flow which dominates the energy spectrum.

of their large energy NIWs have a strong impact on the ocean dynamics. The downward propagation of wind-generated NIWs is the main process of transporting kinetic energy into the deep ocean [2]. The dominant contribution to vertical shear makes NIW to be one of the main sources of turbulent mixing. Interestingly, recent numerical studies [55, Straub and Tayler personal communication] suggests that NIWs could provide an answer to one of the main open question in ocean climate – the closure of the oceanic energy budget [48] – by acting as an energy sink for the measoscale oceanic flow. This is the possibility that the present chapter explains, and we have an estimation of this new effect to be of the same order as well-studied mean-flow dissipation mechanisms, such as bottom drag (for details of the oceanic energy budget, see [131]).

Linear wave theories have been applied to understand the dynamics of NIWs under the influence of a mean flow. Under the assumption that the spatial scales of NIWs are much smaller than mean-flow scales, a WKB approach can be applied [91, 92]; it shows in particular that the vorticity of the balanced flow shifts the frequency of NIWs away from f_0 [69]. However, in the mixed layer of the ocean, where they are generated by large-scale winds, NIWs usually have horizontal scales larger than or comparable to these of the mean flow. Motivated by this, Young and Ben Jelloul [137] (referred to as YBJ hereafter) relaxed the assumption of spatial scale separation to derive a model of the NIW modulation by a mean flow. This model captures various mechanisms: advection, dispersion and refraction. In a simple situation of a barotropic mean flow, the YBJ equation reads

$$\partial_t M_{zz} + \underbrace{\boldsymbol{U}\cdot\nabla M_{zz}}_{\text{advection}} + \underbrace{\mathrm{i}\frac{N^2}{2f_0}\nabla^2 M}_{\text{dispersion}} + \underbrace{\mathrm{i}\frac{\nabla^\perp\cdot\boldsymbol{U}}{2}M_{zz}}_{\text{refraction}} = 0,$$

where $\boldsymbol{U}$ is a horizontal mean flow, $\nabla = (\partial_x, \partial_y)$, and $\nabla^\perp = (-\partial_y, \partial_x)$. Here M_z is the NIW amplitude defined from the wave velocity by

$$u + \mathrm{i}v = M_z(\boldsymbol{x}, t)\mathrm{e}^{-\mathrm{i}f_0 t} \quad \text{and} \quad w = \frac{1}{2}(M_x - \mathrm{i}M_y)\mathrm{e}^{-\mathrm{i}f_0 t} + \text{c.c.}.$$

Note that the dispersion term leads to a dispersion relation $\omega = f_0 + N^2|\boldsymbol{k}|^2/(2f_0 m^2)$ for plane wave. This can be recognized as a two term Taylor expansion of the dispersion relation (4.1). Here the NIW frequency shift associated with the mean vorticity is straightforwardly captured by the refraction term.

The YBJ equation describes the impact of mean flow on NIWs. The counterpart of this, namely, the feedback of the NIWs on the mean flow, is what we study in this

chapter, since it is the key to the role of NIWs on the ocean energy budget. Specifically, we study the interaction between NIWs and a mesoscale mean flow and develop a simple coupled model – a combination of the YBJ equation and a modified quasi-geostrophic potential vorticity equation – to describe this interaction. A important feature of this model is its conservation structure, which proves highly illuminating. This chapter is largely based on the paper [134].

4.1 Introduction

NIWs, that is, inertia-gravity waves with frequencies close to the local Coriolis frequency f_0, play an important role in the dynamics of the ocean [e.g. 52]. They account for almost 50% of the wave energy [e.g. 48] and thus make a strong contribution to processes associated with inertia-gravity waves such as diapycnal mixing, vertical motion and primary production. Several features explain their dominance [54]: their minimum frequency in the inertia-gravity-wave spectrum, the low frequency of the atmospheric winds that generate them, the presence of turning latitudes, nonlinear interactions [87], and the transfer of tidal energy through parametric subharmonic instability [138].

In view of their large energy, it is natural to expect that NIWs affect the large-scale circulation of the ocean. One possibility is that they do so through enhanced diapycnal mixing in the regions of the ocean where they dissipate [e.g. 131]. Another, more remarkable perhaps, is that they alter the slow, balanced oceanic circulation directly through wave–mean-flow interaction processes. Gertz and Straub [55] put forward the idea that NIWs provide an energy sink for this circulation. Their numerical simulations suggest that this process may be significant and, along with other mechanisms including bottom and surface friction [e.g. 95, 43] and loss of balance [e.g. 123, 31], help resolve the long-standing puzzle posed by the dissipation of the (inverse energy-cascading) balanced oceanic flow.

The aim of the present chapter is to develop a theoretical tool that enables a detailed analysis of the interactions between NIWs and balanced flow. Because the YBJ model makes no assumption on spatial scales, it is well suited to examine the realistic scenario of NIWs forced by atmospheric winds at horizontal scales larger than those of the ocean flow, therefore we extend the YBJ model to account for the feedback of the NIWs on the balanced flow. Specifically, we derive a new model that couples the YBJ model with a modified quasi-geostrophic (QG) model. The modification – a change in the relation between the advected potential vorticity (PV) and advecting velocity – captures this feedback. As detailed below, we work in the framework of non-dissipative generalised

Lagrangian-mean theory [GLM, see, e.g., 22] and pay close attention to the conservation laws satisfied by the coupled model. These turn out to be particularly important: based on the conservation of NIW action (in fact, the NIW kinetic energy divided by f_0) and total energy alone, we identify a novel mechanism providing a sink of energy for the balanced flow. In this mechanism, the reduction in the horizontal scale of NIWs that results from advection and refraction is accompanied by an increase in the NIW potential energy and, consequently, a decrease in the energy of the balanced flow.

A key to the derivation of wave–mean-flow models of the kind we develop is to separate the motion between mean and wave contributions, relying on the time-scale separation to define the mean as an average over the inertial period $2\pi/f_0$. The GLM theory of Andrews and McIntyre [5] offers a general framework for this separation and for the systematic derivation of equations governing the coupled wave–mean dynamics (see Bühler 22 for an account). The theory has achieved notable successes but suffers from a deficiency in that the (Lagrangian) mean velocity it defines is divergent even for an incompressible fluid. Soward and Roberts [115] proposed a variant of GLM, termed 'glm', which yields a divergence-free mean velocity. Because it is convenient, we adopt this approach in the main body of the chapter but show in an Appendix that the same leading-order model can also be obtained from standard GLM. We also adopt a variational approach that ensures that conservation laws and their link to symmetries are preserved when the primitive equations are reduced asymptotically (see, e.g., Salmon [107], Grimshaw [58], Holm et al. [63]). Specifically, we derive the Lagrangian-mean and perturbation equations by introducing a wave–mean decomposition of the flow map into the primitive-equation Lagrangian, following closely the method proposed by Salmon [108] (see Gjaja and Holm 56 for a related approach). Because the wave component consists of rapidly oscillating NIWs, the resulting Lagrangian can be averaged in time in the manner of Whitham [128]. Variations with respect to the mean flow map (or rather its inverse) and to the NIW amplitude then lead to a coupled primitive-equation–YBJ system; applying a QG approximation reduces this system to a simple, energy conserving YBJ-QG coupled model. (See Vanneste [124] for a related variational derivation of the original YBJ equation.)

The chapter is organised as follows. The coupled YBJ-QG model is introduced without a derivation in § 4.2. Some key properties of the model and the key scaling assumptions underlying its derivation are also discussed there. The derivation itself is carried out in § 4.3 which also records the complete primitive-equation–YBJ model. The Hamiltonian structure of the YBJ-QG model and associated conservation laws are presented in § 4.4. Sections 4.3 and 4.4 are technical; the reader mainly interested in applications

can skip them and move directly to § 4.5 which considers the possible implications of the wave–mean-flow interactions represented in the model for ocean energetics. Section 4.6 examines two simplified models deduced from the full YBJ-QG model assuming certain symmetries. These models are two-dimensional and hence easily amenable to numerical simulations. We take advantage of this and present the results of two sets of simulations demonstrating (i) the slow down of a one-dimensional barotropic jet by NIWS, and (ii) the deflection of a vortex dipole under the influence of vertically travelling NIWs. The chapter concludes with a brief Discussion in § 4.7. Three Appendices provide details of some of the computations and alternative derivations.

4.2 Coupled model

4.2.1 Model

We start with the hydrostatic–Boussinesq equations written in the form

$$\partial_t u + \boldsymbol{u}\cdot\nabla u + w\partial_z u - (f_0 + \beta y)v = -\partial_x p, \tag{4.2a}$$

$$\partial_t v + \boldsymbol{u}\cdot\nabla v + w\partial_z v + (f_0 + \beta y)u = -\partial_y p, \tag{4.2b}$$

$$\theta = \partial_z p, \tag{4.2c}$$

$$\nabla\cdot\boldsymbol{u} + \partial_z w = 0, \tag{4.2d}$$

$$\partial_t\theta + \boldsymbol{u}\cdot\nabla\theta + w\partial_z\theta = 0, \tag{4.2e}$$

where $\boldsymbol{u} = (u, v)$ is the horizontal velocity, w is the vertical velocity, p is the pressure, and θ is the buoyancy, defined as $-g$ times the density variations relative to a constant density ρ_0 [e.g. 121]. We have used the β-plane approximation to write the Coriolis parameter as $f_0 + \beta y$, with constant f_0 and β. Throughout the chapter, $\nabla = (\partial_x, \partial_y)$ denotes the horizontal gradient.

Inertial oscillations are characterised by a linear balance between inertia and the Coriolis force in (4.2a)–(4.2b) and thus satisfy

$$\partial_t u - f_0 v = 0 \quad \text{and} \quad \partial_t v + f_0 u = 0. \tag{4.3}$$

The solution can written in complex form as

$$u + \mathrm{i}v = M_z\, \mathrm{e}^{-\mathrm{i}f_0 t} \tag{4.4}$$

for some complex amplitude $M(x, y, z)$. Here we follow YBJ in writing this amplitude as

a z-derivative so that the vertical velocity, deduced from the incompressibility condition (4.2d), takes the simple form

$$w = -M_s \mathrm{e}^{-\mathrm{i}f_0 t} + \text{c.c.}, \tag{4.5}$$

where $s = x + \mathrm{i}y$, $\partial_s = (\partial_x - \mathrm{i}\partial_y)/2$, and c.c. denotes the complex conjugate of the preceding term. The position $\boldsymbol{x} = (x, y, z)$ of fluid particles in the inertial field (4.4)–(5.24) can be obtained by integration. If this position is written as

$$\boldsymbol{x} = \boldsymbol{X} + \boldsymbol{\xi}, \tag{4.6}$$

the displacement $\boldsymbol{\xi} = (\xi, \eta, \zeta)$ satisfies

$$\xi + \mathrm{i}\eta = \chi_z \, \mathrm{e}^{-\mathrm{i}f_0 t} \quad \text{and} \quad \zeta = -\chi_s \mathrm{e}^{-\mathrm{i}f_0 t} + \text{c.c.}, \tag{4.7}$$

where $\chi = \mathrm{i}M/f_0$ in the linear approximation. The mean position $\boldsymbol{X}$ can be regarded as an integration constant identifying the fluid particle, and the displacement $\boldsymbol{\xi}$ and amplitude χ can be thought of as functions of $\boldsymbol{X}$.

For NIWs propagating in a flow, the description leading to (4.7) is overly simplified. However, it can be extended to capture the two-way interactions between the NIWs and the flow: this is achieved by regarding $\boldsymbol{X}$ as a suitably defined, time-dependent Lagrangian-mean position (in fact, a mean map $\boldsymbol{X}(\boldsymbol{a}, t)$ mapping the particle labelled by $\boldsymbol{a}$ to its mean position at time t), and by taking the amplitude $\chi(\boldsymbol{X}, t)$ to be a function of both time and mean position in typical GLM fashion [e.g. 22]. The main achievement of this chapter is the derivation of equations governing the joint evolution of the NIW amplitude χ and of the mean map $\boldsymbol{X}(\boldsymbol{a}, t)$ or, rather, of the corresponding Lagrangian-mean velocity.

We leave the details of this derivation for the next section and present here the final equations. These are particularly simple when the Lagrangian-mean flow is assumed to be quasi-geostrophic and hence derived from a streamfunction ψ according to $(\bar{\boldsymbol{u}}^{\mathrm{L}}, \bar{w}^{\mathrm{L}}) = (\nabla^{\perp}\psi, 0)$, with $\nabla^{\perp} = (-\partial_y, \partial_x)$. In this approximation, and using $\boldsymbol{x}$ rather than $\boldsymbol{X}$ to denote the independent spatial variables (the mean positions), the coupled model takes

the form

$$\chi_{zzt} + (\partial(\psi, \chi_z))_z + \mathrm{i}\beta y \chi_{zz} + \frac{\mathrm{i}}{2}\left(\left(\frac{N^2}{f_0} + \psi_{zz}\right)\nabla^2\chi + \nabla^2\psi\,\chi_{zz} - 2\nabla\psi_z\cdot\nabla\chi_z\right) = 0, \tag{4.8a}$$

$$q_t + \partial(\psi, q) = 0, \tag{4.8b}$$

where $\partial(\cdot,\cdot)$ denotes the two-dimensional Jacobian (with $\partial(f,g) = f_x g_y - g_x f_y$), and N is the Brunt–Väisälä frequency which generally depends on z. The first equation can be recognised as a version of the YBJ model, specifically their complete Eq. (3.2) rather than the simplified model given by their Eq. (1.2). It is supplemented by the boundary conditions at the top and bottom boundaries $z = z^{\pm}$,

$$\chi = \text{const}^{\pm} \quad \text{at} \quad z = z^{\pm}, \tag{4.9}$$

ensuring a vanishing NIW vertical velocity there. The second equation is the material conservation of the quasi-geostrophic potential vorticity (QGPV) q. This is related to the streamfunction ψ and to χ through

$$q = \beta y + \Delta\psi + \frac{\mathrm{i}f_0}{2}\partial(\chi_z^*, \chi_z) + f_0 G(\chi^*, \chi), \tag{4.10}$$

where

$$\Delta = \nabla^2 + \partial_z\left(f_0^2/N^2\partial_z\right), \tag{4.11}$$

is the familiar quasi-geostrophic potential vorticity operator,

$$G(\chi^*, \chi) = \frac{1}{4}\left(2|\nabla\chi_z|^2 - \chi_{zz}\nabla^2\chi^* - \chi_{zz}^*\nabla^2\chi\right), \tag{4.12}$$

and * denotes complex conjugate. In a familiar way, (4.10) should be interpreted as an inversion equation which relates the streamfunction ψ and hence the advecting velocity $\nabla^\perp\psi$ to the dynamical variables, here q and χ. This inversion necessitates boundary conditions. In the vertical they are provided by the advection of the Lagrangian-mean buoyancy at the top and bottom boundaries, that is,

$$\partial_t\theta^{\pm} + \partial(\psi^{\pm}, \theta^{\pm}) = 0, \quad \text{where} \quad \psi^{\pm} = \psi|_{z=z^{\pm}} \quad \text{and} \quad \theta^{\pm} = f_0\,\psi_z|_{z=z^{\pm}}\,. \tag{4.13}$$

For horizontally periodic or unbounded domains, as assumed in what follows, Eqs.

(4.8)–(4.13) define the new model completely.[1] The YBJ equation (4.8a) describes the weak dispersion that arises from a finite horizontal scale (through the term $\mathrm{i}N^2\nabla^2\chi/(2f_0)$) and as well the various effects that the mean flow has on the NIWs: advection (term $(\partial(\psi,\chi_z))_z$), and refraction by the mean vorticity (term $\mathrm{i}\nabla^2\psi\,\chi_{zz}/2$) and by vertical shear (term $-\mathrm{i}\nabla\psi_z\cdot\nabla\chi_z$). The simple QGPV equation (4.8b) governs the mean flow. Here the effect of the NIWs is a modification of the relation between ψ and q by the quadratic wave terms in (4.10). This structure is expected from GLM theory which interprets the quadratic wave terms as a potential vorticity contribution stemming from the wave pseudomomentum [23, 22, 108].

4.2.2 Some properties

An important feature of the coupled model is its sets of conservation laws. The model conserves the total energy

$$\mathcal{H} = \frac{1}{2}\int\left(|\nabla\psi|^2 + \frac{f_0^2}{N^2}\psi_z^2 + f_0\beta y|\chi_z|^2 + \frac{N^2}{2}|\nabla\chi|^2\right)\mathrm{d}\boldsymbol{x}, \tag{4.14}$$

and the wave action

$$\mathcal{A} = \frac{f_0}{2}\int|\chi_z|^2\,\mathrm{d}\boldsymbol{x}. \tag{4.15}$$

The wave action can be recognised as the kinetic energy of the NIWs divided by f_0. Its conservation does not follow from an analogous conservation in the hydrostatic–Boussinesq equations; rather it stems from an adiabatic invariance associated with the large time-scale separation between the fast oscillations of the NIWs and the slow evolution of their amplitude and of the mean flow [cf. 27]. Since, in the NIW limit, the leading-order wave energy is entirely kinetic and their frequency is f_0, the familiar form of wave action, namely the ratio of wave energy to frequency, reduces to (4.15). The conservation of $\mathcal{H}$ is directly inherited from the energy conservation for the hydrostatic–Boussinesq equations. The first two terms in (4.14) are recognised as the quasi-geostrophic kinetic and potential energy associated with the mean flow. The third term is associated with the β-effect. The fourth and final term can be interpreted as the time-averaged potential energy of the NIWs; indeed, using the vertical displacement in (4.7) and denoting averaging over the wave time scale f_0^{-1} by $\langle\cdot\rangle$, we compute this as

$$\left\langle\int\frac{N^2\zeta^2}{2}\,\mathrm{d}\boldsymbol{x}\right\rangle = \frac{1}{4}\int N^2|\nabla\chi|^2\,\mathrm{d}\boldsymbol{x}. \tag{4.16}$$

[1] In a bounded domain, regions near boundary need special consideration.

Here the left-hand side is the standard expression for the quadratic part of the potential energy in a Boussineq fluid in terms of vertical displacements [e.g. 62]. The total energy in the model could alternatively be defined as $\mathcal{H} + f_0\mathcal{A}$. However, since $f_0\mathcal{A} \gg \mathcal{H}$ is conserved independently, and $\mathcal{H}$ is the Noetherian conserved quantity associated with time invariance (see § 4.4), our separation appears more natural.

The energy and action are not the only conserved quantities for the coupled model. Clearly, the enstrophy and more generally the integrals

$$\int f(q)\,\mathrm{d}\boldsymbol{x} \tag{4.17}$$

of arbitrary smooth functions f of the PV are conserved, as in the standard quasi-geostrophic model. In fact, as we discuss in § 4.4, the coupled model is Hamiltonian and additional conservation laws (e.g. linear and angular momentum) can be derived using Noether's theorem.

4.2.3 Scaling assumptions

Our derivation of the coupled model relies on a number of approximations which we now detail. The focus on NIWs, as opposed to more general inertia-gravity waves, implies that the parameter measuring the relative frequency shift compared with f_0, namely $\epsilon^2/2$, where

$$\epsilon = \frac{Nk}{f_0 m}, \tag{4.18}$$

with k and m typical horizontal and vertical wavenumbers, is small: $\epsilon \ll 1$. The parameters characterising the mean flow are the Rossby and Burger number

$$\mathrm{Ro} = \frac{U_{\mathrm{QG}}}{f_0 L} \quad \text{and} \quad \mathrm{Bu} = \frac{N^2 H^2}{f_0^2 L^2}, \tag{4.19}$$

where U_{QG} is a typical mean velocity, and L and H are horizontal and vertical scales of the mean flow. These parameters are taken to satisfy $\mathrm{Ro} \ll 1$ and $\mathrm{Bu} = O(1)$ in accordance with quasi-geostrophic theory. In the YBJ model (4.8a), dispersion and mean-flow effects have similar orders of magnitudes provided that $\mathrm{Ro} = O(\epsilon^2)$, which we also assume. Note that there is no specific assumption about the relative size of the wave and mean horizontal scales which can be taken to satisfy $kL = O(1)$.

The last relevant parameter controls the NIW amplitude and is defined as

$$\alpha = \frac{U_{\mathrm{NIW}}}{f_0 L}, \tag{4.20}$$

where U_{NIW} is a typical NIW horizontal velocity. We choose the relative scaling of Ro and α in order that the NIW feedback affect the mean motion at the same order as nonlinear vorticity advection. This imposes that

$$\alpha = O(\epsilon) \quad \text{and} \quad \mathrm{Ro} = O(\alpha^2). \tag{4.21}$$

This scaling indicates that $U_{\mathrm{NIW}}/U_{\mathrm{QG}} = \alpha^{-1} \gg 1$, as is relevant to strong NIWs generated by intense storms [e.g. 33]. It leads to a mean equation that is a modification of the quasi-geostrophic equation by wave effects. Had a smaller wave amplitude been assumed in order to model quieter conditions, say by taking $\mathrm{Ro} = O(\alpha)$, the wave effects would have been an $O(\mathrm{Ro})$-factor smaller than advection in (4.8b) and of comparable order as balanced corrections to quasi-geostrophy [cf. 139]. Because these corrections do not alter the qualitative properties of the quasi-geostrophic model, we prefer the scaling (4.21) to retain a model that is as simple as possible.

It is important to note that our model is not fully consistent from an asymptotic viewpoint. The assumption of two different aspects ratios for NIWs and mean flow, implied by the condition $\epsilon \ll 1$ and $\mathrm{Bu} = O(1)$ are best thought of as resulting from a disparity in vertical scales, $mH \gg 1$, is not generally consistent. Indeed, small-scale NIWs generally lead to small-scale wave terms in (4.10) and hence to a pair q and ψ that varies on the wave scale (with a vertically-planar NIW field $\chi \propto \exp(\mathrm{i}mz)$ a notable exception, see § 4.6.2). A consistent assumption would be to take $\mathrm{Bu} = O(\epsilon^2) \ll 1$. But this assumption is less relevant to most of the ocean; it leads to a different balanced dynamics, namely frontal dynamics, with negligible wave–mean interactions [139].

While the model is heuristic, we regard it as valuable for its simplicity and because it respects key properties including conservation laws. The variational derivation of the wave–mean equations as detailed in the next sections makes this possible. This derivation starts with that of a coupled YBJ–primitive-equation (Eqs. (4.36)–(4.38) below) which makes no assumption of quasi-geostrophy for the mean flow. This model, naturally more complex than (4.8), is asymptotically consistent provided that $\alpha \ll \mathrm{Ro}^{1/2}/\epsilon^{1/2}$ so that the wave–wave interactions are negligible. It could serve as basis to obtain a balanced model for the mean flow that is more accurate than quasi-geostrophic and/or with relaxed assumptions on Bu so as to be fully consistent with the YBJ equation.

4.3 Derivation of the coupled model

We follow Salmon [108] in deriving the Lagrangian-mean and wave equations from a variational formulation of the fluid equations rather than from the equations themselves. This is advantageous since it guarantees that the wave–mean model inherits conservation laws from the original hydrostatic–Boussinesq model. While Salmon [108] develops a general theory making no specific assumptions on the form of the perturbations to the mean flow, we focus on NIWs, assuming that the displacements $\boldsymbol{\xi}$ satisfy (4.7). With this assumption, which can be viewed as a form of closure relying on a hypothesis of small wave amplitude, a natural step is to average the Lagrangian in the manner of Whitham [128] to obtain a reduced Lagrangian that is a functional of the mean map $\boldsymbol{X}$ and of the NIW amplitude χ. This is described in § 4.3.1. Variations with respect to $\boldsymbol{X}$ (or rather its inverse) and χ are carried out in § 4.3.2 to obtain the mean and wave (YBJ) equations.

4.3.1 Lagrangian and wave–mean decomposition

The hydrostatic–Boussinesq equations (4.2) can be derived from the Lagrangian

$$\mathcal{L}[\boldsymbol{x}, p] = \int \left(\frac{1}{2}\left(\dot{x}^2 + \dot{y}^2\right) - \left(f_0 y + \frac{1}{2}\beta y^2 \right) \dot{x} + \theta z + p \left(\left| \frac{\partial \boldsymbol{x}}{\partial \boldsymbol{a}} \right| - 1 \right) \right) \mathrm{d}\boldsymbol{a}, \tag{4.22}$$

where $\boldsymbol{a} = (a, b, \theta)$ are particle labels, with the (materially conserved) buoyancy taken as third component, and $\boldsymbol{x}(\boldsymbol{a}, t)$ is the flow map [e.g. 108]. The pressure $p(\boldsymbol{x}, t)$ is a Lagrange multiplier enforcing the incompressibility constraint. Following standard GLM practice, we introduce the mean-map $\boldsymbol{X}(\boldsymbol{a}, t)$ and displacement $\boldsymbol{\xi}(\boldsymbol{x}, t)$, with

$$\boldsymbol{x}(\boldsymbol{a}, t) = \boldsymbol{X}(\boldsymbol{a}, t) + \boldsymbol{\xi}(\boldsymbol{X}(\boldsymbol{a}, t)). \tag{4.23}$$

Following Salmon [108], we regard the Lagrangian as a functional of the inverse of the mean flow map, $\boldsymbol{a}(\boldsymbol{X}, T) = \boldsymbol{X}^{-1}(\boldsymbol{X}, t)$, with $T = t$. Using the chain rule, (4.22) can be shown to take the form

$$\begin{aligned} \mathcal{L}[\boldsymbol{a}, \boldsymbol{\xi}, p] \;=\; & \int \left(J \left(\frac{1}{2}\left((U + D_T\xi)^2 + (V + D_T\eta)^2 \right) - \left(f_0(Y + \eta) + \frac{1}{2}\beta(Y + \eta)^2 \right) \right.\right. \\ & \left.\left. \times (U + D_T\xi) + \theta(Z + \zeta) \right) + p(\boldsymbol{X}) \left(\left| \frac{\partial(\boldsymbol{X} + \boldsymbol{\xi})}{\partial \boldsymbol{X}} \right| - J \right) \right) \mathrm{d}\boldsymbol{X}, \end{aligned} \tag{4.24}$$

where $D_T = \partial_T + \boldsymbol{U}\cdot\nabla_3$, with $\boldsymbol{U} = \dot{\boldsymbol{X}} = \bar{\boldsymbol{u}}^{\mathrm{L}}$ the Lagrangian-mean velocity and ∇_3 the three-dimensional gradient with respect to $\boldsymbol{X}$, and $J = |\partial \boldsymbol{a}/\partial \boldsymbol{X}|$ is the Jacobian of the inverse mean map. In this expression, $\boldsymbol{U}$ should be thought as a differential function of $\boldsymbol{a}(\boldsymbol{X}, T)$; an explicit form for it is obtained from the material invariance of the labels, $D_T \boldsymbol{a} = 0$, as

$$U = -\frac{1}{J}\frac{\partial(a,\ b,\ \theta)}{\partial(T,\ Y,\ Z)},\ V = -\frac{1}{J}\frac{\partial(a,\ b,\ \theta)}{\partial(X,\ T,\ Z)},\ W = -\frac{1}{J}\frac{\partial(a,\ b,\ \theta)}{\partial(X,\ Y,\ T)}. \tag{4.25}$$

We next introduce the expansion

$$\boldsymbol{\xi} = \boldsymbol{\xi}^{(1)} + \boldsymbol{\xi}^{(2)} + \ldots, \tag{4.26}$$

of the NIW displacement into the Lagrangian (4.24), with $|\boldsymbol{\xi}^{(n)}| = O(\alpha^n)$. Retaining only terms in α^n, $n \leq 2$, which amounts to linearising the NIW dynamics, and averaging over the fast time scale f_0^{-1} lead to the averaged Lagrangian

$$\begin{aligned}
\langle \mathcal{L} \rangle \quad = \quad & \int \Bigg(\frac{1}{2} J \left(U^2 + V^2 + 2U D_T \left\langle \xi^{(2)} \right\rangle + 2V D_T \left\langle \eta^{(2)} \right\rangle \right. \\
& \left. + \left\langle \left(D_T \xi^{(1)} \right)^2 \right\rangle + \left\langle \left(D_T \eta^{(1)} \right)^2 \right\rangle \right) - J \left(f_0 Y + \frac{1}{2}\beta Y^2 \right) \left(U + D_T \left\langle \xi^{(2)} \right\rangle \right) \\
& - J \left(f_0 + \beta Y \right) \left(\left\langle \eta^{(2)} \right\rangle U + \left\langle \eta^{(1)} D_T \xi^{(1)} \right\rangle \right) - J \frac{1}{2}\beta \left\langle \left(\eta^{(1)} \right)^2 \right\rangle U + J\theta Z \\
& + J\theta \left\langle \zeta^{(2)} \right\rangle + P \nabla_3 \cdot \left(\left\langle \boldsymbol{\xi}^{(2)} \right\rangle - \frac{1}{2} \left\langle \boldsymbol{\xi}^{(1)} \cdot \nabla_3 \boldsymbol{\xi}^{(1)} \right\rangle \right) + P(1 - J) \Bigg) \, \mathrm{d}\boldsymbol{X}.
\end{aligned} \tag{4.27}$$

where $\langle \cdot \rangle$ denotes the average. It is standard in GLM theories that this average be defined as an arbitrary ensemble average. Here, a natural ensemble is that formed by a family of NIWs differing by a phase shift. Thus, an ensemble parameter $\gamma \in [0, 2\pi]$ is introduced in (4.7) to obtain the ensemble of leading-order wave fields

$$\xi^{(1)} + \mathrm{i}\eta^{(1)} = \chi_Z \, \mathrm{e}^{-\mathrm{i}(f_0 T + \gamma)} \quad \text{and} \quad \zeta^{(1)} = -\chi_S \mathrm{e}^{-\mathrm{i}(f_0 T + \gamma)} + \text{c.c.} \tag{4.28}$$

with $S = X + \mathrm{i}Y$ and $\partial_S = (\partial_X - \mathrm{i}\partial_Y)/2$. When there is a time-scale separation between the (fast) oscillation at frequency f_0 and the (slow) evolution of the amplitude χ, averaging over γ amounts to averaging over the fast time scale f_0^{-1}. Thus the ensemble average becomes physically relevant, and it leads to an averaged dynamics identical to that obtained by explicit perturbation expansions as demonstrated by Whitham [128]. Note that our notation $\boldsymbol{\xi}^{(1)}(\boldsymbol{x}, t)$ does not make the dependence of $\boldsymbol{\xi}^{(1)}$ on the ensemble

parameter γ explicit; our compact notation is justified by the fact that parameter γ disappears completely from the problem after the (Whitham) average has been performed. Note also that the truncation of the Lagrangian (4.27) to $O(\alpha)$ can be regarded as a closure in which the nonlinearity of wave dynamics is neglected.

To derive (4.27), we have used that $\left\langle \boldsymbol{\xi}^{(1)} \right\rangle = 0$, that $\nabla_3 \cdot \boldsymbol{\xi}^{(1)} = 0$ (stemming from the divergence-free property of NIWs), and that

$$\left| \frac{\partial(\boldsymbol{X} + \boldsymbol{\xi})}{\partial \boldsymbol{X}} \right| = 1 + \nabla_3 \cdot \boldsymbol{\xi}^{(2)} + \frac{1}{2} \nabla_3 \cdot \left(\boldsymbol{\xi}^{(1)} \nabla_3 \cdot \boldsymbol{\xi}^{(1)} - \boldsymbol{\xi}^{(1)} \cdot \nabla_3 \boldsymbol{\xi}^{(1)} \right) + O(\alpha^3), \tag{4.29}$$

as well as integration by parts. Importantly, we do not assume that $\left\langle \boldsymbol{\xi}^{(2)} \right\rangle = 0$ as is standard in GLM theory. Instead, we follow Soward and Roberts' (2010) glm prescription which ensures that the mean motion is divergence free. As detailed in Appendix B, at the order we consider, this prescription amounts to taking

$$\left\langle \boldsymbol{\xi}^{(2)} \right\rangle = \frac{1}{2} \left\langle \boldsymbol{\xi}^{(1)} \cdot \nabla_3 \boldsymbol{\xi}^{(1)} \right\rangle. \tag{4.30}$$

As (4.29) indicates, this ensures that the map $\boldsymbol{X} \mapsto \boldsymbol{X} + \boldsymbol{\xi}$ from mean to perturbed position is volume preserving: since the map $\boldsymbol{a} \mapsto \boldsymbol{X} + \boldsymbol{\xi}$ is volume preserving, this is also true for the map $\boldsymbol{a} \mapsto \boldsymbol{X}$, so the Lagrangian-mean velocity is divergence free.

At this point, we can substitute the NIW-ansatz (4.7), rewritten here as

$$\xi^{(1)} + \mathrm{i}\eta^{(1)} = \chi_Z \, \mathrm{e}^{-\mathrm{i}f_0 t} \quad \text{and} \quad \zeta^{(1)} = -\chi_S \mathrm{e}^{-\mathrm{i}f_0 t} + \text{c.c.}, \tag{4.31}$$

with $S = X + \mathrm{i}Y$ and $\partial_S = (\partial_X - \mathrm{i}\partial_Y)/2$, into (4.27) to obtain the averaged Lagrangian in terms of $\boldsymbol{a}$, P and χ. This leads to

$$\begin{aligned} \langle \mathcal{L} \rangle \quad = \quad & \int \left(\frac{1}{2} J(U^2 + V^2) - J \left(f_0 Y + \frac{1}{2} \beta Y^2 \right) U + J\theta Z \right. \\ & + J \left(-\frac{\mathrm{i}f_0}{4} (\chi_Z D_T \chi_Z^* - \chi_Z^* D_T \chi_Z) - \frac{1}{2} f_0 \beta Y |\chi_Z|^2 \right) \\ & \left. + J \left(-f_0 Y D_T \left\langle \xi^{(2)} \right\rangle - f_0 \left\langle \eta^{(2)} \right\rangle U + \theta \left\langle \zeta^{(2)} \right\rangle \right) + P(1 - J) \right) \mathrm{d}\boldsymbol{X}. \end{aligned} \tag{4.32}$$

To obtain this expression, we have retained only wave terms that are $O(1)$ or $O(\alpha^2/\mathrm{Ro})$ relative to the size U_{QG}^2 of the first term, assuming that $\beta L/f = O(\mathrm{Ro})$ so that only a single wave term involving β remains. Note that the linearisation of the NIW dynamics entailed by ignoring cubic terms in $\langle \mathcal{L} \rangle$ is asymptotically consistent: averaging eliminates

cubic terms in $\boldsymbol{\xi}^{(1)}$, leaving cubic terms involving higher harmonics (with frequency $2f$), whose size can be estimated as $\epsilon\alpha^4/\mathrm{Ro}^2 = O(\alpha)$. The absence of resonant cubic terms has been noted by Falkovich et al. [47] and Zeitlin et al. [139] and is related to the possible elimination of advective nonlinearities by means of Lagrangian coordinates [47, 65].

The Lagrangian (4.32) governs the NIW–mean flow system: when (4.30)–(4.31) are used to express $\boldsymbol{\xi}^{(2)}$ explicitly as

$$\left\langle \xi^{(2)} \right\rangle = \frac{1}{4}(\chi_Z \chi^*_{ZS} - \chi_S \chi^*_{ZZ}) + \text{c.c.}, \tag{4.33a}$$

$$\left\langle \eta^{(2)} \right\rangle = \frac{\mathrm{i}}{4}(\chi_Z \chi^*_{ZS} - \chi_S \chi^*_{ZZ}) + \text{c.c.}, \tag{4.33b}$$

$$\left\langle \zeta^{(2)} \right\rangle = \frac{1}{2}(-\chi_Z \chi^*_{SS^*} + \chi_S \chi^*_{ZS^*}) + \text{c.c.}, \tag{4.33c}$$

$\mathcal{L}$ is a functional of $\boldsymbol{a}$, χ and P from which primitive equations for the mean flow coupled to a YBJ-like equation for the NIWs can be derived systematically. This is carried out in the next subsection, § 4.3.2. The reduced quasi-geostrophic model (4.8) is then derived in § 4.3.3.

4.3.2 Coupled YBJ–primitive-equation model

Taking the variation δP of the action $\int \langle \mathcal{L} \rangle \, \mathrm{d}t$ with the Lagrangian (4.32) and using (4.33) we obtain

$$J = 1, \tag{4.34}$$

confirming that the mean map is volume preserving. Thus the Lagrangian-mean velocity is divergence free:

$$\nabla_3 \cdot \boldsymbol{U} = 0. \tag{4.35}$$

The mean equations of motion can now obtained from the stationarity of $\int \langle \mathcal{L} \rangle \, \mathrm{d}t$ with respect to variations $\delta \boldsymbol{a}$. It is convenient to use the energy-momentum formalism as proposed by Salmon (2013). Computations detailed in Appendix C lead to the

momentum equations in the form

$$\begin{aligned} D_T U - (f_0+\beta Y)V + \partial_X P =& \frac{\mathrm{i}f_0}{2}\left(D_T\chi_Z\chi^*_{XZ} - D_T\chi^*_Z\chi_{XZ}\right) - \frac{1}{2}f_0\beta\partial_X(Y|\chi_Z|^2) \\ &+ f_0\left\langle D_T\eta^{(2)} - U\eta^{(2)}_X + V\xi^{(2)}_X\right\rangle + \theta\left\langle\zeta^{(2)}_X\right\rangle, \qquad (4.36a) \\ D_T V + (f_0+\beta Y)U + \partial_Y P =& \frac{\mathrm{i}f_0}{2}\left(D_T\chi_Z\chi^*_{YZ} - D_T\chi^*_Z\chi_{YZ}\right) - \frac{1}{2}f_0\beta\partial_Y(Y|\chi_Z|^2) \\ &+ f_0\left\langle -D_T\xi^{(2)} - U\eta^{(2)}_Y + V\xi^{(2)}_Y\right\rangle + \theta\left\langle\zeta^{(2)}_Y\right\rangle, \qquad (4.36b) \\ -\theta + \partial_Z P =& \frac{\mathrm{i}f_0}{2}\left(D_T\chi_Z\chi^*_{ZZ} - D_T\chi^*_Z\chi_{ZZ}\right) - \frac{1}{2}f_0\beta\partial_Z(Y|\chi_Z|^2) \\ &+ f_0\left\langle -U\eta^{(2)}_Z + V\xi^{(2)}_Z\right\rangle + \theta\left\langle\zeta^{(2)}_Z\right\rangle. \qquad (4.36c) \end{aligned}$$

These are completed by the buoyancy equation

$$D_T\theta = 0 \qquad (4.37)$$

which expresses that θ is a label. The left-hand sides of Eqs. (4.35)–(4.37) recover the hydrostatic–Boussinesq equations (4.2) for the mean flow; the right-hand sides, which can be written completely in terms of χ, describe the impact of the NIWs on the mean flow.

Taking the variation $\delta\chi^*$ of the Lagrangian (4.32) after using (4.33) for $\boldsymbol{\xi}^{(2)}$ leads to the wave equation

$$\begin{aligned} (D_T\chi_Z)_Z - \mathrm{i}\beta Y\chi_{ZZ} &+ \frac{\mathrm{i}}{2}\left((V\chi_Z)_{ZS} - (V\chi_S)_{ZZ} - (V\chi_{ZS*})_Z + (V\chi_{ZZ})_{S*}\right) \\ &+ \frac{1}{2}\left((U\chi_Z)_{ZS} - (U\chi_S)_{ZZ} - (U\chi_{ZS^*})_Z - (U\chi_{ZZ})_{S^*}\right) \qquad (4.38) \\ &+ \frac{\mathrm{i}}{f_0}\left(-(\theta\chi_Z)_{SS^*} + (\theta\chi_S)_{ZS^*} + (\theta\chi_{SS^*})_Z - (\theta\chi_{ZS})_{S^*}\right) = 0. \end{aligned}$$

This equation can be interpreted as a generalisation of the YBJ equations which makes no assumption that the mean flow is quasi-geostrophic or steady.

Together, Eqs. (4.36), (4.37) and (4.38) constitute a closed model for the joint evolution of the wave and the mean flow. This model is complex and we prefer to focus our analysis on its quasi-geostrophic approximation introduced in § 4.2 and derived in the next subsection. It is nonetheless worth noting that the full model has two simple conservation laws. The first is obtained by multiplying (4.38) by χ^* and adding the complex conjugate of the resulting equation. Integrating over space and making liberal

use of integration by parts yields the wave-action conservation

$$\frac{\mathrm{d}}{\mathrm{d}t}\int |\chi_Z|^2\,\mathrm{d}\boldsymbol{X} = 0. \tag{4.39}$$

This conservation law is associated with the obvious symmetry $\chi \mapsto \mathrm{e}^{\mathrm{i}\gamma}\chi$, $\gamma \in \mathbb{R}$, of the Lagrangian (4.32) and can therefore also be obtained from Noether's theorem in the form

$$\frac{\mathrm{d}}{\mathrm{d}T}\int \left(\mathrm{i}\chi\frac{\delta}{\delta\chi_T} - \mathrm{i}\chi^*\frac{\delta}{\delta\chi_T^*}\right)\langle\mathcal{L}\rangle\,\mathrm{d}\boldsymbol{X} = 0, \tag{4.40}$$

thus justifying the terminology of action. The second conservation law is that of energy. It is best obtained from the Lagrangian (4.32). The general form of the conserved energy stems the time symmetry $T \to T + \delta T$, namely

$$\int \left(a_T^i\frac{\delta}{\delta a_T^i} + \chi_T\frac{\delta}{\delta\chi_T} + \chi_T^*\frac{\delta}{\delta\chi_T^*} - 1\right)\langle\mathcal{L}\rangle\,\mathrm{d}\boldsymbol{X}, \tag{4.41}$$

implies that the energy is readily deduced from $\mathcal{L}$ using the following rules: terms that are quadratic in $\boldsymbol{U}$ (and hence in a_T^i) or χ_T are retained, terms that are linear are omitted, and terms that contain no time derivatives change sign. So the energy conservation reads

$$\frac{\mathrm{d}}{\mathrm{d}t}\int \left(\frac{1}{2}(U^2+V^2) - \theta(Z + \left\langle\zeta^{(2)}\right\rangle) + \frac{1}{2}f_0\beta Y|\chi_Z|^2\right)\mathrm{d}\boldsymbol{X} = 0 \tag{4.42}$$

using that $J = 1$. This is a remarkably simple expression in which the effect of the waves arises only through the potential-energy term $-\theta\left\langle\zeta^{(2)}\right\rangle$ and the β-term. Surprisingly perhaps, it is simpler than the analogous energy that is conserved in the (uncoupled) YBJ model [124].

4.3.3 Quasi-geostrophic approximation

We now derive an approximation to the mean and wave equations in the quasi-geostrophic limit $\mathrm{Ro} \to 0$. The standard quasi-geostrophic model cannot be derived in a simple manner from the variational formulation of the primitive equations [see 15, 99, however], and the same difficulty arises here. We therefore derive the quasi-geostrophic approximation of the mean equations directly from the momentum equations (4.36), retaining a variational argument for the wave part only. That the approximations made in both parts of the model are consistent is confirmed by the fact that the resulting coupled model has a Hamiltonian structure, as discussed in § 4.4.

In the quasi-geostrophic approximation, the buoyancy is decomposed into a Z-dependent mean part and a perturbation according to

$$\theta = \bar{\theta}(Z) + \theta' = \int^Z N^2(z')\,\mathrm{d}z' + \theta'. \tag{4.43}$$

To leading order in Ro, the mean equations (4.36) then reduce to

$$\begin{aligned} f_0 V &= \partial_X \left(P - \bar{\theta} \left\langle \zeta^{(2)} \right\rangle \right), && (4.44)\\ -f_0 U &= \partial_Y \left(P - \bar{\theta} \left\langle \zeta^{(2)} \right\rangle \right), && (4.45)\\ \theta' &= \partial_Z \left(P - \bar{\theta} \left\langle \zeta^{(2)} \right\rangle - \int^Z \mathrm{d}z \int^z N^2(z')\,\mathrm{d}z' \right) + N^2 \left\langle \zeta^{(2)} \right\rangle, && (4.46) \end{aligned}$$

and are recognised as expressing geostrophic and hydrostatic balance. This leads to the introduction of a streamfunction ψ such that

$$U = -\psi_Y, \quad V = \psi_X \quad \text{and} \quad \theta' = f_0 \psi_Z + N^2 \left\langle \zeta^{(2)} \right\rangle. \tag{4.47}$$

Using this, the buoyancy conservation becomes

$$D_T^0 \left(f_0 \psi_Z + N^2 \left\langle \zeta^{(2)} \right\rangle \right) + N^2 W = 0, \tag{4.48}$$

where $D_T^0 = \partial_T + \partial(\psi, \cdot)$.

A closed equation for ψ can now be derived from (4.36) and (4.48) in a familiar way: taking the horizontal curl of (4.36a)–(4.36b) and keeping terms up to $O(U^2/L^2)$ we obtain

$$D_T^0 \left(\beta Y + V_X - U_Y + \frac{\mathrm{i}f}{2} \partial(\chi_Z, \chi_Z^*) + f_0 (\left\langle \xi_X^{(2)} \right\rangle + \left\langle \eta_Y^{(2)} \right\rangle) \right) - f_0 W_Z = 0. \tag{4.49}$$

Substituting (4.48) to eliminate W leads to the conservation equation

$$D_T^0 q = 0, \quad \text{where} \quad q = \beta Y + \Delta\psi + \frac{\mathrm{i}f_0}{2} \partial(\chi_Z^*, \chi_Z) + f_0 \nabla_3 \cdot \left\langle \boldsymbol{\xi}^{(2)} \right\rangle \tag{4.50}$$

is the QGPV. A direct computation using (4.33) gives the last term explicitly as

$$\nabla_3 \cdot \left\langle \boldsymbol{\xi}^{(2)} \right\rangle = G(\chi^*, \chi), \tag{4.51}$$

with the symmetric bilinear operator G defined in (4.12). Replacing $\boldsymbol{X}$ by $\boldsymbol{x}$ as inde-

pendent variable reduces the QGPV equation (4.50) to the form announced in (4.8b). An alternative derivation based on potential-vorticity conservation and valid for an arbitrary definition of the Lagrangian average is presented in Appendix D. The vertical boundary conditions (4.13) associated with the QGPV equation are derived by applying the no-normal-flow condition $W = 0$ at $z = z^{\pm}$ to (4.48) and noting from (4.30) that $\langle \zeta^{(2)} \rangle = 0$ at $z^{\pm}$ follows from the fact that $\zeta^{(1)} = 0$ there.

The NIW equation associated with (4.50) is best derived by introducing the geostrophic and hydrostatic conditions into the averaged Lagrangian (4.32) then taking variations with respect to χ or χ^*. The wave part of the Lagrangian is readily found from (4.32) to be

$$\begin{aligned} \langle \mathcal{L} \rangle_{\mathrm{NIW}} \;=\; \int \Bigg(& -\frac{\mathrm{i}f_0}{4}(\chi_Z D_T^0 \chi_Z^* - \chi_Z^* D_T^0 \chi_Z) - \frac{1}{2} f_0 \beta Y |\chi_Z|^2 \\ & - f_0 \psi \nabla_3 \cdot \left\langle \boldsymbol{\xi}^{(2)} \right\rangle + \int^Z N^2(z)\, \mathrm{d}z \left\langle \zeta^{(2)} \right\rangle \Bigg)\, \mathrm{d}\boldsymbol{X}, \end{aligned} \tag{4.52}$$

where we have used that $J = 1$, integration by parts, and neglected a term in $\langle \zeta^{(2)} \rangle^2$ The terms depending on $\boldsymbol{\xi}^{(2)}$ can now be written in terms of χ using (4.51) and the observation that

$$\left\langle \zeta^{(2)} \right\rangle = \frac{1}{2} \partial_Z \left\langle \left(\zeta^{(1)} \right)^2 \right\rangle + \cdots = \frac{1}{4} \partial_Z |\nabla \chi|^2 + \cdots, \tag{4.53}$$

where $\cdots$ denotes the horizontal divergence of an irrelevant vector. This simplifies (4.52) into

$$\begin{aligned} \langle \mathcal{L} \rangle_{\mathrm{NIW}} \;=\; -\int \Bigg(& \frac{\mathrm{i}f_0}{4}(\chi_Z D_T^0 \chi_Z^* - \chi_Z^* D_T^0 \chi_Z) + \frac{1}{2} f_0 \beta Y |\chi_Z|^2 \\ & + f_0 \psi G(\chi^*, \chi) + \frac{1}{4} N^2 |\nabla \chi|^2 \Bigg)\, \mathrm{d}\boldsymbol{X}. \end{aligned} \tag{4.54}$$

To take the variations of the corresponding action, it is convenient to introduce the symmetric bilinear operator $\hat{G}$ dual to G in the sense that

$$\int \psi G(\chi^*, \chi)\, \mathrm{d}\boldsymbol{X} = \int \chi^* \hat{G}(\psi, \chi)\, \mathrm{d}\boldsymbol{X}. \tag{4.55}$$

The variation $\delta\chi^*$ then gives

$$(D_T^0 \chi)_Z + \mathrm{i}\beta Y \chi_{ZZ} + \frac{\mathrm{i}N^2}{2f_0} \nabla^2 \chi - 2\mathrm{i}\hat{G}(\psi, \chi) = 0. \tag{4.56}$$

From its definition and (4.12) $\hat{G}(\psi,\chi)$ is calculated to be

$$\hat{G}(\psi,\chi)=\frac{1}{4}\left(2\nabla\psi_Z\cdot\nabla\chi_Z-\nabla^2\psi\chi_{ZZ}-\psi_{ZZ}\nabla^2\chi\right) \tag{4.57}$$

and is recognised as the negative of YBJ's bracket $[[\cdot,\cdot]]$. Introducing (4.57) into (4.56), dropping the superscript 0 from D_T^0 and replacing $\boldsymbol{X}$ by $\boldsymbol{x}$ leads to the YBJ equation in the form (4.8a).

4.4 Conservation laws and Hamiltonian structure

We now derive conservation laws satisfied by the coupled model (4.8). We start by the conservation law identified in YBJ: multiplying (4.8a) by χ^* and integrating yields

$$\int\left(-\chi_z^*\partial_t\chi_z+\psi\partial(\chi_z^*,\chi_z)-\mathrm{i}\beta y|\chi_z|^2-\frac{\mathrm{i}N^2}{2f_0}|\nabla\chi|^2-2\mathrm{i}\psi G(\chi^*,\chi)\right)\mathrm{d}\boldsymbol{x}=0, \tag{4.58}$$

after using integration by parts. Adding the complex conjugate and using the symmetry of G and antisymmetry of $\partial(\cdot,\cdot)$ gives

$$\frac{\mathrm{d}}{\mathrm{d}t}\int|\chi_z|^2\,\mathrm{d}\boldsymbol{x}=0. \tag{4.59}$$

Thus, the wave action $\mathcal{A}$ defined in (4.15) is conserved. This conservation law is identical to that obtained for the YBJ–primitive-equation model in (4.39) and, as checked below using the Hamiltonian structure of the YBJ-QG model, also associated with an invariance with respect to phase shifts of the amplitude χ.

Next we derive an energy conservation law. Multiplying the QGPV equation (4.8b) by ψ, integrating and using the definition (4.10) of q gives

$$\int\left(\frac{1}{2}\partial_t\left(|\nabla\psi|^2+\frac{f_0^2}{N^2}\psi_z^2\right)-\frac{\mathrm{i}f_0\psi}{2}\left(\partial(\chi_{zt}^*,\chi_z)+\partial(\chi_z^*,\chi_{zt})\right)\right.$$
$$\left.-f_0\psi\left(G(\chi_t^*,\chi)+G(\chi^*,\chi_t)\right)\right)\mathrm{d}\boldsymbol{x}=0. \tag{4.60}$$

Multiplying the YBJ equation (4.8a) by $\mathrm{i}f_0\partial_t\chi^*/2$, integrating and adding the complex

conjugate gives

$$\int \left(\frac{\mathrm{i} f_0 \psi}{2} \left(\partial(\chi_{zt}^*, \chi_z) + \partial(\chi_z^*, \chi_{zt}) \right) + \frac{f_0 \beta Y}{2} \partial_t |\chi_z|^2 \right.$$
$$\left. + \frac{N^2}{4} \partial_t |\nabla \chi|^2 + f_0 \psi \left(G(\chi_t^*, \chi) + f_0 G(\chi^*, \chi_t) \right) \right) \mathrm{d}\boldsymbol{x} = 0, \quad (4.61)$$

where the relation (4.55) between G and $\hat{G}$ is used. Adding (4.60) and (4.61) leads to

$$\frac{\mathrm{d}}{\mathrm{d}t} \int \frac{1}{2} \left(|\nabla \psi|^2 + \frac{f_0^2}{N^2} \psi_z^2 + \beta y |\chi_z|^2 + \frac{1}{2} N^2 |\nabla \chi|^2 \right) \mathrm{d}\boldsymbol{x} = 0, \quad (4.62)$$

and hence to the conservation of the energy $\mathcal{H}$ in (4.14). This energy conservation can be recognised as the QG approximation of primitive-equation energy (4.42): the first two terms are the usual QG approximation of the mean kinetic and potential energy; the third term in unchanged; the fourth term is an approximation to $\theta \left\langle \zeta^{(2)} \right\rangle$ obtained by noting that $\theta \approx \int^z N^2(z') \, \mathrm{d}z'$ and using (4.53). It is interesting to notice that the wave action conservation indicates that the beta-effect does not influence the total energy budget, which is a reason that in the later two-dimensional models we set $\beta = 0$.

The coupled model (4.8) is in fact Hamiltonian. The Hamiltonian structure [e.g. 111], which can be obtained by inspection, is conveniently written using the amplitude of the horizontal NIW displacement $\phi = \chi_z$, its complex conjugate ϕ^*, q and $\theta^\pm$ as dynamical variables. Grouping these in a vector $\boldsymbol{\phi}$, it can be checked that the governing equations (4.8) are recovered from

$$\boldsymbol{\phi}_t = \mathcal{J} \frac{\delta \mathcal{H}}{\delta \boldsymbol{\phi}}, \quad (4.63)$$

where

$$\mathcal{J} = \begin{pmatrix} 0 & -2\mathrm{i}/f_0 & 0 & 0 & 0 \\ 2\mathrm{i}/f_0 & 0 & 0 & 0 & 0 \\ 0 & 0 & -\partial(q, \cdot) & 0 & 0 \\ 0 & 0 & 0 & (N^+)^2 f_0^{-1} \partial(\theta^+, \cdot) & 0 \\ 0 & 0 & 0 & 0 & -(N^-)^2 f_0^{-1} \partial(\theta^-, \cdot) \end{pmatrix} \quad (4.64)$$

and the Hamiltonian is

$$\mathcal{H} = \frac{1}{2}\int \left(|\nabla\psi|^2 + \frac{f_0^2}{N^2}|\psi_z|^2 + f_0\beta y|\phi|^2 + \frac{N^2}{2}\left|\nabla\int^z \phi(z')\,\mathrm{d}z'\right|^2 \right) \mathrm{d}\boldsymbol{x}. \tag{4.65}$$

The streamfunction ψ is here regarded as a functional of $\boldsymbol{\phi}$ defined by

$$\psi = \Delta^{-1}\left(q - \beta y - \frac{\mathrm{i}f_0}{2}\partial(\phi^*,\phi) - f_0 G\left(\int^z \phi^*(z')\,\mathrm{d}z', \int^z \phi(z')\,\mathrm{d}z'\right)\right) \tag{4.66}$$

with $\psi_z|_{z=z^\pm} = f_0^{-1}\theta^\pm$. Even though it is not easy to generally check that a bracket satisfies the Jacobi identity, we can easily see that our bracket (4.4) does because it is a combination of a 2-by-2 canonical matrix at top-left and a diagonal matrix where each element identifies the bracket of a quasi-geostrophic flow.

The Hamiltonian structure provides a systematic route to the derivation of conservation laws using Noether's theorem. We note that the Hamiltonian flow associated with the wave action $\mathcal{A} = f_0\int|\phi|^2\,\mathrm{d}\boldsymbol{x}/2$, namely $\mathcal{J}\delta\mathcal{A}/\delta\boldsymbol{\phi}$, is $(-\mathrm{i}\phi, \mathrm{i}\phi^*, 0, 0, 0)^T$. This is recognised as the generator of the continuous transformation $\phi \mapsto \phi\exp(-\mathrm{i}\gamma)$, $\gamma\in\mathbb{R}$, an obvious symmetry of $\mathcal{H}$. The invariance of $\mathcal{H}$ with respect to translations and horizontal rotations gives rise to conserved linear and angular momenta. For instance, the conserved x-momentum is readily shown to be

$$\begin{aligned}\mathcal{M}_x &= \int\left(\frac{\mathrm{i}f_0}{4}\left(\phi^*\phi_x - \phi_x^*\phi\right) - qy\right)\mathrm{d}\boldsymbol{x} + f_0\int\left((N^+)^{-2}\theta^+ - (N^-)^{-2}\theta_-\right) y\,\mathrm{d}x\mathrm{d}y \\ &= \int U\,\mathrm{d}\boldsymbol{x}.\end{aligned} \tag{4.67}$$

Additional conserved quantities are of course the same Casimir invariants as in three-dimensional quasi-geostrophic dynamics, namely the volume integrals of arbitrary functions of q and surface integrals of arbitrary functions of $\theta^\pm$ [111].

4.5 Implications

We now discuss some implications of the conservation of energy (4.14) and action (4.15) for ocean dynamics. First, we note that the action conservation implies that the NIW amplitude remains zero if it is initially so: thus spontaneous generation of NIWs is impossible in this model, unsurprisingly since it is expected to be exponentially small in Ro [123] and thus much smaller than neglected terms.

Another, more striking, conclusion is that conservation laws show unambiguously

that oceanic NIWs forced by atmospheric winds provide an energy sink for the mean flow. To see how, consider NIWs forced at some initial time $t = 0$ with horizontal scales large enough that $\chi_0 = \chi(t = 0)$ has negligible horizontal gradient i.e. $\nabla\chi_0 \approx 0$. This is a reasonable approximation since NIWs are generated by atmospheric storms whose scales are ten or more times the scale of oceanic eddies. Initially, NIWs make no contribution to the energy $\mathcal{H}$ which then purely consists of the mean-flow energy. As time progresses, the advection and refraction of the waves by the mean flow lead to a scalar cascade in the NIW field, producing horizontal scales similar to, or smaller than, the eddy scale. As a result, $|\nabla\chi|$ grows since $|\chi|$ is constrained by wave-action conservation. According to (4.14), the contribution of $|\nabla\chi|^2$ to the energy must be balanced by a decrease in the energy of the mean flow. Physically, the mechanism for this energy exchange is clear: as the horizontal scale of the NIWs decreases, their potential energy increases, necessarily at the expense of the mean energy since the NIW kinetic energy $f_0\mathcal{A}$ is conserved. This mechanism can be suggestively termed 'stimulated wave generation' to distinguish it from spontaneous generation (ruled out in our model) and complete an electromagnetic analogy [e.g. 13].

The explicit form of (4.14) and (4.15) enables us to make quantitative predictions. Suppose that the NIWs initially have a typical vertical scale m_0^{-1}, corresponding for example to the depth of the mixed layer. Suppose too that at some final time t, the various processes governing their dynamics have led to typical horizontal and vertical scales k^{-1} and m^{-1} and to typical amplitudes $|\chi|$. The conservation of wave action (4.15) implies that

$$\frac{f_0 m_0^2}{2}|\chi_0|^2 \approx \frac{f_0 m^2}{2}|\chi|^2. \tag{4.68}$$

Correspondingly, the kinetic energy of the NIW per unit volume, $\mathcal{K}_{\rm NIW} \approx f_0^2 m^2|\chi|^2/2$ remains unchanged. The potential energy, on the other hand, increases from 0 to $\mathcal{P}_{\rm NIW} \approx N^2k^2|\chi|^2/4$. We therefore conclude that the NIWs extracts from the mean-flow an energy

$$-\mathcal{E}_{\rm QG} = \mathcal{P}_{\rm NIW} = \frac{N^2k^2}{2f_0^2m^2}\mathcal{K}_{\rm NIW} = \frac{\epsilon^2}{2}\mathcal{K}_{\rm NIW} \tag{4.69}$$

per unit volume.

Since one of the main open questions in ocean dynamics concerns the dissipation of mesoscale energy, it is natural to ask whether the mechanism we have identified could be a significant contributor. Assuming that the process of NIW generation followed by their cascade to small scale occurs in a continuous fashion, (4.69) can be turned into an

expression for the power rate extracted from the mean flow,

$$-\dot{\mathcal{E}}_{\mathrm{QG}} = \frac{\epsilon^2}{2}\dot{\mathcal{K}}_{\mathrm{NIW}}, \tag{4.70}$$

where $\dot{\mathcal{K}}_{\mathrm{NIW}}$ is the power injected into NIWs by winds. Integrating over the whole ocean, this power is estimated as 0.6 TW in Wunsch and Ferrari [131]. It is unclear what a realistic value of $\epsilon^2/2$ might be: if we take k and m as representative of typical NIWs, $\epsilon^2/2 = \Delta\omega/f_0$ can be interpreted as the width of the inertial peak relative to f_0, and a value of $\epsilon^2/2 = 0.2$ is plausible. This leads to a sink of 0.12 TW, comparable, for instance, with the 0.1 TW estimated for the dissipation caused by bottom drag [131]. There is considerable uncertainty in these estimates however, in particular because it is not clear what the final values of k and m ought to be and whether the impact of NIWs is restricted to the upper parts of the ocean. Furthermore, the scale cascade can be expected to lead to values of $\epsilon^2/2$ that are not small, e.g. through the mechanism of wave capture [7, 24] which suggests that ϵ stabilises at $O(1)$ values. While our model ceases to be valid then – and the crucial feature of conserved wave kinetic energy ceases to hold – one can expect energy to be transferred from mean flow to the waves throughout the cascading process. Our argument above, necessarily limited to $\epsilon \ll 1$, may therefore underestimate the amount of energy extracted from the mean flow. It would certainly be valuable to test the efficiency of the process through detailed numerical simulations.

4.6 Two-dimensional models

In this section we discuss two two-dimensional models that are deduced from the YBJ-QG model under certain symmetry assumptions. These models are useful to study the NIW-mean interactions in a simplified context.

4.6.1 Slice model

Neglecting the β-effect, we consider solutions that are independent of y. This reduces (4.8) to

$$\chi_{zzt} + \frac{\mathrm{i}N^2}{2f_0}\chi_{xx} + \frac{\mathrm{i}}{2}(\psi_{xx}\chi_{zz} + \psi_{zz}\chi_{xx} - 2\psi_{xz}\chi_{xz}) = 0, \tag{4.71a}$$

$$\partial_t\left(\psi_{xx} + \partial_z\left(\frac{f_0^2}{N^2}\psi_z\right) + \frac{f_0}{4}(2|\chi_{xz}|^2 - \chi_{zz}\chi_{xx}^* - \chi_{zz}^*\chi_{xx})\right) = 0. \tag{4.71b}$$

Because advection disappears, (4.71b) can be integrated in time to provide the streamfunction in terms of χ, leaving (4.71a) as the sole prognostic equation.

We illustrate the interest of this model by presenting the result of a numerical simulation examining the impact of NIWs on a barotropic mean flow using a setup based on that of Balmforth et al. [9]. In this setup, NIWs initialised near the surface propagate vertically as a result of their interactions with the one-dimensional mean flow

$$\nabla^\perp \psi = (0, U_{\mathrm{QG}} \sin(2\pi x/L)), \tag{4.72}$$

where L is the length of the domain. The coupled model enables us to study the feedback of the NIWs on this mean flow.

We carried out simulations using a pseudospectral implementation of (4.71), with a domain $(x, z) \in [0, L] \times [-H, 0]$ where $L = 80$ km and $H = 4\,200$ m. The Coriolis frequency is taken as $f_0 = 10^{-4}\,\mathrm{s}^{-1}$ and a constant Brunt–Väisälä frequency $N = 8 \times 10^{-3}\,\mathrm{s}^{-1}$, somewhat smaller than that in [9], is used. The maximum mean velocity is $U_{\mathrm{QG}} = 0.08\,\mathrm{m\,s}^{-1}$. The NIWs are initially confined within the mixed layer with a characteristic depth $H_{\mathrm{m}} = 50\,\mathrm{m}$, with the form $\chi_{0z} = U_{\mathrm{NIW}} \exp(-(z/H_m)^2)$ where $U_{\mathrm{NIW}} = 0.8\,\mathrm{m\,s}^{-1}$. The corresponding dimensionless parameters are $\mathrm{Ro} = 0.01$, $\alpha = 0.1$ and $\epsilon = 0.05$, so $\mathrm{Ro}^{1/2} = \alpha \approx \epsilon$, consistent with our scaling assumptions.

Figure 4.3 shows the evolution of the change in mean energy, wave potential energy and total energy from their initial values in a 14-days simulation. Here, the mean and wave potential energies are the two terms

$$\frac{1}{2}\int \left(\psi_x^2 + \frac{f_0^2}{N^2}\psi_z^2\right) \mathrm{d}\boldsymbol{x} \quad \text{and} \quad \frac{N^2}{4}\int |\chi_x|^2 \,\mathrm{d}\boldsymbol{x} \tag{4.73}$$

which make up the constant total energy. The figure confirms that, overall, NIWs act as an energy sink for the mean flow. The net energy transfer from mean flow to NIWs is concentrated within the first 5 days; afterwards, the energy exchange is much smaller and its sign alternates. The NIW amplitude $|\chi_z|$ and the change in the mean velocity $V = \psi_x$ are shown in Figure 4.4. Their feedback results in a slowing down of the mean flow, consistent with the energy loss and collocated with the NIW wavepacket. An important feature of the mean-flow evolution is that it is reversible: at each location, the flow velocity returns to its initial value once the NIWs have propagated away. This is a particularity of the slice model, specifically of the diagnostic relation existing between the mean flow and the NIW amplitude. We next consider another two-dimensional model in which the NIW–mean-flow interactions lead to an irreversible behaviour.

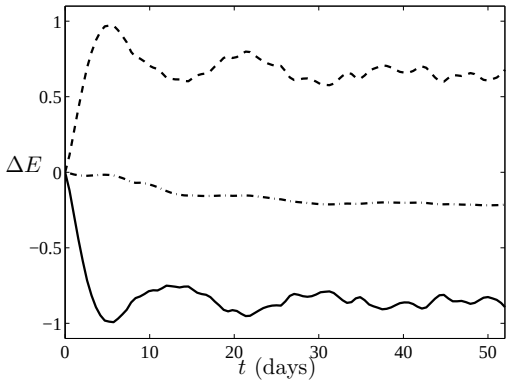

Figure 4.3: Energy exchange in the slice model: the changes in the mean energy (solid line), NIW energy (dashed line) and total energy (dotted line) are shown as functions of time. These energy changes are normalized by the initial mean flow energy in the mixed layer, $z \in [-50, 0]$ m. The increase of NIW (potential) energy is offset by a mean energy loss, resulting in a total energy that is conserved up to a small hyperviscous dissipation added for numerical stability.

4.6.2 Vertically plane wave

A simple two-dimensional model in the (x, y) plane is obtained by assuming that the wave field takes the form of a plane wave in the vertical, that is, $\chi_z = \varphi(x, y, t)\mathrm{e}^{\mathrm{i}mz}$ for some complex function φ and vertical wavenumber m. This is consistent with a barotropic mean flow $\psi = \psi(x, y, t)$. Introducing this restricted form of the solution into the coupled model (4.8) reduces it to

$$\partial_t \varphi + \partial(\psi, \varphi) + \mathrm{i}\beta y\varphi - \frac{\mathrm{i}N^2}{2m^2 f_0}\nabla^2\varphi + \frac{\mathrm{i}}{2}\nabla^2\psi\,\varphi = 0, \tag{4.74a}$$

$$\partial_t q + \partial(\psi, q) = 0, \tag{4.74b}$$

where

$$q = \beta y + \nabla^2\psi + \frac{\mathrm{i}f_0}{2}\partial(\varphi^*, \varphi) + \frac{f_0}{4}\nabla^2|\varphi|^2. \tag{4.75}$$

As an illustration, we consider the propagation of a vorticity dipole in a NIW field on the f-plane ($\beta = 0$). We carry out simulations initialising the streamfunction ψ to

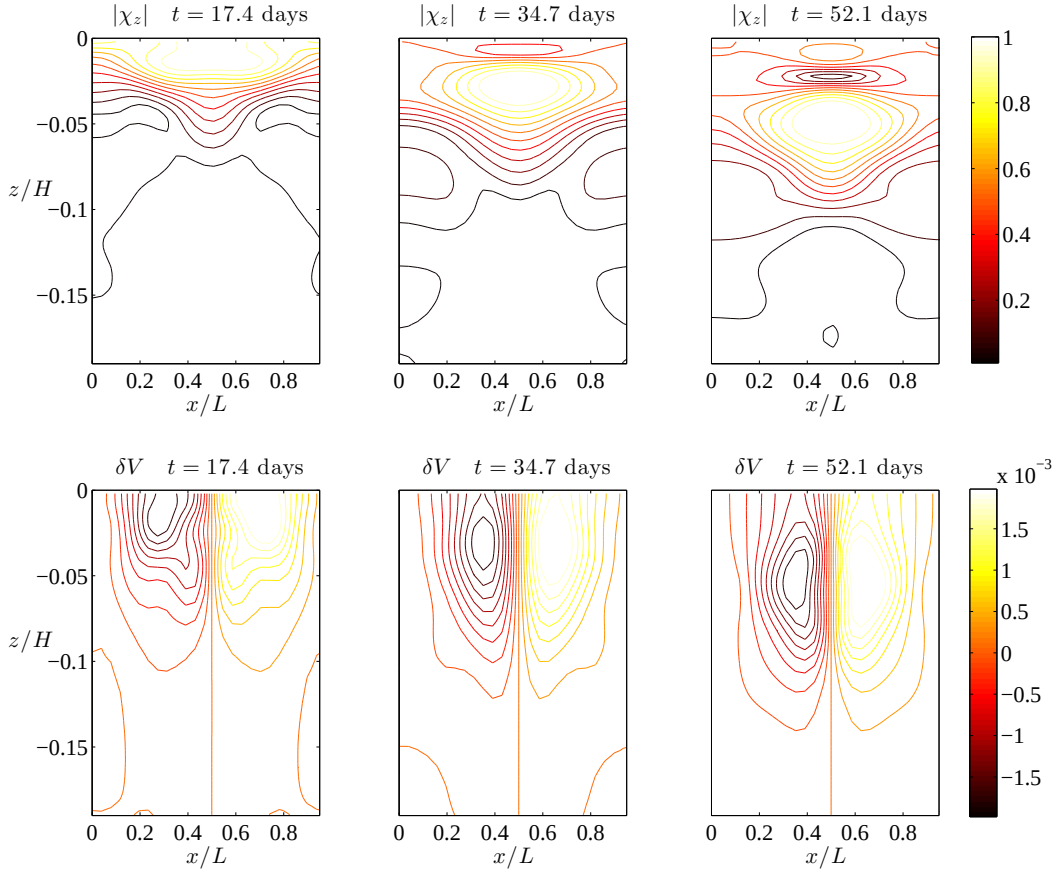

Figure 4.4: Wave amplitude $|\chi_z|$ (upper panels) and change in the mean velocity $V = \psi_x$ (lower panels) in the slice model. $|\chi_z|$ and V are nondimensionalized by αL and U_{QG}, respectively. The downward propagating NIWs induce a mean flow change, which slows down the original mean flow.

match the vorticity

$$\omega = \nabla^2\psi = \begin{cases} \dfrac{2kU}{J_0(\kappa a)} J_1(\kappa r)\sin\theta, & r < a \\ 0, & r > a \end{cases}, \tag{4.76}$$

of the Lamb [70] dipole propagating at speed U in the y-direction. Here (r, θ) are polar coordinates, a characterises the spatial scale of the dipole, J_n are the Bessel functions of the first kind of order n, and κ is determined by solving the matching condition $J_1(\kappa a) = 0$.

We carry out a numerical simulation in a periodic domain of size 500 km × 500 km using a pseudospectral method. Because of the periodisation, the vorticity (4.76) does not exactly correspond to that of a dipole steadily propagating a speed U; however, for the dipole size $a = 40\,\mathrm{km}$ that we take, the differences are minor. We take the other parameters to be $U = 0.05\,\mathrm{ms}^{-1}$, $f_0 = 10^{-4}\,\mathrm{s}^{-1}$, and $N = 0.01\,\mathrm{s}^{-1}$. Taking $L = a$ gives a Rossby number $\mathrm{Ro} = 0.0125$. The initial wave amplitude is chosen as the Gaussian

$$\varphi = A\mathrm{e}^{-(k_0(y-y_0))^2}, \tag{4.77}$$

where $A = 1.5\,\mathrm{km}$, $k_0 = 2 \times 10^{-5}\,\mathrm{m}^{-1}$ and $y_0 = 250$ km. This implies that $\alpha = A/L = 0.0375$ and $U_{\mathrm{NIW}} = 0.15\,\mathrm{m\,s}^{-1}$. The vertical scale of wave is taken as $m = 0.02\,\mathrm{m}^{-1}$, so $\epsilon = 0.125$. We therefore have that $\mathrm{Ro} < \alpha < \epsilon \approx \mathrm{Ro}^{1/2}$, consistent with our scaling. The initial position of the dipole ($r = 0$) and wavepacket (maximum of $|\varphi|$) are (0.5, 0.3) and $y = 0.5$ when distances are normalised by the domain size of 500 km.

We report the results of an integration time of $t = 1.5 \times 10^7\,\mathrm{s} \approx 173\,\mathrm{days}$, within which the dipole travels about $1\frac{1}{2}$ domain size. The changes in mean and wave energies (normalised by the initial mean energy) are shown as functions of time in Figure 4.5. As in the slice model, the increase of NIW energy is compensated by a loss of mean-flow energy. Using (4.69) and $\epsilon = 0.1$, we can estimate the relative mean energy change to be about 0.05, in agreement with the numerical results. The initial and final streamfunction ψ and wave amplitude $|\varphi|$ are shown in Figure 4.6. This also shows the trajectories of the vorticity maximum and minimum as an indication of the dipole's trajectory. The impact of the NIWs on the mean flow is obvious: instead of propagating in a straight line $x = \text{const.}$, the dipole deforms and is deflected to the left. This illustrates the irreversible nature of the wave–mean flow interactions when, unlike in the slice model, the potential vorticity is not constant.

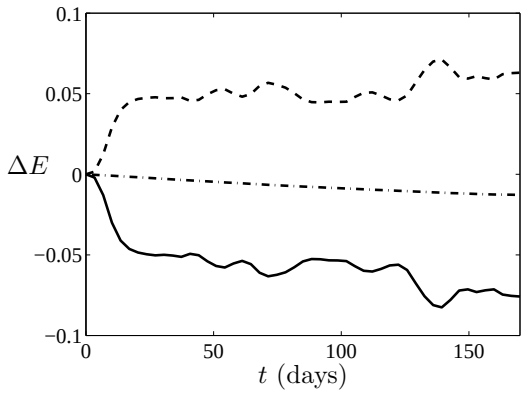

Figure 4.5: Same as Figure 4.3 but for the simulation of a vortex dipole propagating in a field of vertically travelling NIWs. The energy changes are normalized by the initial mean flow energy.

4.7 Discussion

In this chapter, we derive and study a model of the interactions between slow balanced motion and fast NIWs in the ocean. The model is obtained within the GLM framework [e.g. 22] or, more precisely, its glm variant [115], and neglects dissipative effects. In its simplest form (4.8), the model consists of the YBJ model of NIW propagation [137] coupled with a modified quasi-geostrophic equation. As expected from general GLM theory [23, 22, 108], the modification consists solely in a change in the relation between streamfunction and potential vorticity which adds to the standard QGPV a quadratic wave contribution.[2] Thus NIWs impact the dynamics of potential vorticity by changing its advection in what is, in general, an irreversible manner. The assumption that the waves are near inertial leads to drastic simplifications, reducing the wave part of the dynamics to the YBJ equation for a single (complex) amplitude χ evolving on the same time scale as the balanced flow.

Our YBJ-QG coupled model can be thought of as providing a parameterisation of NIW effects, with the fast NIWs regarded as a subgrid phenomenon in time. In this view, the YBJ is an asymptotically motivated closure for the NIWs: it provides enough information about the NIWs to compute their impact on the balanced flow. We emphasise that the derivation relies on a scale separation in time only and does not assume that the waves have a small spatial scales, unlike previous applications of

[2] A comparison between averaging formalisms (glm, GLM and others) in Appendix D shows that this wave contribution arises as the sum of the curl of a pseudomomentum, a wave-induced mean-stratification change and a mean-density change, with the exact form of each term depending on the formalism.

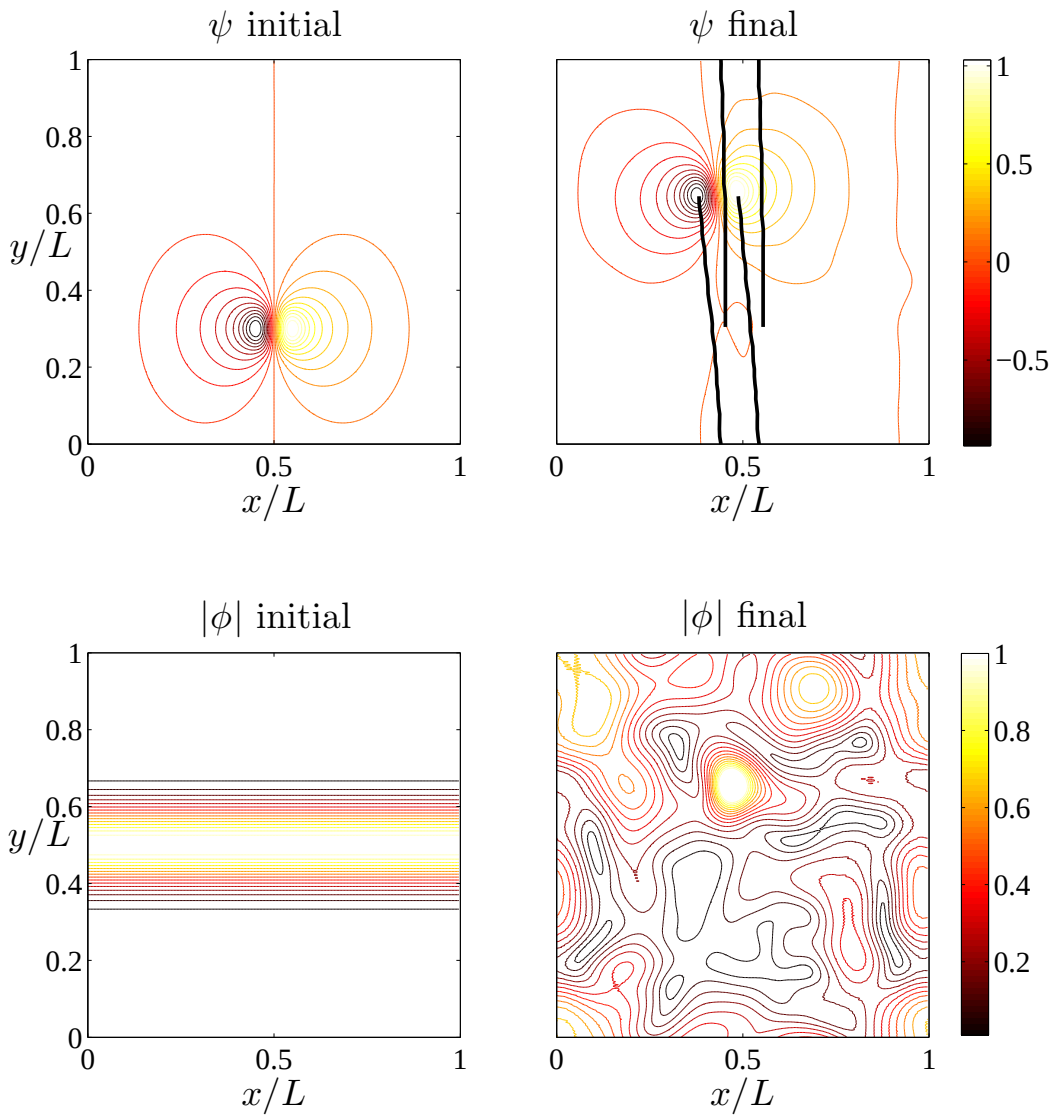

Figure 4.6: NIW-dipole interaction: initial (left panels) and final (right panels) stream-function ψ (top) and NIW amplitude $|\varphi|$ (bottom). Both ψ and $|\varphi|$ have been normalised by their maximum value at the initial time. The trajectories of the vorticity maximum and minimum shown by the thick black lines in the top right panel indicate the motion of the dipole during the simulation (colour online).

GLM [56, 23]. This is crucial for NIWs since they are forced by atmospheric winds at horizontal scales that are much larger than the oceanic mesoscales. It is also practically convenient since the YBJ and QG equations can be solved numerically on the same grid, so that the coupled model requires only about three times as much computational effort as the standard QG equation.

As discussed in § 4.2, the model is not fully consistent asymptotically. This is because the different aspect ratios it assumes for NIWs and balanced motion, specifically $m/k = \epsilon^{-1} N/f_0 \gg N/f_0$ and $L/H = O(N/f_0)$, cannot be expected to persist: the feedback of the NIWs implies that their aspect ratio is imprinted onto the balanced flow, leading to an increase in L/H and potentially to a breakdown of the assumption of order-one Burger number that underlies the quasi-geostrophic approximation. In practice this may not be significant: the NIWs contribute to the quasi-geostrophic velocity $\nabla^\perp\psi$ through a term that is twice smoother in the vertical than the NIWs amplitude χ_z itself (because of the Helmholtz inversion in (4.10)). As a result, short vertical fluctuations in χ_z have a limited impact on $\nabla^\perp\psi$. Furthermore, in the case of locally planar NIWs, it is the envelope scale that is imprinted onto $\nabla^\perp\psi$ rather than the (much shorter) wavelength. Finally, the existence of a coupled YBJ–primitive-equation model with conservations of potential vorticity, energy and action analogous to those of the YBJ-QG model suggests that conclusions inferred from the latter model are robust.

In this chapter, we discuss some qualitative aspects of the interactions between balanced flow and NIWs in the ocean, mostly based on the remarkably simple action and energy conservation laws of the YBJ-QG model. The conservation of action implies the complete absence of spontaneous NIW generation in the model, consistent with the expected exponentially smallness of this phenomenon [123]. The conservation laws further indicate that NIWs forced at large scales by atmospheric winds provide an energy sink for the oceanic balanced motion through a mechanism that can be termed 'stimulated wave generation'. This is potentially significant: several mechanisms have been proposed to explain the dissipation of mesoscale energy but it is far from clear whether they are efficient enough to balance the flux imposed by the energy source (mainly baroclinic instability). We offer a rough estimate of the power extracted from the mean flow by the mechanism we have identified; this suggests that further consideration is worthwhile. More reliable estimates would require intensive numerical simulations of the YBJ-QG or of the primitive equations and are well beyond the scope of this chapter.

Chapter 5

Topographic wave-shear flow interaction

In the previous chapter 4 we studied the interactions between NIWs and mean flow in an inviscid setup relevant to the large spatial scales of geophysical flows. Even though it is true that the spatial scales of geophysical fluids are usually large enough that viscosity can be omitted, flows often evolve into small-scale structures where viscous dissipation becomes important. Even though small-scale structures are typical in the turbulent flows in geophyysical fluids, such as geostrophic turbulence [103] and turbulence in the mixed-layer [32], they also arise in much simpler situations. One example is wave propagation in a nonuniform medium, when refraction can lead to wavenumbers that are much larger than that of the wave source. Considering IGWs with a nonzero background mean flow, e.g. a x-directional flow, the dispersion relation (4.1) becomes

$$\omega = Uk \pm \sqrt{f_0^2 + \frac{N^2|\boldsymbol{k}|^2}{m^2}}. \tag{5.1}$$

This dispersion relation exhibits a singularity with the vertical wavenumber $m \to \infty$ whenever the relation $\omega = Uk \pm f_0$ is satisfied. When this happens the infinitely small wavelength makes viscous effects unavoidable. In reality, the scenario is more complicated because nonlinearity can become important too, something that we do not consider here (see [50] for a reference).

Different kinds of IGWs can be classified according to their sources. In this chapter we focus on the all-important IGWs generated by topography, the so-called mountain or lee waves. In the atmosphere, topographic IGWs are often observed to influence cloud patterns [129]; they are the main mechanism for transporting momentum from the tro-

posphere to the stratosphere and higher up [50]. In the ocean, energy is transferred from large-scale flows to IGWs mainly through the process of IGW generation by topography at the bottom. The dominant flow, tidal oscillations and geostrophic mean flow generate, two kinds of IGWs, tidal IGWs and lee waves. In numerical simulations the energy transferred to the tide IGWs and lee waves is about 1 TW [130] and 0.2 – 0.4 TW (the last two value are estimated by Nikurashin and Ferrari [94] and Scott et al. [109]).

In this chapter, we study steady ($\omega = 0$) topographic IGWs and their interactions with the unidirectional uniform shear flow $U = \Lambda z$. Thus, from (5.1) the singularities can be calculated explicitly. When rotation is negligible, $f_0 = 0$, the singularity is the critical level at $z = 0$; when $f_0 \neq 0$, there are two singularities at the inertial levels with $z = \pm f_0/(k\Lambda)$. Because of viscous effects the wave behaviour has a dramatic change across these singularities. Specifically, considering the wave-mean flow interaction we care about, there is a decrease in the wave (pseudo)momentum flux (ref. [85] for clarifying the nomenclatures), which has a large effect on the mean flow. Thus, the viscosity affects the mean flow in an indirect way, through its influence on IGWs which plays the role of a catalyst. An example of mean flow generation is the quasi-biannual oscillation forced by gravity waves and Kelvin waves around critical levels, which is one of the most remarkable flow pattern in the tropical stratosphere. (See [8] for a review.)

The interaction between IGWs and mean flow is not only theoretically interesting but also practically useful. IGWs are important for large-scale geophysical fluid dynamics; but, as a sub-grid phenomenon, they have to be parameterized in the atmospheric and oceanic models. So the results of this chapter could lead to new topographic wave parameterization in numerical models.

5.1 Introduction

Inertia-gravity wave (IGW), a class of geophysical fluid waves maintained by the restoring force due to both Coriolis effects and density stratification, is important for the large-scale circulation in both the atmosphere [50] and oceans [130, 94, 109]. Eliassen and Palm [46] pioneered the IGW-mean flow interaction by studying the lee-wave-generating mean flow; the non-dissipative interaction between a non-inertial gravity wavepacket and a mean flow was first studied by Bretherton [19]. Practically, in general circulation models, the IGWs are a sub-grid phenomena that needs to be parameterized [90, 78], so it is important to study the mean effect due to IGWs theoretically.

Among the many mechanisms of IGW generation – topography, convection, shear instability, jet-front systems and loss of balance – this chapter focuses on topographic

lee IGWs generated by shear flow. IGWs in a shear flow have been intensively studied in the literature. On the one side, the shear flow can modify the propagation of IGW packets [20, 67], on the other side, in addition to the mean-flow generation, the IGWs are considered as the main object responsible for the shear flow instability [88, 89]. An exact solution of IGW propagating in shear flow has been obtained by Yamanaka and Tanaka [135], and in the large Richardson number limit Lott et al. [80] use the WKB approximation, which is the theoretical foundation of this paper.

The singularities – the critical level with zero shear flow and the two inertial levels where the Doppler-shifted phase velocity matching the Coriolis frequency – are important for the wave behaviour. The IGWs tends to break around singularities through the mechanism such as instability and onset of turbulence. We are going to apply the breaking mechanism in the zero-viscosity limit introduced by Bretherton [20], where the wave absorption is manifested by the branch choice through an infinitesimal imaginary wave frequency.

These singularities are also crucial for wave-mean flow interaction. For an inviscid fluid, i.e. if there is no singularity, the zonal averaged Eliassen-Palm (EP) flux is conserved due to the symmetry of background flow (e.g. [46, 5, 58]), so the divergence of an EP flux is zero and therefore the wave does not influence the mean flow. This conclusion is understood as the non-acceleration theorem in literature [25]. When singularities exist, the wave momentum (or EP flux or pseudomomentum, see [22] for a reference) is not conserved when crossing or being reflected by the singularities. Booker and Bretherton [16] studied the non-inertial gravity wave and they concluded that the vertical momentum flux[1] of the gravity wave (GW) packet is preserved until it reaches the critical level; and when the gravity wave is stable, where the Richardson number Ri is larger than 1/4 [88], the amplitude of GW is attenuated by a factor of $e^{-2\pi\sqrt{\mathrm{Ri}-1/4}}$ after crossing the critical level. Parallel to the momentum flux of the GW packet, angular-momentum flux of an IGW packet is preserved when it is away from the singularities [67]. Here the angular-momentum flux is identical with the EP flux and pseudomomentum, which can be understood as the Lagrangian mean momentum of IGWs [120]. Similar as in the GW situation, it is calculated by Lott et al. [79, 80] in the large Richardson number limit that across the inertial level, the EP flux of IGWs has an attenuation proportional to $e^{-\pi\sqrt{\mathrm{Ri}}}$ in two-dimensional case. This consistency of IGW and GW attenuation can be understood by the contour integration in the complex domain [81].

In order to understand the dynamics of the IGW and the mean flow generation in

[1] In the original paper of Booker and Bretherton [16], they use the word "momentum", but in the wave-mean flow interaction context the "momentum flux" is a more suitable word (Ref. [85]).

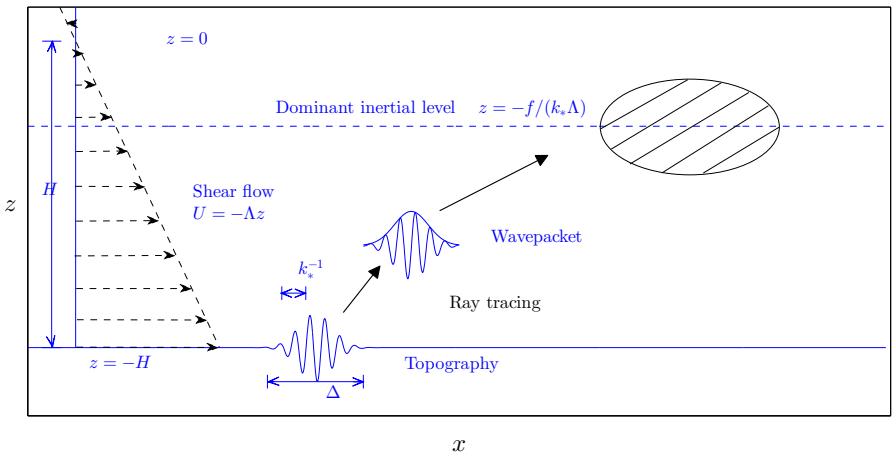

Figure 5.1: Schematic representation of the topographic wave-shear mean flow interaction seen in the $x - z$ intersection.

the vicinity of the inertial levels, this chapter considers the interaction between a steady topographic wave generated by a multiscale mountain and an unidirectional uniform-shear mean flow. The design of this new setup stems from two considerations – the capture of spatial structures and finite amplitude wave force on a mean flow. The first point is achieved by considering the multiscale mountain, which generates a multiscale topographic wavepacket, which is the difference between our setup and the one by Shutts [113]. Then we can obtain large-scale flow structures by applying small-scale averaging. The sudden change of wave behaviour across the singularities induce local force on the mean flow, so one way to avoid singular force is to separate locations of singularities of different wavenumbers. In our setup, the combination of rotation and shear flow realizes this idea.

The structure of this chapter is as follows. We formulate the problem in Section 5.2; In Section 5.3 we approximate the wave expression in different regimes using a steepest descent method. In Section 5.4 we use the approximated wave solutions to calculate the EP flux and then solve the mean quasi-geostrophic potential vorticity equation to obtain the mean-flow response. Finally, we summarize and discuss our results in Section 5.5.

5.2 Formulation

In this chapter we consider the interaction between a steady topographic wave and a backward uniform-shear flow in the idealized setup shown in Fig. 5.1. The background

flow is chosen as a unidirectional uniform shear flow $\boldsymbol{U}_0 = (U_0, 0)$ where $U_0 = -\Lambda z$ ($\Lambda > 0$). The distance between the zero background velocity level (critical level) and the bottom boundary is H. It is proven convenient to use a slightly unusual vertical coordinate such that $z = 0$ and $z = -H$ correspond to the critical level and bottom boundary, respectively. The topographic wave is generated by the idealised multiscale mountain with height

$$\begin{aligned} h_{\mathrm{t}}(x,y) &= \mathrm{Re}\left\{h\mathrm{e}^{-(x^2+y^2)/(2\Delta^2)}\mathrm{e}^{\mathrm{i}\boldsymbol{k}_*\cdot\boldsymbol{x}}\right\} \\ &= \frac{\Delta^2 h}{2\pi}\mathrm{Re}\left\{\int_{-\infty}^{\infty}\int_{-\infty}^{\infty}\mathrm{e}^{-|\boldsymbol{k}-\boldsymbol{k}_*|^2\Delta^2/2}\mathrm{e}^{\mathrm{i}\boldsymbol{k}\cdot\boldsymbol{x}}\mathrm{d}k\mathrm{d}l\right\}, \end{aligned} \tag{5.2}$$

where $\boldsymbol{x} = (x, y)$, $\boldsymbol{k} = (k, l)$, $\boldsymbol{k}_* = (k_*, l_*)$ is the dominant wave vector, h is the characteristic height of topography and Re denotes the real part. Here k_*^{-1} and Δ control the scale of the oscillation and envelope scale of the topography so that the parameter $k_*\Delta \gg 1$ characterize their separation. In Fig. 5.1 the shaded ellipse indicates the region where the wave influence the men flow, and dynamics of the wave and mean flow is what we focus on.

The fluid satisfies the f-plane hydrostatic Boussinesq equations

$$\partial_t\mathbf{u} + \mathbf{u}\cdot\nabla\mathbf{u} + w\partial_z\mathbf{u} + f\boldsymbol{e_z}\times\mathbf{u} = -\nabla\phi, \tag{5.3a}$$

$$\partial_z\phi = b, \tag{5.3b}$$

$$\partial_t b + \mathbf{u}\cdot\nabla b + w\partial_z b + N^2 w = 0, \tag{5.3c}$$

$$\nabla\cdot\mathbf{u} + \partial_z w = 0, \tag{5.3d}$$

where $\mathbf{u} = (u, v)$ is the horizontal velocity, w the vertical velocity, ϕ a scaled pressure, b the buoyancy, f the local Coriolis frequency, $\boldsymbol{e_z}$ the unit vertical vector pointing upward, N the Brunt-Väisälä frequency taken to be a constant, and $\nabla = (\partial_x, \partial_y)$ is the horizontal gradient.

We apply the zero normal flow boundary condition at the bottom boundary:

$$w = \mathbf{u}_{\mathrm{b}}\cdot\nabla h_{\mathrm{t}} \quad \text{at} \quad z = -H + h_{\mathrm{t}}, \tag{5.4}$$

where the subscript "b" denotes the value on the bottom boundary.

5.3 Wave solution

5.3.1 Preliminaries

In this paper we consider small-amplitude waves such that the wave governing equations are obtained by linearizing the primitive equations (5.3) around the background state. We take small Rossby number $\mathrm{Ro} = U_\mathrm{b}/(f\Delta) \ll 1$ where Δ is taken as the mean horizontal scale, the scale of the range of the mountain, so the leading background flow is in geostrophic balance, hence the prescribed background shear flow corresponds to the state:

$$U_0 = -\partial_y \Psi_0, \quad V_0 = \partial_x \Psi_0, \quad W_0 = 0, \quad B_0 = f\partial_z \Psi_0, \quad \Phi_0 = f\Psi_0, \quad \text{and} \quad \Psi_0 = \Lambda yz. \tag{5.5}$$

We consider a distinguished regime where the advection and Coriolis effect are of the same order, so when the background flow velocity is characterized by the value at the bottom boundary this distinguished regime indicated that $\mathrm{Ro} = O((k_*\Delta)^{-1})$. Therefore the leading order equations governing the waves are

$$\partial_t \mathbf{u}_1 - \Lambda z \partial_x \mathbf{u}_1 + \Lambda w_1 \boldsymbol{e_x} + f\boldsymbol{e_z} \times \mathbf{u}_1 = -\nabla \phi_1, \tag{5.6a}$$

$$\partial_z \phi_1 = b_1, \tag{5.6b}$$

$$\partial_t b_1 - \Lambda z \partial_x b + f\Lambda v + N^2 w_1 = 0, \tag{5.6c}$$

$$\nabla \cdot \mathbf{u}_1 + \partial_z w_1 = 0. \tag{5.6d}$$

where $\nabla = (\partial_x, \partial_y)$ is the horizontal gradient, $\boldsymbol{e_x}$ is the x-component unit vector and the subscript "1" denotes the leading order wave.

The amplitude of the wave is found from the linearization of the boundary condition (5.4):

$$w_1 = U_\mathrm{b} \partial_x h_t, \tag{5.7}$$

where $U_\mathrm{b} = \Lambda H$ is the background velocity at the bottom boundary. From the governing equations (5.6a)–(5.6d) the horizontal wave velocity is estimated as $u_1 = O(N/(k_* U_\mathrm{b}) w_1)$, then considering $w_1 = O(U_\mathrm{b} k_* h)$ obtained from the boundary condition (5.7), we obtain $u_1 = O(Nh)$. So the small amplitude wave $u' \ll U_\mathrm{b}$ requires that

$$\frac{Nh}{U_\mathrm{b}} = J\frac{h}{H} \ll 1, \tag{5.8}$$

which is the inverse of Froude number. Here $J = N/\Lambda = \mathrm{Ri}^{1/2}$ with Ri the Richardson

number. Based on this small parameter we introduce the convection of subscript "i" ($i = 1, 2, 3 \dots$) denoting the flow of ith order such that

$$u_i = O\left(\left(J\frac{h}{H}\right)^i U_\mathrm{b}\right). \tag{5.9}$$

Applying a Fourier transform and manipulating simplifies (5.6) into the single equation

$$\frac{1-\zeta^2}{\zeta^2}\hat{w}_{\zeta\zeta} - \left(\frac{2}{\zeta^3} - \frac{2\mathrm{i}\nu}{\zeta^2}\right)\hat{w}_\zeta - \left(\frac{(1+\nu^2)J^2}{\zeta^2} + \frac{2\mathrm{i}\nu}{\zeta^3}\right)\hat{w} = 0, \tag{5.10}$$

where $\nu = l/k$. This equation is identical to (4) in [135]. The independent variable is $\zeta = -k\Lambda z/f$ which is a scaled vertical coordinate, and $\hat{w}$ is the horizontal Fourier transform of w_1, such that:

$$w_1 = \frac{1}{2\pi}\int_{-\infty}^{\infty}\int_{-\infty}^{\infty}\hat{w}(k,l)\mathrm{e}^{\mathrm{i}\boldsymbol{k}\cdot\boldsymbol{x}}\mathrm{d}k\mathrm{d}l. \tag{5.11}$$

The other dependent variables are linked to $\hat{w}$ through the polarization relations

$$\hat{u} = \mathrm{i}\frac{-\Lambda}{f}\left(\frac{\zeta - \mathrm{i}\nu}{\zeta(1+\nu^2)}\hat{w}_\zeta + \frac{\nu^2}{\zeta(1+\nu^2)}\hat{w}\right), \tag{5.12a}$$

$$\hat{v} = \frac{\Lambda}{f}\left(\frac{1 - \mathrm{i}\nu\zeta}{\zeta(1+\nu^2)}\hat{w}_\zeta + \frac{\mathrm{i}\nu}{\zeta(1+\nu^2)}\hat{w}\right), \tag{5.12b}$$

$$\hat{b} = \mathrm{i}\frac{\Lambda^2}{f}\left(\frac{1 - \mathrm{i}\nu\zeta}{\zeta^2(1+\nu^2)}\hat{w}_\zeta + \left(\frac{\mathrm{i}\nu}{\zeta^2(1+\nu^2)} + \frac{\mathrm{Ri}}{\zeta}\right)\hat{w}\right). \tag{5.12c}$$

One of the key characteristics of IGWs in shear flow is the possible existence of singularities: the two inertial levels, where the Doppler-shifted phase velocity matches the background velocity, and the critical level, where the backgroud velocity vanishes. These singularities can be identified from the wave equation (5.10) with the two inertial levels and critical level corresponding to $\zeta = \pm 1$ and $\zeta = 0$, respectively. The critical level is an apparent singularity that can be removed by Galilean transform. The exact solution of (5.10) is obtained by Yamanaka and Tanaka [135], and it indicates that for a single frequency the wave properties, such as wave amplitude, differ in different regions divided by the singularities. And as we will point out in §5.4, this sudden change of wave properties due to singularities is the main reason for wave forcing the mean flow. When there is no rotation, only one critical level exists[2], and so because of the independence of the critical level on wavenumber, different wavenumbers have

[2] We can also think that the two inertial level and the critical coincide.

the same singularity. But it is not the same here where rotation is not negligible. Our specific topographic wave problem hinges on the inertial levels closer to topography, with $\zeta = 1$. The difference between the critical level and inertial level is that because the independent variable ζ depends on both k and z and is rescaled by Λ/f, the shear flow with rotation separates the inertial levels of different wavenumbers in a wavepacket into different vertical positions. So corresponding to the characteristic wavepacket spectrum width, these vertical positions expand to an inertial layer with a characteristic thickness:

$$\delta_* = -\frac{z_*}{k_*}\delta k = \frac{f}{k_*^2 \Lambda \Delta}, \tag{5.13}$$

where we have taken into account that in the topography expression (5.2) the wavepacket width in spectral space $\delta k = O(\Delta^{-1})$, and

$$z_* = -\frac{f}{k_* \Lambda} \tag{5.14}$$

denotes the dominant inertial level where the wave with single dominant wavenumber k_* reaches its inertial level. In Section 5.4, we will show that for a uniform-shear background flow, in contrast to the no rotation situation, wave force on the mean flow is not singular in the finite-thickness inertial layer when rotation is considered. The similar idea of smearing the singularities across different altitudes can also be applied to the non-rotational case, for which the background flow is chosen to be a more complicate flow, such as the directional shear flow in [83].

Even though the wave equation (5.10) is linear, the singularities make the wave expression non-trivial. As pointed out by Lott et al. [80], the single-frequency wave solution is well expressed by WKB approximation in large Richardson number limit. We approximate the wave solution based on their results in the scalings

$$J = O(k_* \Delta) \quad \text{and} \quad \mathrm{Ro} = O((k_* \Delta)^{-1}), \tag{5.15}$$

where the former, large Richardson number validates the WKB approximation[3] and the latter as we discussed ensures the distinguished regime of wave dynamics. In our specific setup we further require that $\mathrm{Ro} k_* \Delta > 1$ to ensure that $z_* > -H$, so the dominant inertial level is above the bottom topography.

Using the WKB approximation by Lott et al. [80], the wave's vertical structure function calculated from (5.10) can be expressed in different regions. In the region $\zeta > 1$

[3] We can also choose a different scaling $J = O((k_* \Delta)^\gamma)$ with $\gamma > 0$, but here we choose $\gamma = 1$ as a specific example to carry out approximations and for different γ's the calculations are similar.

we obtain

$$\tilde{w} = \frac{\zeta}{\zeta_\mathrm{b}} \left(\frac{\zeta_\mathrm{b} - 1}{\zeta - 1} \right)^{1/4 - \mathrm{i}\nu/2} \left(\frac{\zeta_\mathrm{b} + 1}{\zeta + 1} \right)^{1/4 + \mathrm{i}\nu/2} \mathrm{e}^{-\mathrm{i}J\sqrt{1+\nu^2}\left(\ln(\zeta + \sqrt{\zeta^2 - 1}) - \ln(\zeta_\mathrm{b} + \sqrt{\zeta_\mathrm{b}^2 - 1})\right)} \tag{5.16}$$

where $\zeta_\mathrm{b} = k\Lambda H/f$. Even though we consider a steady wave, we need to choose the branch corresponding to upward group velocity – in the exponential of (5.16) the minus sign is chosen instead of a plus – to be physically sensible in the perspective of steady wave generation. This branch choice is a consequence of the assumption that the far-field wave condition above the singularity only contains an upward propagating wave. In fact we can choose different far-field conditions or boundary conditions to include wave reflection, but because the wave field is linear it will only digress us from our aim of understanding the wave and mean flow behaviour around the singularities. In the vicinity of $\zeta = 1$, specifically $|\zeta - 1| = O(J^{-2})$, $\hat{w}$ is expressed by Hankel functions. And when $\zeta < 1$, $\hat{w}$ is exponentially small.

Substituting the topography expression (5.2) into the boundary condition (5.7) we obtain the spectral expression of the wave boundary condition:

$$w_{1\mathrm{b}} = \frac{U_\mathrm{b} h \Delta^2}{2\pi} \int_{-\infty}^{\infty} \int_{-\infty}^{\infty} \mathrm{i}k \mathrm{e}^{-|\boldsymbol{k} - \boldsymbol{k}_*|^2 \Delta^2/2} \mathrm{e}^{\mathrm{i}\boldsymbol{k}\cdot\boldsymbol{x}} \mathrm{d}k\mathrm{d}l, \tag{5.17}$$

so the wavepacket solution can be expressed by the using the WKB result (5.16) as

$$w_1 = \frac{\mathrm{i}U_\mathrm{b} h \Delta^2}{2\pi} \int_{-f\Lambda^{-1}z^{-1}}^{\infty} \int_{-\infty}^{\infty} k \mathrm{e}^{-|\boldsymbol{k} - \boldsymbol{k}_*|^2 \Delta^2/2} \tilde{w} \mathrm{e}^{\mathrm{i}\boldsymbol{k}\cdot\boldsymbol{x}} \mathrm{d}k\mathrm{d}l. \tag{5.18}$$

Here, from the definition of inertial level – $\zeta = 1$ – the integration limit $(-f\Lambda^{-1}z^{-1}, \infty)$ captures the wavenumbers whose inertial level above z with an omission of high order terms. The exponentially small $\zeta < 0$ contribution is directly neglected, while the $|\zeta - 1| = O(J^{-2})$ contribution is neglected because the region is of high order smaller than the effective integration region which we will verify later, and the Hankel function does not contain singularity in this region. This wavenumber truncation approximates the branch choice with the minus sign in the exponential of (5.16) across the inertial level when the terms in the square root become negative, so with an exponentially small error the lower integration limit can be replaced by $-\infty$. This phenomenon of wave absorption across the singularity further results in EP flux loss, which is crucial for topographic wave–shear mean flow interaction.

5.3.2 Approximated solution

The wave solution (5.18) can be further simplified by taking advantage of the assumptions $J \gg 1$ and $k_*\Delta \gg 1$ to apply a steepest descent method. The key is of course to identify the dominant terms in the argument of the exponential functions. To avoid defining several new nondimensionless numbers for the relations of J, $k_*\Delta$ and Ro, it is expedient to introduce a bookkeeping parameter ϵ which keeps track of the size of the various terms. This parameter is treated as formally small and used as a basis for the steepest descent method, but at the end of the computation it can be set to 1 to obtain convenient asymptotic formulas. Here we need to emphasize that this bookkeeping parameter is different from the nondimensional parameters, where the former is simply a mark to remind the orders of different terms while the latter are real parameters controlling the system. In our specific problem the bookkeeping parameter is introduced through the changes

$$k_*\Delta \mapsto \epsilon^{-1}k_*\Delta, \quad J \mapsto \epsilon^{-1}J \quad \text{and} \quad \mathrm{Ro} \mapsto \epsilon\mathrm{Ro}, \tag{5.19}$$

corresponding to topographic scale separation, large Richardson number and small Rossby number, separately.

Thus the solution of w_1 (5.18) can be expressed as

$$w_1 = \frac{\mathrm{i}U_\mathrm{b}hk_*\Delta^2}{2\pi\epsilon}\int_{-f\Lambda^{-1}z^{-1}}^{\infty}\int_{-\infty}^{\infty}\mathrm{e}^{-|\boldsymbol{k}-\epsilon^{-1}\boldsymbol{k}_*|^2\Delta^2/2}\hat{w}\mathrm{e}^{\mathrm{i}\boldsymbol{k}\cdot\boldsymbol{x}}\mathrm{d}k\mathrm{d}l, \tag{5.20}$$

where

$$\hat{w} = \frac{\zeta}{\zeta_\mathrm{b}}\left(\frac{\zeta_\mathrm{b}-1}{\zeta-1}\right)^{1/4-\mathrm{i}\nu/2}\left(\frac{\zeta_\mathrm{b}+1}{\zeta+1}\right)^{1/4+\mathrm{i}\nu/2}\mathrm{e}^{-\mathrm{i}\epsilon^{-1}J\sqrt{1+\nu^2}\left(\ln(\zeta+\sqrt{\zeta^2-1})-\ln(\zeta_\mathrm{b}+\sqrt{\zeta_\mathrm{b}^2-1})\right)},$$

and we have estimated the leading order spatial derivation by the dominant wavenumber which is latter justified by detailed calculations proofing that the integration is controlled by a wavenumber close to k_*.

A first approximation of (5.20) can be made by carrying out the integration with respect to l, noting that $\hat{w}$ is independent of l. Because the wavepacket is localised in frequency space we can rewrite the l-component wavenumber as

$$l = \epsilon^{-1}l_* + L, \tag{5.21}$$

where $\epsilon L/l_* \ll 1$, leading to the following expressions

$$\nu = \frac{l_*}{\epsilon k}\left(1+\epsilon\frac{L}{l_*}\right), \tag{5.22}$$

$$\sqrt{1+\nu^2} = \sqrt{1+\left(\frac{l_*}{\epsilon k}\right)^2}+\epsilon\frac{l_* L}{\epsilon k\sqrt{(\epsilon k)^2+l_*^2}}+O\left(\left(\epsilon\frac{L}{l_*}\right)^2\right), \tag{5.23}$$

where ϵk is not a small term since k is centred around $\epsilon^{-1}k_*$.

After substituting the above expansion (5.23) and truncating until $O((\epsilon L/l_*)^2)$, (5.20) can be expressed as

$$\begin{aligned} w_1 = {} & \frac{\mathrm{i}U_\mathrm{b}hk_*\Delta^2}{2\pi\epsilon}\int_{-f\Lambda^{-1}z^{-1}}^{\infty}\int_{-\infty}^{\infty} \mathrm{e}^{-(\Delta L)^2/2-\mathrm{i}\frac{Jl_*}{\epsilon k\sqrt{(\epsilon k)^2+l_*^2}}D(\zeta)L+\mathrm{i}Ly}\mathrm{d}L \\ & \times \mathrm{e}^{-(k-\epsilon^{-1}k_*)^2\Delta^2/2}\frac{\zeta}{\zeta_\mathrm{b}}\left(\frac{\zeta_\mathrm{b}-1}{\zeta-1}\right)^{1/4-\mathrm{i}\nu_*/2}\left(\frac{\zeta_\mathrm{b}+1}{\zeta+1}\right)^{1/4+\mathrm{i}\nu_*/2}\mathrm{e}^{-\mathrm{i}J\epsilon^{-1}\sqrt{1+\left(\frac{l_*}{\epsilon k}\right)^2}D(\zeta)+\mathrm{i}kx}\mathrm{d}k \\ \doteq {} & \frac{\mathrm{i}U_\mathrm{b}hk_*\Delta}{\epsilon\sqrt{2\pi}}\int_{-f\Lambda^{-1}z^{-1}}^{\infty}\mathrm{e}^{-\frac{1}{2\Delta^2}\left(y-\frac{Jl_*}{\epsilon k\sqrt{(\epsilon k)^2+l_*^2}}D(\zeta)\right)^2} \\ & \times \mathrm{e}^{-(k-\epsilon^{-1}k_*)^2\Delta^2/2}\frac{\zeta}{\zeta_\mathrm{b}}\left(\frac{\zeta_\mathrm{b}-1}{\zeta-1}\right)^{1/4-\mathrm{i}\nu_*/2}\left(\frac{\zeta_\mathrm{b}+1}{\zeta+1}\right)^{1/4+\mathrm{i}\nu_*/2}\mathrm{e}^{-\mathrm{i}J\epsilon^{-1}\sqrt{1+\left(\frac{l_*}{\epsilon k}\right)^2}D(\zeta)+\mathrm{i}kx}\mathrm{d}k, \end{aligned} \tag{5.24}$$

where

$$D(\zeta) = \ln(\zeta+\sqrt{\zeta^2-1})-\ln(\zeta_\mathrm{b}+\sqrt{\zeta_\mathrm{b}^2-1}), \tag{5.25}$$

and the symbol "$\doteq$" denotes the equality of amplitude, specifically, here in (5.24) the difference between the l.h.s. and the r.h.s. is $\mathrm{e}^{\mathrm{i}\epsilon^{-1}l_*y}$. Here all the ν's are approximated by $\nu_* = l_*/k_*$ except the one in the exponential with a ϵ^{-1} in front because the wavepacket is concentrated around k_*. We introduce this amplitude equality because instead of the phase the wave amplitude not only reveals the shape of the wave but also is crucial for wave-mean flow interaction: the spatial averaged EP flux, which is quadratic in wave quantities, only depends on the amplitude of wave.

The appearance of bookkeeping parameter ϵ^{-1} in the exponential in expression (5.24) motivates a saddle point approximation. Specifically, we need to compare the following leading terms in the exponentials:

$$(k-\epsilon^{-1}k_*)^2\Delta^2/2 \quad \text{and} \quad \mathrm{i}J\epsilon^{-1}\sqrt{1+\left(\frac{l_*}{\epsilon k}\right)^2}D(\zeta), \tag{5.26}$$

where the first term comes from the topographic-spectrum width and the $\zeta(z)$-dependent second term capture the vertical wave structure.

Our next step is to find the distinguished regimes where the leading order terms in (5.26) balance. First, we need to approximate $D(\zeta)$ to determine its order. This approximation is not trivial since $D(\zeta)$ has different orders depending on the range of ζ, so we will obtain different distinguished regimes with different height ranges. Mathematically, different height ranges can be captured by different values of α in the following expansion of z

$$z = z_* \left(1 + \left(\frac{\epsilon}{k_*\Delta}\right)^{\alpha} Z\right), \tag{5.27}$$

where $Z = O(1)$ and because of the introduction of bookkeeping parameter $z_* = -\epsilon f/(k_*\Lambda)$. This expansion captures the distance to the dominant inertial level: the larger α the closer it is to the dominant region. It is important to note that Z and z have a sign difference.

Because of the k and z dependence of ζ, we also need to expand k to find the dominant range in the wavenumber space. Since the wavepacket is concentrated around k_*, the wave number k can be expressed as

$$k = \epsilon^{-1} k_* \left(1 + \left(\frac{\epsilon}{k_*\Delta}\right)^{\beta} K\right) \quad \text{with} \quad K = O(1) \quad \text{and} \quad \beta \geq 0. \tag{5.28}$$

Combining the z expansion (5.27) and the k expansion (5.28) we obtain

$$\zeta = -\frac{k\Lambda z}{f} = 1 + \left(\frac{\epsilon}{k_*\Delta}\right)^{\beta} K + \left(\frac{\epsilon}{k_*\Delta}\right)^{\alpha} Z + O\left(\left(\frac{\epsilon}{k_*\Delta}\right)^{\alpha+\beta}\right). \tag{5.29}$$

So as to the expansion of $D(\zeta)$ there are two situations: (i) When $\alpha = 0$ the wavepacket is away from the dominant inertial level, and we obtain

$$D(\zeta) = D(1 + Z) + O\left(\left(\frac{\epsilon}{k_*\Delta}\right)^{\beta}\right). \tag{5.30}$$

(ii) When $\alpha > 0$, the expansion become

$$D(\zeta) = D(1) + O\left(\left(\frac{\epsilon}{k_*\Delta}\right)^{\min\{\alpha,\beta\}/2}\right). \tag{5.31}$$

Because in these two expansions (5.30) and (5.31) the leading order terms are independent of k, hence do not contribute to the k integration of (5.24), the order of the second

terms are crucial. So the different orders of β and $\min\{\alpha,\beta\}/2$ indicate different distinguished regimes namely Regime I with $\alpha=0$ and $\beta=1$, Regime II with $\alpha=\beta=2/3$. Here, we only repeat the final approximations for w_1 referring the reader to the Appendix for the details of the steepest descent derivation.

In Regime I, we find that

$$w_1 \doteq \mathrm{i}hf(1+Z_{\mathrm{I}})\left(\frac{(k_*\Delta)^2\mathrm{Ro}^2-1}{2Z_{\mathrm{I}}+Z_{\mathrm{I}}^2}\right)^{1/4}\mathrm{e}^{-\frac{1}{2\Delta^2}\left(y-\frac{J\nu_*}{k_*\sqrt{1+\nu_*^2}}D_I\right)^2}\mathrm{e}^{-\frac{X_{\mathrm{I}}^2}{2\Delta^2}}, \tag{5.32}$$

where

$$X_{\mathrm{I}} = x-\frac{J}{k_*}\left[\sqrt{1+\nu_*^2}\left(\frac{1+Z_{\mathrm{I}}}{\sqrt{2Z_{\mathrm{I}}+Z_{\mathrm{I}}^2}}-\frac{k_*\Delta\mathrm{Ro}}{\sqrt{(k_*\Delta)^2\mathrm{Ro}^2-1}}\right)-\frac{\nu_*^2}{\sqrt{1+\nu_*^2}}D_{\mathrm{I}}\right] \tag{5.33}$$

with $D_{\mathrm{I}}=\ln(1+Z_{\mathrm{I}}+\sqrt{2Z_{\mathrm{I}}+Z_{\mathrm{I}}^2})-\ln(\zeta_{\mathrm{b}*}+\sqrt{\zeta_{\mathrm{b}*}^2-1})$, $Z_{\mathrm{I}}=z/z_*-1$ and $\zeta_{\mathrm{b}*}=k_*\Lambda H/f$.

In this regime we show that the wavepacket remains its bell-shape and horizontal scale of the wavepacket is the same as the topography envelope scale Δ. In addition, in the Appendix E.1 we can see that the derivation of (5.32) is in fact the derivation of ray tracing, which indicates the wavepacket's scales. Note that the ray tracing result suggests that the wavepacket tends to $x\to\infty$ as z approaches z_*. In our solution, we apply an implicit dissipation corresponding to the branch choice [16] in the solution of (5.10) to obtain a physically reasonable result.

In regime II,

$$w_1 \doteq \frac{\mathrm{i}U_{\mathrm{b}}hk_*^2\Delta}{2^{1/4}\epsilon^{5/4}(k_*\Delta)^{3/4}}q(K_s)\sqrt{\frac{1}{p''(K_s)}}\mathrm{e}^{-\frac{1}{2\Delta^2}\left(y-\frac{J\nu_*}{k_*\sqrt{1+\nu_*^2}}D_{\mathrm{II}}\right)^2}\mathrm{e}^{(k_*\Delta)^{2/3}P(K_{\mathrm{s}})}, \tag{5.34}$$

where

$$\begin{aligned} q(K_{\mathrm{s}}) &= \frac{1}{(K_{\mathrm{s}}+Z_{\mathrm{II}})^{1/4}}, \\ p(K_{\mathrm{s}}) &= -\frac{K_{\mathrm{s}}^2}{2}-\mathrm{i}J(k_*\Delta)\sqrt{1+\nu_*^2}\sqrt{2(K_{\mathrm{s}}+Z_{\mathrm{II}})}+\mathrm{i}K_{\mathrm{s}}X_{\mathrm{II}}, \end{aligned} \tag{5.35}$$

with K_s is the saddle point that $p'(K_\mathrm{s})=0$, where the prime denotes derivative and

$$X_\mathrm{II}=\epsilon^{1/3}\left(k_*(k_*\Delta)^{-4/3}x+J(k_*\Delta)^{-4/3}\left[\sqrt{1+\nu_*^2}\frac{k_*\Delta\mathrm{Ro}}{\sqrt{(k_*\Delta)^2\mathrm{Ro}^2-1}}+\frac{\nu_*^2}{\sqrt{1+\nu_*^2}}D_\mathrm{II}\right]\right) \tag{5.36}$$

with $D_\mathrm{II}=-\ln(\zeta_{\mathrm{b}*}+\sqrt{\zeta_{\mathrm{b}*}^2-1})$ and $Z_\mathrm{II}=(k_*\Delta)^{2/3}(z/z_*-1)$.

In addition to the two distinguished regimes, we are also interested in a regime that denotes the solution in the inertial layer where the change of EP flux is significant. This is the layer $|z-z_*|=O(\delta_*)$ with δ_* given in (5.13). Thus relevant range of z expressed by (5.27) becomes

$$Z=k_*\Delta\left(\frac{z}{z_*}-1\right) \tag{5.37}$$

corresponding to $\alpha=1$. This is in fact a limit of Regime II as it contains less terms compared with Regime II, and we term it Regime $\mathrm{II_B}$. In Regime $\mathrm{II_B}$ the wave solution can be approximated by

$$w_1\doteq\frac{\mathrm{i}hfJ^{1/2}\left(1+\nu_*^2\right)^{1/4}\left((k_*\Delta)^2\mathrm{Ro}^2-1\right)^{1/4}}{(k_*\Delta)^{1/2}}\mathrm{e}^{-\frac{1}{2\Delta^2}\left(y-\frac{J\nu_*}{k_*\sqrt{1+\nu_*^2}}D_\mathrm{II}\right)^2}\frac{1}{X}\mathrm{e}^{-\frac{1}{2}\left(\frac{J^2\left(1+\nu_*^2\right)}{2(k_*\Delta)^2X^2}-Z\right)^2}, \tag{5.38}$$

where

$$X=\epsilon^{1/2}\left(k_*(k_*\Delta)^{-3/2}x-J(k_*\Delta)^{-3/2}\left[\sqrt{1+\nu_*^2}\frac{(k_*\Delta)\mathrm{Ro}}{\sqrt{(k_*\Delta)^2\mathrm{Ro}^2-1}}+\frac{\nu_*^2}{\sqrt{1+\nu_*^2}}D_\mathrm{II}\right]\right). \tag{5.39}$$

See Appendix E for details.

In x-component, the peak of wave amplitude is calculated to be

$$X=X_\mathrm{c}=\left(\frac{J^2\left(1+\nu_*^2\right)}{(k_*\Delta)^2(Z+\sqrt{2+Z^2})}\right)^{1/2}. \tag{5.40}$$

Considering the definition of X by (5.39), where x is rescaled by $(k_*\Delta)^{1/2}\Delta$, the wavepacket in the inertial layer expands to an $O((k_*\Delta)^{1/2}\Delta)$ width streamwise and the peak of the wavepacket is an $O((k_*\Delta)^{1/2}\Delta)$ distance downstream from the mountain. This finite-distance behaviour of the wavepacket at the dominant inertial level is distinctive from the standard ray tracing method prediction that the wavepacket goes to infinity. In addition, because of the nonnegligible rotation effect, the wave amplitude does not

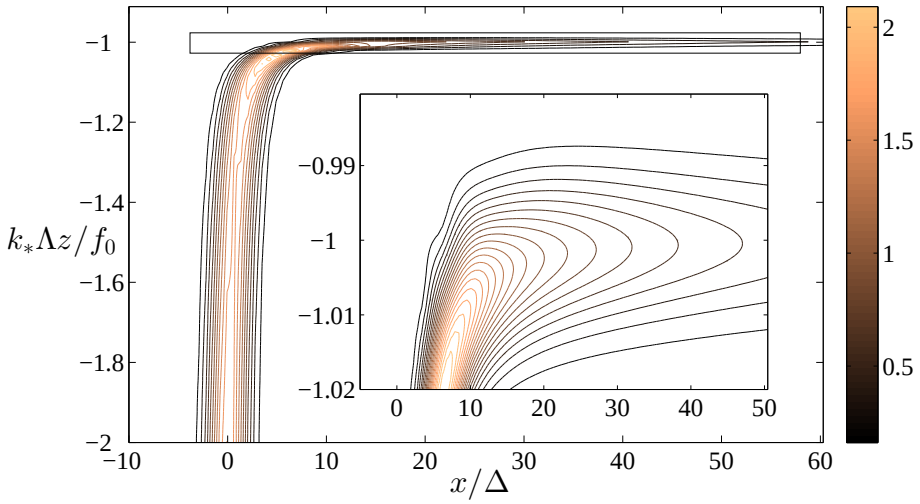

Figure 5.2: Contour plot of the wave vertical velocity amplitude w_1, normalized by $Uhk_*\Delta^2/(2\pi)$, from direct numerical integration of (5.20). The inset is a zoom in the rectangle region in the main figure.

tends to infinity when the wave packet tends to the dominant inertial level.

In summary, these three regimes correspond to three physical mechanisms. The regime I is the region where the singular effect of IGW does not affect; in Regime II the singular effect due to the vertical structure function of a single-frequency wave starts to influence the wave packet; in Regime $\mathrm{II_B}$, another singular effect – inertial level absorption – is dominant, and the region width calculated from the definition of inertial level is controlled by the spectrum width of the mountain.

5.3.3 Numerical results

We compare the approximate results with numerical results in Figure 5.2 and 5.3 in the following parameter regime: $\mathrm{Ro} = 0.02$, $k_*\Delta = 100$, $l_*\Delta = 100$, $J = 100$ and $\nu_* = 1$, so $\zeta_{\mathrm{b}*} = k_*\Delta\mathrm{Ro} = 2$. In this regime very distinctive parameters are used to check the validity of the approximations. Here, we show the wave amplitude in $x - z$ intersection at the peak in the y-direction. Because the y-component structure simply resembles the mountain shape we do not show it.

Figure 5.2 shows the contour plot of the wave vertical velocity amplitude. When the wave is away from the dominant inertial level, $k_*\Lambda z/f = -1$, the wavepacket only has a sight deflection from vertical. When the wavepacket is much closer to the dominant inertial level, the wavepacket shows a significant bend, and we can read from the inset

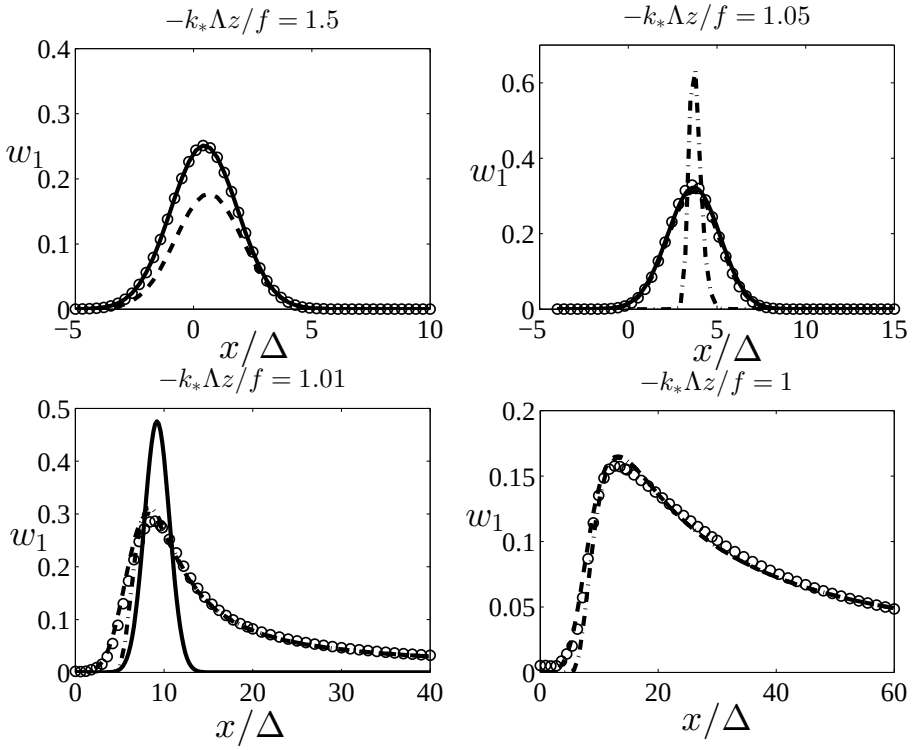

Figure 5.3: (a)–(d) show the amplitude of w normalized by $U_{\mathrm{b}}hk_*\Delta/(\sqrt{2\pi}\epsilon)$ at $-k_*\Lambda z/f = 1.5, 1.05, 1.01, 1$ corresponding to Regime I, II, $\mathrm{II_B}$ and dominant inertial level. Here the circles, solid line, dashed line and dot-dashed line denote the direct numerical result, Regime I, II and $\mathrm{II_B}$ approximations respectively.

that the peak of the wavepacket at the dominant inertial level $k_*\Lambda z/f = -1$ is around $x/\Delta = 12$, which accords with the peak predicted by expression (5.39) with $X_{\mathrm{c}} = 2^{1/4}$. This figure is more a qualitative illustration than a quantitative comparison, the latter which is shown in the Figure 5.3.

In Figure 5.3, subfigure (a) shows w_1 as a function of x for fixed z in Regime I ($-k_*\Lambda z/f = 1.5$) where the ray tracing method is valid (the match between the numerical circles and the ray tracing solid curve) and the wavepacket keeps the bell shape inherited from the boundary condition. Here the Regime II approximation is not valid so that the dashed curve does not agree with the numerical circles. In the subfigure (b), results in Regime II are shown. Even though it is not in Regime I the Regime I approximation is still valid (overlapping between the circles and solid curve) and the wavepacket resembles the bell shape. Because here the Regime II approximation is also valid (overlapping between the circled curve and dashed curve), we can see the match-

ing between Regime I and regime II approximations. Here we also plot the Regime $\mathrm{II_B}$ approximation (dot-dashed curve) to show its invalidity. When the wavepacket is closer to the dominant inertial level and reach Regime $\mathrm{II_B}$, the Regime II approximation is valid (overlapping between the circled curve and dashed curve) but not the Regime I approximation (mismatch between the circled curve and the solid curve) as is shown in the subfigure (c), so this divergence confirms that the Regime I and Regime II are two distinguished regimes. Now the Regime $\mathrm{II_B}$ approximation works (overlapping between the circled curve and dot-dashed curve), the wavepacket is no longer bell shaped and the peak of the wavepacket has a $O((k_*\Delta)^{1/2}\Delta)$ shift ($x/\Delta \approx 10 = (k_*\Delta)^{1/2}$) in agreement with (5.39) and (5.40). In the subfigure (d) we show the validity of Regime $\mathrm{II_B}$ approximation at the dominant inertial level, which ensures that we can calculate the EP flux change by applying the Regime $\mathrm{II_B}$ approximation. Here, at the dominant inertial level the peak of the wavepacket remains at a finite $O((k_*\Delta)^{1/2}\Delta)$ position, which is different from the ray tracing result, we observe a significant decrease of wave amplitude and increase of the wavepacket's width associated with the wave absorption at inertial levels.

Even though we can take the physical quantities as $N = 1.4 \times 10^{-2}\,\mathrm{s}^{-1}$, $f = 1 \times 10^{-4}\,\mathrm{s}^{-1}$, $\Lambda = 1.4 \times 10^{-4}\,\mathrm{s}^{-1}$, $H = 5\,\mathrm{km}$, $\Delta = 3.5 \times 10^{2}\,\mathrm{km}$ and $k_* = 2.8 \times 10^{-4}\mathrm{m}^{-1}$ to obtain a physically reasonable scenario to validate the above parameter regime, the physical applications usually relate to larger small parameters – the Rossby number and the (inverse of) Richardson number. So in Figure 5.4 we compare our approximate results with the numerical results in the parameter regime: $\mathrm{Ro} = 0.4$, $k_*\Delta = 5$, $l_*\Delta = 5$, $J = 5$ and $\nu_* = 1$, so $\zeta_{\mathrm{b}*} = k_*\Delta\mathrm{Ro} = 2$. Here, results corresponding to direct numerical simulation and Regime I, II and $\mathrm{II_B}$ are show in all the four panels, except that in the subfigure (d), the Regime I result is not shown because the wavepacket goes to infinity.

5.4 Wave-mean flow interaction

From §5.3 we know that the wave behaviour has sudden change across the singularities, so in this section based on the wave approximate solutions we derive that this sudden change will force mean flow and calculate the mean-flow response. For wave-mean flow interaction, the important quantity is the EP flux, which has been recognized as a diagnostic for waves on mean flow in literature, starting from Eliassen and Palm [46] and later by Andrews and McIntyre [4], by Boyd [17] and by Edmon et al. [45]. There are two kinds of mean flow response – far-field response and local response. The far-field response is the net change of the mean flow that persist when the flow is downstream far away from the mountain. It is a consequence of the net EP flux change due to EP

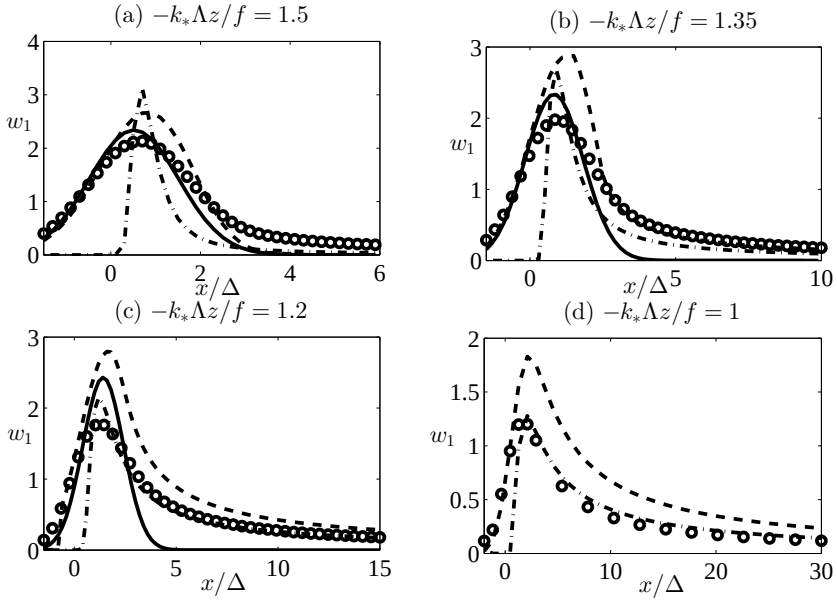

Figure 5.4: Wave field approximation with parameter Ro = 0.4, $k_*\Delta = 5$, $l_*\Delta = 5$, $J = 5$ and $\nu_* = 1$. The notations are the same as those in Figure 5.3. Here $-k_*\Lambda z/f = 1.5, 1.35, 1.2, 1$ corresponding to Regime I, II, II_B and the dominant inertial level.

flux absorption. In contrast, the local response is the mean flow change due to the local EP flux change which has no far-field effect. As we have discussed in the §5.3, the net EP flux change happens in the Regime II_B denoting the inertial layer; for the rest of the region, waves are transient in space that leave no net mean-flow response: the mean flow generation only exists within the range of wavepacket but not outside. In accord with the non-acceleration theorem, if zonal (streamwise) integration is taken, this local mean-flow generation does not appear.

In this section we focus on the calculation of the far-field response. First we derive the governing equation for this mean-flow response in §5.4.1. Physically speaking, there are two main questions in wave-mean flow interaction: The first question is how much force is generated by the wave field at the inertial layer? This force on the mean flow brings about a permanent mean flow change. This question is answered by calculating the EP flux in §5.4.2. The second question is what flow pattern the mean flow acquires as a result of this force? This question is answered by solving (5.43) in §5.4.3. These two subsections show the general procedure for the calculation, and we provide explicit results in a specific example in §5.4.4. A brief discussion on the mean-flow generation is given in §5.4.5.

5.4.1 Governing equation

Taking advantage of the small Rossby number, the mean flow is calculated using quasi-geostrophic theory. By taking the horizontal curl of the horizontal momentum equation (5.3a), taking $\partial_z f/N^2$ on f times (5.3c) and using the incompressibility (5.3d), we obtain

$$\partial_t \left(v_x - u_y + \partial_z \left(\frac{f}{N^2} b \right) \right) + \underbrace{(\partial_{xx} - \partial_{yy})(uv) + \partial_{xy}(v^2 - u^2)}_{(1)} + \underbrace{\partial_z \left(\frac{f}{N^2} \partial_z (wb) \right)}_{(2)} + \underbrace{\partial_{xz} \left(wv + \frac{f}{N^2} ub \right) - \partial_{yz} \left(wu - \frac{f}{N^2} vb \right)}_{(3)} = 0. \tag{5.41}$$

Taking advantage of the scale separation, the waves and mean flow are identified by the small scale average defined as

$$\langle \ \cdot \ \rangle = \frac{1}{D^2} \int_x^{x+D} \int_y^{y+D} \cdot \, \mathrm{d}\boldsymbol{x}', \tag{5.42}$$

where $\Delta \gg D \gg k_*^{-1}$. Applying this small scale average to (5.41) and retaining the leading order terms for both wave and mean flow based on both the small wave amplitude and small Rossby number we obtain

$$(\partial_t + \boldsymbol{U} \cdot \nabla) \left(\nabla^\perp \cdot \boldsymbol{U} + \partial_z \left(\frac{f}{N^2} B \right) \right) + \nabla^\perp \cdot \partial_z \boldsymbol{F} = 0, \tag{5.43}$$

where the leading mean flow is geostrophic such that $\boldsymbol{U} = (U, V) = (-\partial_y \Psi, \partial_x \Psi)$, $W = 0$ and $B = f \partial_z \Psi$, $\nabla^\perp = (-\partial_y, \partial_x)$ is the horizontal curl, and

$$\boldsymbol{F} = \left(\langle u_1 w_1 \rangle - \frac{f}{N^2} \langle v_1 b_1 \rangle , \langle v_1 w_1 \rangle + \frac{f}{N^2} \langle u_1 b_1 \rangle \right) \tag{5.44}$$

is the Eliassen-Palm (EP) flux [46]. In (5.43) only the terms denoted by (3) in (5.41) remains: The term denoted by (3) has zero average because w_1 and b_1 are out of phase in large J limit (see (5.12c)); The terms denoted by (1) is of $O(\delta_*/H)$ smaller compared with terms denoted by (3) due to the vertically thin inertial layer. If there is no wave effect, $\mathcal{F} = 0$, (5.43) reduces to the quasi-geostrophic potential vorticity equation.

One significant feature of the EP flux is its conservation when the background flow possesses certain symmetry, and this conservation leads to the non-acceleration theorem [25]: the waves do not force the mean flow unless there exists a singularity or some

dissipation. In our setup, the background shear flow has x- and y-symmetry. Applying the polarization relation (5.12) to (5.44) the single-wavenumber x-component EP flux is obtained as

$$F^k = \frac{-\Lambda}{f}\frac{1}{1+\nu^2}\mathrm{Re}\left\{\mathrm{i}\frac{1-\zeta^2}{\zeta^2}\hat{w}_\zeta(\boldsymbol{k})\hat{w}(\boldsymbol{k})^* - \nu\frac{\hat{w}(\boldsymbol{k})\hat{w}(\boldsymbol{k})^*}{\zeta^2}\right\}. \tag{5.45}$$

The EP flux conservation can be obtained from (5.10) by multiplying the $\hat{w}$'s complex conjugate $\hat{w}^*$ and subtracting the conjugate of resulting equation to find

$$\partial_z F^k = 0, \tag{5.46}$$

where only the x-component EP flux in wavenumber space is expressed and the y-component of EP flux equals ν times the x-component EP flux.

However, the EP flux conservation (5.46) does not hold across the inertial level singularities: the single-wavenumber EP flux attenuates to an exponentially small value across its inertial level; therefore the wave forces the mean flow in the inertial layer (Regime $\mathrm{II}_{\mathrm{IIB}}$).

The mean boundary condition can be obtained by taking small-scale average in (5.4) and retaining until the second order

$$\begin{aligned}\langle w_2\rangle &= \langle \mathbf{u_1}\cdot\nabla h_\mathrm{t} - h_\mathrm{t}\partial_z w_1 - \Lambda h_\mathrm{t}\partial_x h_\mathrm{t}\rangle \\ &= \langle \mathbf{u_1}\cdot\nabla h_\mathrm{t} + h_\mathrm{t}\nabla\cdot\mathbf{u_1} + -\Lambda h_\mathrm{t}\partial_x h_\mathrm{t}\rangle \\ &= \left\langle \nabla\cdot(\mathbf{u_1}h) - \Lambda\partial_x\left(\frac{h_\mathrm{t}^2}{2}\right)\right\rangle = 0,\end{aligned} \tag{5.47}$$

where $\mathbf{u_1} = (u_1, v_1)$, and the incompressibility of wave (5.6d) is used.

5.4.2 Eliassen-Palm flux

In (5.43) the wave and the mean flow interact through the EP flux defined by (5.44). As a wave quantity, it is calculated using the approximate expressions for the waves obtained in §5.3. The x and y component EP flux differs by a factor $\nu = \nu_* + \mathrm{h.o.t.}$, which to the leading order is a same constant for all wavenumbers, here we concentrate on calculating the x-component.

It can be seen from the W_1 approximation that by applying the steepest descent method to a wavepacket its expression is controlled by a single frequency (complex) – the saddle point k_s, for which $k_\mathrm{s} = k_*$ in ray tracing Regime I is a special case. Because of

this single-frequency dominance, the polarization relation (5.12) for a single wavenumber is inherited by the wave packet with the replacement of k by k_s, correspondingly ζ by $\zeta_\mathrm{s} = -k_\mathrm{s}\Lambda z/f$, ν by ν_*, and the functions in spectrum space by their inverse Fourier transform, so it reads

$$u_1 = \frac{\mathrm{i}(\zeta_\mathrm{s} - \mathrm{i}\nu_*)}{k_\mathrm{s}\zeta_\mathrm{s}(1+\nu_*^2)} w_{1z} - \frac{\mathrm{i}\Lambda\nu_*^2}{f\zeta_\mathrm{s}(1+\nu_*^2)} w_1, \tag{5.48a}$$

$$v_1 = -\frac{1 - \mathrm{i}\nu_*\zeta_\mathrm{s}}{k_\mathrm{s}\zeta_\mathrm{s}(1+\nu_*^2)} w_{1z} + \frac{\mathrm{i}\Lambda\nu_*}{f\zeta_\mathrm{s}(1+\nu_*^2)} w_1, \tag{5.48b}$$

$$b_1 = -\frac{\mathrm{i}\Lambda(1 - \mathrm{i}\nu_*\zeta_\mathrm{s})}{k_\mathrm{s}\zeta_\mathrm{s}^2(1+\nu_*^2)} w_{1z} + \mathrm{i}\frac{\Lambda^2}{f}\left(\frac{\mathrm{i}\nu_*}{\zeta_\mathrm{s}^2(1+\nu_*^2)} + \frac{\mathrm{Ri}}{\zeta_\mathrm{s}}\right) w_1. \tag{5.48c}$$

Thus the x-component EP flux becomes

$$F = \frac{-\Lambda}{f}\frac{1}{1+\nu^2}\mathrm{Re}\left\{\mathrm{i}\frac{-f}{k_\mathrm{s}\Lambda}\frac{1-\zeta_\mathrm{s}^2}{\zeta_\mathrm{s}^2} w_{1z} w_1^* - \nu\frac{w_1 w_1^*}{\zeta_\mathrm{s}^2}\right\}. \tag{5.49}$$

As we have already discussed that the net change of the EP flux by wave absorption is only important in the inertial layer represented by the Regime $\mathrm{II_B}$, the relation (5.48) can be simplified to

$$u_1 = \frac{\mathrm{i}(\zeta_\mathrm{s} - \mathrm{i}\nu_*)}{k_\mathrm{s}\zeta_\mathrm{s}(1+\nu_*^2)} w_{1z}, \tag{5.50a}$$

$$v_1 = -\frac{1 - \mathrm{i}\nu_*\zeta_\mathrm{s}}{k_\mathrm{s}\zeta_\mathrm{s}(1+\nu_*^2)} w_{1z}, \tag{5.50b}$$

$$b_1 = \mathrm{i}\frac{\Lambda^2}{f}\frac{\mathrm{Ri}}{\zeta_\mathrm{s}} w_1, \tag{5.50c}$$

which leads to the approximation of EP flux

$$F = \frac{1-\zeta_\mathrm{s}^2}{k_\mathrm{s}\zeta_\mathrm{s}^2}\mathrm{Re}\left\{\mathrm{i}w_{1z}w_1^*\right\}. \tag{5.51}$$

The calculation of w_1 in Appendix E.3 we obtain

$$\begin{aligned} w_{1z} \doteq & \mathrm{i}\Lambda h J^{1/2} k_*(k_*\Delta)\left((k_*\Delta)^2\mathrm{Ro}^2 - 1\right)^{1/4}\left(1+\nu_*^2\right)^{1/4} \\ & \times \mathrm{e}^{-\frac{1}{2\Delta^2}\left(y - \frac{J\nu_*}{k_*\sqrt{1+\nu_*^2}} D_\mathrm{II}\right)^2} \mathrm{e}^{-\frac{1}{2}\left(\frac{J^2\left(1+\nu_*^2\right)}{2(k_*\Delta)^2 X^2} - Z\right)^2}. \end{aligned} \tag{5.52}$$

Combining with

$$\zeta_\mathrm{s} = 1 + \frac{1}{k_*\Delta}(K_s + Z), \tag{5.53}$$

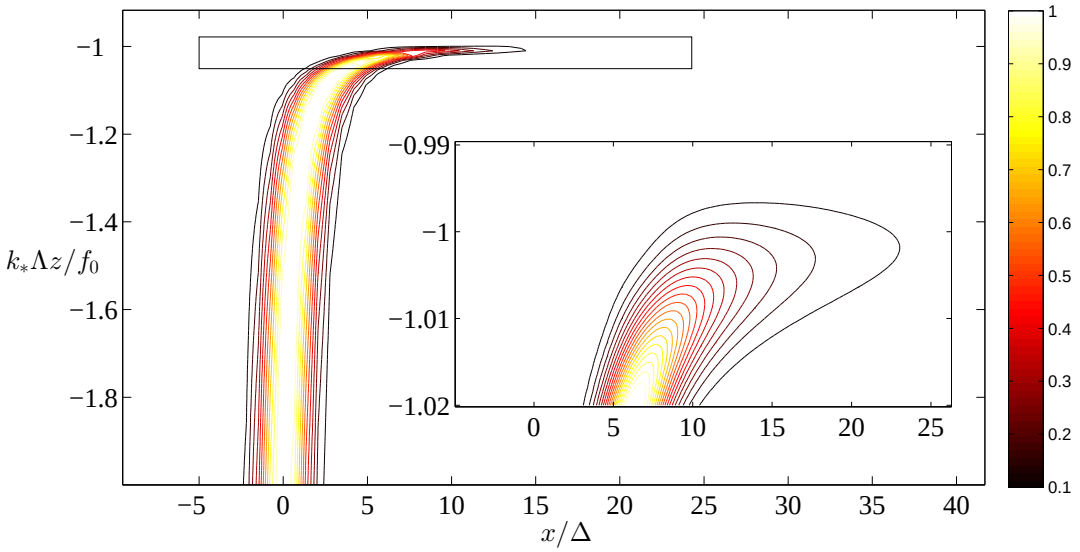

Figure 5.5: Contour plot of the EP flux. Compared with the wave field w shown in Figure 5.2, the centre of the EP flux is closer to the mountain, but the scalings are the same. The inset is the rectangular region in the large figure.

where K_s is expressed in (E.20), the EP flux becomes

$$F = E\mathrm{e}^{-\frac{1}{\Delta^2}\left(y-\frac{J\nu_*}{k_*\sqrt{1+\nu_*^2}}D_{\mathrm{II}}\right)^2}\frac{1}{X^3}\mathrm{e}^{-\left(\frac{J^2\left(1+\nu_*^2\right)}{2(k_*\Delta)^2X^2}-Z\right)^2}, \tag{5.54}$$

where

$$E = \frac{J^3\Lambda h^2 f\left((k_*\Delta)^2\mathrm{Ro}^2-1\right)^{1/2}\left(1+\nu_*^2\right)^{1/2}}{2(k_*\Delta)^{5/2}}. \tag{5.55}$$

With the same parameters as the wave numerical solutions, the EP flux contour and the EP flux at the dominant inertial level are shown in figure 5.5 and figure 5.6 separately.

By integrating the expression (5.54) over x and y components[4], we obtain the horizontal-integrated EP flux:

$$\overline{F(Z)} = \frac{\pi J\Delta^2\Lambda h^2 f\left((k_*\Delta)^2\mathrm{Ro}^2-1\right)^{1/2}}{4\left(1+\nu_*^2\right)^{1/2}}(1+\mathrm{erf}(Z)), \tag{5.56}$$

[4]We in fact integrate for $x \in [0, \infty)$ instead $x \in (-\infty, \infty)$ for the reason that this expression only valid in $x \in [0, \infty)$ and the wave amplitude in $x < 0$ region is exponentially small hence negligible.

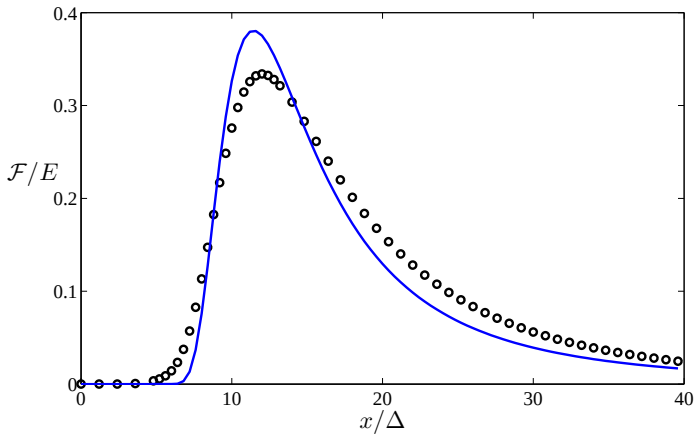

Figure 5.6: EP flux at the dominant inertial level. Circles denotes the numerical result and the solid line represents the Regime $\mathrm{II_B}$ approximation.

where the error function clearly captures the wave absorption. When $Z \to -\infty$, the wave has been totally absorbed so $\overline{\mathcal{F}} = 0$, and when $Z \to \infty$ we obtain the total EP flux:

$$\overline{F}_{\mathrm{tot}} = \frac{\pi J \Delta^2 \Lambda h^2 f \left((k_* \Delta)^2 \mathrm{Ro}^2 - 1\right)^{1/2}}{2\left(1 + \nu_*^2\right)^{1/2}}. \tag{5.57}$$

From (5.56) we can also estimate the EP force per unit area defined as the vertical derivative of horizontal-integrated EP flux divided by Δ^2:

$$\overline{f(Z)} = \partial_z \overline{F(Z)} = -\frac{\sqrt{\pi}}{2} \Lambda N \Delta h^2 k_*^2 \frac{k_*}{|\boldsymbol{k}_*|} ((k_* \Delta)^2 \mathrm{Ro}^2 - 1)^{1/2} \mathrm{e}^{-Z^2}, \tag{5.58}$$

where $|\boldsymbol{k}_*| = \sqrt{k_*^2 + l_*^2}$ is the amplitude dominant wavenumber. When we compare the coefficient (5.58) to the coefficient in the non-inertial gravity wave case (Martin and Lott [83]), we can find the common terms $N\Lambda\Delta h^2 k_*^2$. The difference is that the inertial layer thickness is controlled by f whose zero limit results in infinite force as the inertia layer thickness tends to zero (see (5.13)). But we will see in the detailed calculation in §5.4.4 that this $f \to 0$ limit does not bring about a singularity in calculating the large-scale mean-flow response.

5.4.3 PV equation

After calculating the EP flux we can obtain the steady mean-flow response from the mean potential vorticity equation (5.43). In this section we apply matched asymptotics to solve this equation by dividing the whole region ($z > -H$) into the inner region corresponding to inertial layer (Regime $\mathrm{II_B}$) and an outer region. We denote the streamfunction change in the inner and outer regions as $\Psi(X, y, Z)$ and $\psi(X, y, z)$, respectively.

In the inner region, considering the scalings in Regime $\mathrm{II_B}$, the governing equation (5.43) in steady state ($\partial_t = 0$) become

$$\epsilon^{1/2} k_*(k_*\Delta)^{-3/2}(U_*\partial_X + \nabla^\perp\Psi\cdot\nabla)(\epsilon k_*^2(k_*\Delta)^{-3}\partial_{XX}\Psi + \partial_{yy}\Psi + \frac{k_*^4\Delta^2}{\epsilon^2 J^2}\partial_{ZZ}\Psi) = \frac{k_*^2\Lambda\Delta}{\epsilon^2 f}\partial_{yZ}F, \tag{5.59}$$

where ∇ and $\nabla^\perp$ are based on scaled variables (X, y) but we keep the notations for simplicity, $U_* = -\Lambda z_* = f/k_*$ is the background velocity at the dominant inertial level, and at the r.h.s. F only means the x-component EP flux because the y-component derivative is $O((k_*\Delta)^{1/2})$ larger than that of x-component.

It can be inferred from the energy budget that the streamfunction change is small compared with the background streamfunction as a result of the small wave amplitude. Later the consistency of this small streamfunction change is checked in the detailed calculation. So to the leading order we obtain the linearized equation

$$\frac{k_*^3(k_*\Delta)^{1/2}}{\epsilon^{3/2}J^2}U_*\partial_{XZZ}\Psi = \frac{k_*^2\Lambda\Delta}{\epsilon^2 f}\partial_{yZ}F. \tag{5.60}$$

By taking into account the boundary condition at $X = -\infty$ that the PV change is zero due to no wave effect, we can take the x-integration so (5.60) become

$$\partial_{ZZ}\Psi = Q, \tag{5.61}$$

where

$$Q = \frac{J^2\Lambda(k_*\Delta)^{1/2}}{\epsilon^{1/2}U_* k_*^2 f}\int_{-\infty}^{X}\partial_{yZ}\mathcal{F}(X', y, Z)\mathrm{d}X' \tag{5.62}$$

is the PV change.

When $Z > 0$ the solution of (5.61) is

$$\Psi(Z) = \int_0^Z\int_0^S Q(R)dRdS + C_1 Z + C_2. \tag{5.63}$$

Because F is localized vertically in the inertial layer, when $Z \to \infty$ we obtain

$$\Psi(Z) \to Z(\int_0^{\infty} Q(R)dR + C_1) + C_2^+, \tag{5.64}$$

where C_1 and C_2^+ are Z-independent and $C_2^+ = C_2 - \int_0^{\infty} RQ(R)\mathrm{d}R$.

Similarly, as $Z \to -\infty$,

$$\Psi(Z) \to Z(\int_0^{-\infty} Q(R)dR + C_1) + C_2^-, \tag{5.65}$$

where $C_2^- = C_2 - \int_0^{-\infty} RQ(R)\mathrm{d}R$ the coefficients C_1 and C_2 are the same for both $Z > 0$ and $Z < 0$ solutions due to the continuity of (5.64) and (5.65) at $Z = 0$.

In the outer region the steady governing equation (5.43) become

$$(U\partial_x + \nabla^{\perp}\psi\cdot)\nabla(\partial_{yy}\psi + \partial_{xx}\psi + \frac{f^2}{N^2}\partial_{zz}\psi) = 0, \tag{5.66}$$

which to the leading order is

$$U\partial_X(\partial_{yy}\psi + \frac{f^2}{N^2}\partial_{zz}\psi) = 0. \tag{5.67}$$

By taking into account that the streamfunction change is zero at $X = -\infty$ we obtain

$$\partial_{yy}\psi + \frac{f^2}{N^2}\partial_{zz}\psi = 0, \tag{5.68}$$

whose solution can be expressed after Fourier transform

$$\hat{\psi} = \begin{cases} C_3 \mathrm{e}^{-N|l|(z-z_*)/f} & (z > z_*) \\ C_4 \mathrm{e}^{-N|l|(z-z_*)/f} + C_5 \mathrm{e}^{N|l|(z-z_*)/f} & (z < z_*) \end{cases}, \tag{5.69}$$

where the notation $\hat{\cdot}$ now denotes the Fourier transform only in y, C_3, C_4 and C_5 are functions of l, and the vanishing boundary condition at $z \to \infty$ is applied.

The coefficients C_3, C_4 and C_5 are obtained from the boundary condition and the matching between the inner solutions (5.64) and (5.65) with the outer solution (5.69). Because at the bottom boundary the mean vertical velocity is zero (see (5.47)), the buoyancy equation (5.3c) reduces to $U\partial_X\psi_z = 0$, with further consideration of $\psi_z = 0$ at $X = -\infty$, the boundary condition become $\psi_z = 0$ at $z = -H$, which implies

$$-C_4 \mathrm{e}^{-N|l|(-H-z_*)/f} + C_5 \mathrm{e}^{N|l|(-H-z_*)/f} = 0. \tag{5.70}$$

Matching the solution for $z \to z_*^{\pm}$ and $Z \to \pm\infty$ gives

$$C_4 + C_5 - C_3 = \hat{C}_2^+ - \hat{C}_2^- = -\int_{-\infty}^{\infty} Z'\hat{Q}(X, l, Z')\mathrm{d}Z', \tag{5.71}$$

and

$$C_4 - C_5 - C_3 = \frac{k_*^2\Delta}{J|l|}\int_{-\infty}^{\infty} \hat{Q}(X, l, Z')\mathrm{d}Z', \tag{5.72}$$

where the first condition and the second condition match the function values and the first order derivatives, respectively.

Thus, from (5.71), (5.70) and (5.72) the three coefficients C_3, C_4 and C_5 are determined, and their order can be estimated with the help of the order of EP flux (5.54) that

$$C_i = O\left(\frac{J^4}{(k_*\Delta)^2}\left(\frac{h}{H}\right)^2 U_\mathrm{b}\Delta^2\right) \quad (i = 3, 4, 5). \tag{5.73}$$

So to validate the linearized potential vorticity equations (5.60) and (5.67), $C_i \ll 1$ is required, and it is ensured in our scaling that $J = O(k_*\Delta)$ and $J(h/H) \ll 1$. Eq. (5.73) also shows that the mean-flow generation is a second order effect, which is consistent with the energy argument that the wave energy is a quadratic effect of the first order wave.

5.4.4 Mean-flow response: an example

Following the procedure in the above section, we calculate the mean-flow response in a special case with $J = k_*\Delta$, $l_* = 0$ and $\zeta_{\mathrm{b}*} = 2$. So the x-component EP flux has the following expression:

$$F = E\mathrm{e}^{-\frac{y^2}{\Delta^2}}\frac{1}{X^3}\mathrm{e}^{-\left(\frac{1}{2X^2}-Z\right)^2}, \tag{5.74}$$

so

$$Q = -\frac{\sqrt{3}J^5\Lambda^2h^2}{U_*(k_*\Delta)^4\Delta^2}y\mathrm{e}^{-\frac{y^2}{\Delta^2}}\mathrm{e}^{-\left(\frac{1}{2X^2}-Z\right)^2}, \tag{5.75}$$

where we have let the bookkeeping parameter $\epsilon = 1$. So (5.71), (5.70) and (5.72) that are used to fix the coefficients C_3, C_4 and C_5 of outer region large-scale solution (5.69)

now become

$$-C_4 \mathrm{e}^{|l|\Delta} + C_5 \mathrm{e}^{-|l|\Delta} = 0, \tag{5.76a}$$

$$C_4 + C_5 - C_3 = 0, \tag{5.76b}$$

$$C_4 - C_5 - C_3 = C\frac{l}{|l|}\mathrm{e}^{-l^2\Delta^2/4}, \tag{5.76c}$$

where

$$C = -\frac{\mathrm{i}\sqrt{3\pi}J^4\Lambda^2h^2\Delta^2}{2\sqrt{2}(k_*\Delta)^2U_*}. \tag{5.77}$$

Solving the above equations gives

$$C_3 = -(1+\mathrm{e}^{-2|l|\Delta})\frac{C}{2}\frac{l}{|l|}\mathrm{e}^{-l^2\Delta^2/4}, \tag{5.78a}$$

$$C_4 = -\mathrm{e}^{-2|l|\Delta}\frac{C}{2}\frac{l}{|l|}\mathrm{e}^{-l^2\Delta^2/4}, \tag{5.78b}$$

$$C_5 = -\frac{C}{2}\frac{l}{|l|}\mathrm{e}^{-l^2\Delta^2/4}. \tag{5.78c}$$

So the mean-flow response $\delta U = -\partial_y\psi$ can be obtained. It is explicitly shown in Figure 5.7. In this figure we can see that the mean-flow response corresponding to a localized PV anormaly is not localized. The total mean flow change $\int \delta U \mathrm{d}x\mathrm{d}y$ is zero since the streamfunction variation vanishes at infinity. For any given altitude the extreme values of the velocity change locate at the middle ($y = 0$) and at the position close to the boundary of the PV anormaly. Since the extreme values are in opposite signs, horizontal mean shear is generated.

5.4.5 Mean-flow generation transition

It is interesting to notice that Q has an X-independent vertical integration

$$\partial_X \int_{-\infty}^{\infty} Q dZ = 0, \tag{5.79}$$

so the large-scale mean flow generation is nonzero and X-independent in the region corresponding the Regime $\mathrm{II_B}$ with the characteristic scale of $x/\Delta = O((k_*\Delta)^{1/2})$ when $X > 0$. But for $X < 0$, there is no mean-flow generation. This sudden transition indicates that we are working on a larger scale compared with the mean-flow generation transition, So it is natural to ask what is the scale of mean-flow generation transition. This sudden transition is an artifact due to the stationary phase method used in Regime

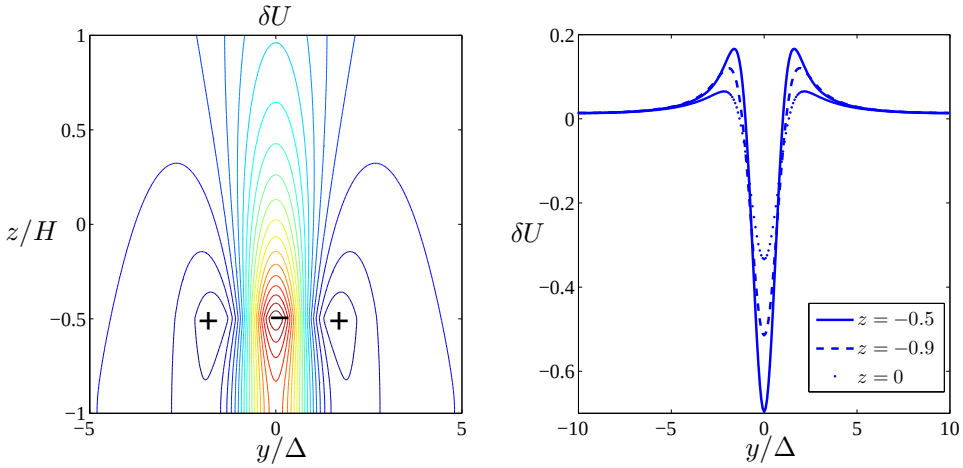

Figure 5.7: Mean-flow response. The left panel shows contour of the mean flow change δU with the sign is indicated by the + and −. The left figure shows the mean flow change profile in level $z/H = -0.9, -0.5, 0$. At $z = -0.5$ corresponding to the dominant inertial level the mean flow change reaches its maximum, at the level above ($z = 0$) and below ($z = -0.9$) the dominant inertial level the velocity profile have a similar shape but with a smaller amplitude. In this figure the nondimensional mean flow change is normalized by $\sqrt{3\pi}J^4\Lambda^2h^2/(2\sqrt{2}(k_*\Delta)^2U_*)$.

$\mathrm{II_B}$, where x has characteristic scales $(k_*\Delta)^{1/2}\Delta$ and z satisfies $z/z_* - 1 = O((k_*\Delta)^{-1})$ (see §E.3). However, when x is smaller, we can obtain from the Regime II result (See §E.2) that the wave packet, hence the EP flux, is localized around $x/\Delta = O((k_*\Delta)^{\alpha/2})$ and $z/z_* - 1 = O((k_*\Delta)^{-\alpha})$ with $\alpha \in [2/3, 1)$. Even though, in this region (E.16) is satisfied and therefore the imaginary part of the exponential in (E.7) is dominant, we cannot apply the stationary phase method because the term $\mathrm{e}^{-(k_*\Delta)^{2-2\alpha}K^2/2} \gg O(1)$. Therefore in this region, the part of Regime II excluding Regime $\mathrm{II_B}$, the solution should be expressed by the Regime II result with characteristic length $x/\Delta = O((k_*\Delta)^{1/3})$. Different from the stationary phase approximation in Regime $\mathrm{II_B}$, the saddle point in Regime II is not purely real and X_{II} and Z_{II} do not appear in the subtle combination as in Regime $\mathrm{II_B}$, so (5.79) is not valid; hence $x/\Delta = O((k_*\Delta)^{1/3})$ is the scale of mean flow generation transition. We need to emphasize that in this region, the mean flow generation includes both local generation and global generation, and as x increases the local generation abates and the global generation grows.

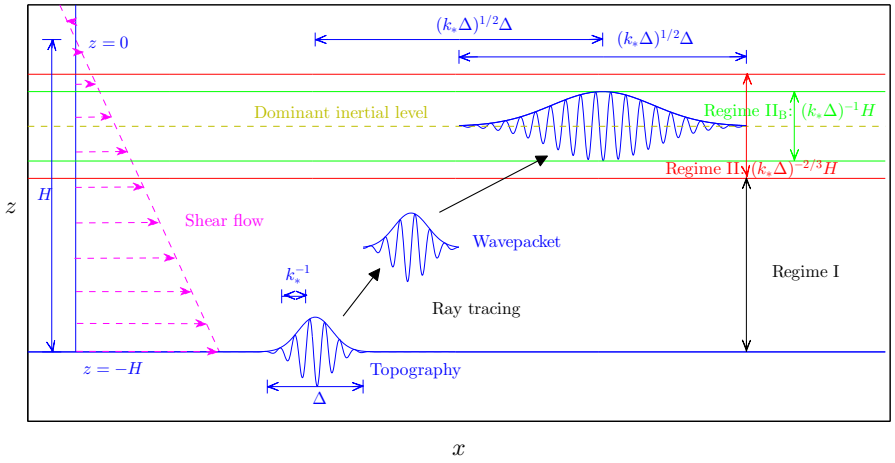

Figure 5.8: Topographic wave in a uniform shear flow. The topographic wave is generated by a backward uniform shear flow passing a multiscale topography whose scale separation is characterized by $k_*\Delta \ll 1$. The two distinctive regimes are Regime I and Regime II with a distance from the dominant inertial level of $O(H)$ and $O((k_*\Delta)^{-2/3}H)$ respectively. In Regime I the wavepacket resembles the topography while in Regime II the wavepacket locates downstream of $O((k_*\Delta)^{1/2}\Delta)$ and disperses to scale $(k_*\Delta)^{1/2}\Delta$. The Regime $\mathrm{II_B}$ is the region with thickness of $O(k_*\Delta H)$ around the dominant inertial level, which is used to capture the EP flux attenuation.

5.5 Conclusion and discussion

In this chapter, we study the behaviour of a topographic wavepacket and the mean flow generation due to inertial-level singularity, where the Doppler-shifted wave frequency matches the Coriolis frequency. In our setup, the Coriolis effect and the shear flow separate the inertial levels of different wavenumbers into different heights, leading to the formation of a finite-thickness inertial layer. By applying a steepest descent method, we obtain the approximate steady wave solutions in different regions distinguished by the relative strength of the singular effect. The corresponding steady mean-flow response is obtained using matched asymptotics. The setup and wave behaviour are illustrated in Figure 5.8.

The wave solution has different approximations in two distinctive regimes – Regime I and Regime II – distinguished by the distance from the dominant inertial level. In Regime I the wave is sufficiently far away from the dominant inertial level that the singular effect is not important. Classic ray-tracing results apply, and the wavepacket resembles the topography, with envelope scale Δ. In Regime II the wavepacket is close to

the dominant inertial level and hence the vertical structure of wave (5.21) associated with the singularity is essential. As a consequence, the ray tracing method is no longer valid and the wavepacket has a characteristic streamwise scale $(k_*\Delta)^{1/3}\Delta$, much longer than the scale of the topography. In Regime $\mathrm{II_B}$, a sublimit of Regime II, the wavepacket is closer still to the dominant inertial level, and the wave absorption is a dominant effect. We pay special attention to this regime, because unlike the other regions, here the singularity is so important that wave absorption causes the horizontally integrated EP flux to vary vertically, leading to a mean flow change. The approximate wave solution obtained in this regime controls the far-field mean-flow response.

Taking advantage of the small Rossby number, the mean flow dynamics is captured by the quasi-geostrophic potential-vorticity equation (5.43) where the wave influence enters through the divergence of the EP flux. In our setup, because of the thinness of inertial layer, the vertical derivative of the EP flux is dominant and the wave force on the mean flow is concentrated in the vertical. The vertical scale is set by the thickness of Regime $\mathrm{II_B}$ which is hence crucial for wave-mean flow interaction. The mean-flow response, however, has a large scale in both horizontal and vertical dimension as a result of the inverse Laplacian operator in the diagnostic relation between the mean potential vorticity and the mean streamfunction.

An interesting feature of the mean-flow generation predicted by the Regime $\mathrm{II_B}$ approximation is that it is zero in the region with $X < 0$ but jumps to an X-independent value for $X \geq 0$. This is the prediction on the scale $X = O(1)$, i.e. $x/\Delta = O((k_*\Delta)^{1/2})$ characteristic of the EP flux losses. A smooth transition in the mean-flow in fact happens over a characteristic scale $x/\Delta = O((k_*\Delta)^{1/3})$, where the mean-flow generation includes both the far-field generation and local generation. This result can be obtained using the Regime II approximations, but we did not carry out detailed calculations since these are complicated by the presence of a branch cut in (5.34). This is left as a subject of future work.

Even though we only calculate the mean-flow response for a special scaling, namely $\mathrm{Ro} = O((k_*\Delta)^{-1})$, $J = O(k_*\Delta)$, with $k_*\Delta \gg 1$, and $Jh/H \ll 1$, the validity of our result in fact only requires that

$$J\frac{h}{H} \ll 1, \quad k_*\Delta \gg 1, \quad J \gg 1, \quad \mathrm{Ro} \ll 1 \quad \text{and} \quad \frac{k_*\Lambda H}{f} > 1, \tag{5.80}$$

corresponding to the validity of the hypothesis of (i) linear wave, (ii) scale separation of the topography, (iii) WKB scaling as in [80], (iv) quasi-geostrophic mean flow, and (v) the dominant inertial level located above the ground. The requirement ensures that

the argument of the squire root in (5.58) is positive. In view of the independence of the large-scale mean-flow response on the detailed structure in the thin inertial layer, our far-field mean-flow generation results are robust as long as the conditions (5.80) is satisfied.

This study provides some indications on improving the topographic wave parameterization in numerical models. Parameterization of gravity waves as a subgrid-scale effect starts from Palmer et al. [100], where momentum flux dissipates due to the gravity wave saturation and this columnar parameterization prevents information transferred between columns. Different dissipation mechanisms are applied in the literature, turbulence is the key dissipative effect for the parameterization of Laurent et al. [72], and in Lott and Guez [77]'s columnar parameterization, same as in our setup, wave absorption is a result of singularity in the zero viscosity limit. The connection between neighbouring columns is accounted for in a ray-tracing based parameterization proposed by Hasha et al. [61]. Our results indicate that when the dissipation is a result of singularity in the zero viscosity limit the information exchange between columns should be taken into account – IGWs force the mean flow of $O((k_*\Delta)^{1/2}\Delta)$ far away from the source and the force range is extended to a large range of $O((k_*\Delta)^{1/2}\Delta)$. However, we also point out that ray tracing is not enough to accomplish this task due to its break down near inertial level singularity.

Due to the coexistence of various dissipation mechanisms, it is important to study which one dominants in specific scenarios. Here we make a comparison between the strength of finite viscosity and zero-viscosity limit wave absorptions, which hinges on the scale of finite viscosity dissipation δ_d and the inertial layer thickness δ_*: if $\delta_d \gg \delta_*$ finite viscosity dissipation dominants, and *vice versa*. We may estimate δ_d from the linear wave equations with usual viscosity form where various viscosity coefficients correspond to different mechanisms. This viscosity introduces a sixth order z-derivative in (5.10), if we want $\delta_d \gg \delta_*$ the J-related term establishes dominant balance with the viscosity term, from which δ_d is estimated. When molecular dissipation is considered this balance reads $\mu^2/(\rho^2 f_0^2)k_*^{-2}\delta_d^{-6} \sim J^2$, where μ and ρ are the molecular dynamic viscosity and density of air, therefore $\delta_d \sim (\mu/(\rho f_0 k_* J))^{1/3} \approx 1\,\mathrm{m}$ taking $\mu = 20\,\mu\mathrm{Pa\,s}$, $\rho = 1\,\mathrm{kg\,m^{-3}}$, $f_0 = 10^{-4}\,\mathrm{s^{-1}}$, $k_* = 10^{-3}\,\mathrm{m^{-1}}$ and $J = 100$. Meanwhile $\delta_* \approx 10\,\mathrm{m}$ indicates that zero viscosity wave absorption mechanism dominates. Turbulent viscosity is much larger than the molecular viscosity, and its importance will depending on specific process, requiring further study.

Chapter 6

Summary and discussion

In this thesis, we study the wave-mean flow interactions at two very distinctive length scales: the nanometre scale where the viscosity is dominant and the megametre scale where the interactions are non-dissipative. Since concluding remarks were made and discussed in chapters 2–5, here we only provide a very brief summary. The main content of this chapter is about how can these specific works help us on understanding wave-mean flow interaction.

6.1 Summary

Viscous wave-mean flow interactions have been studied in two complementary microfluidics problems. In chapter 2, we revisited the classic problem of boundary streaming to include the effect of a slip (Navier) boundary condition. This work identifies a new non-dimensional parameter controlling the strength of streaming and applies matched asymptotics to capture a significant modification to the classic results. In chapter 3, the other microfluidics problem concerns particle dynamics in an acoustic wave field. Our interest there lies more on the mean motion of the particles than on their fast oscillations at the wave frequency We applied a systematic multiscale approach to obtain mean equations which capture relevant physical effects – acoustic pressure, streaming, drag and inertia. This work clarifies the valid regimes of earlier heuristic results and identifies a new regime where the dynamics of the particle and fluid cannot be decoupled and the full Navier-Stokes equation must be solved.

We have studied the non-dissipative wave-mean flow interaction in two geophysical-fluid problems. In chapter 4, the first problem concerns the impact of near-inertial waves (NIWs) on the mesoscale mean flow. By combining generalized Lagrangian mean theory,

Whitham averaging and variational calculus we have obtained a Hamiltonian wave-mean flow coupled model. This model establishes a connection between the familiar quasi-geostrophic theory of mesoscale ocean circulation and the Young & Ben Jelloul model [137] for NIWs. Based on the conservation of energy and action, this work indicates that the NIWs act as an energy sink for the mean flow: as advection and refraction by the mean flow reduce the horizontal scale of the NIWs, the potential energy of NIWs increases at the expense of mean flow energy. This energy sink, whose existence is confirmed by numerical simulations and is estimated to be of comparable importance with the sink caused by bottom friction, implies that NIWs are important for one of the main open question in the oceanography – the mesoscale energy closure.

The second geophysical fluid problem concerns the impact of singularities and is studied in chapter 5. Specifically, it involves the interactions between topographic waves and a unidirectional uniform shear flow in a rotating fluid, in which the interaction concentrates near an inertial level (singularity) where the Doppler-shifted wave frequency matches the Coriolis frequency. By applying a combination of Fourier transform, WKB and saddle-point methods, we obtained asymptotic expressions for the wave in different regions, calculated the quasi-geostrophic mean-flow response, and confirmed the validity of theoretical results by numerical computations. In this problem, the presence of a non-zero vorticity is crucial, even though the results do not depend on the value of viscosity when it is small enough, as we assume.

Even though the wave-mean flow interaction mechanisms we studied differ for different scales, it is clear that vorticity (or potential vorticity) is the key object for understanding the wave-mean flow interaction. In the microfluidics problems, the mean vorticity generation is not a direct result of the mean flow itself but a consequence of viscous vorticity generation by the wave resonant pairs. In the geophysical fluid problems, the conservation of the potential vorticity consists of the mean flow part and the wave part, and the wave-mean flow interaction is about the potential vorticity exchange between these two parts. The difference between these two scenarios is that for small scales (viscosity dominant) the mean vorticity generation by wave effects is responsible for the mean flow generation while the large-scale phenomena are controlled by the potential vorticity exchange (or rather redistribution).

6.2 Wave-mean flow interaction

Regarding the wave-mean flow interaction, we remark that the average is defined artificially in order to make the problems convenient to tackle: In chapters 2–4[1], a time average is applied; in chapter 5, a spatial average is used. One assessment for a good definition of averaging is that the symmetries of the general fluid systems are inherited in the wave-mean flow coupled systems. First, let us think about the inviscid fluid, who possesses a Lagrangian description, corresponding to which the flow is naturally described following fluid elements. Therefore a suitable definition of average should pay attention to the flow map instead of a Eulerian field. This idea naturally leads to the generalized Lagrangian mean theories of both Andrews and McIntyre [5] and Soward and Roberts [115], which are mentioned with details in chapters 1 and 4. For example, in the near-inertial wave–mean flow interaction problem in chapter 4, we observe that the conservation laws, especially the potential-vorticity conservation, control the dynamics of the wave-mean flow interaction. However, for viscous fluids the viscous term does not naturally have a geometrical definition. The important concept "strain", which is responsible for the vortex generation, is naturally expressed in Eulerian terms. So in the two viscosity-dominated microfluidics problems, we simply applied Eulerian averaging.

In a two-dimensional situation there exists a symmetry $\nabla^{\perp} \cdot \boldsymbol{v} = -\nabla \cdot \boldsymbol{v}^{\perp}$, which can express dissipation as a divergence. This symmetry is helpful in deriving wave-mean flow interaction theories. For example, by using this symmetry, the pseudomomentum rule proposed by Mclntyre and Norton [86] is validated mathematically in a shallow water system by Bühler [21]. One perspective of understanding this symmetry is through the Kelvin circulation theorem: by writing the dissipation in the form of flux, two dimensional flows preserve circulation. However, for three-dimensional viscous flow the conservation of circulation is no longer valid, which is even true in the zero-viscosity limit when the flow is turbulent [26]. So it is interesting to ask whether some wave-mean flow interaction theories are still valid in realistic geostrophic fluid applications which are turbulent almost everywhere. Note that for a turbulent flow there is no scale separation, therefore the decomposition of wave and mean flow needs further consideration. For the real geophysical fluid, we may not need to consider a fully three dimensional flow, and future work could focus on a simpler quasi-two dimensional situation due to the strong stratification.

The world contains a rich range of scales. However, "Misfortune may be a blessing in disguise": the multiscale structure of many systems enables approximations based on

[1] In chapter 4, the ensemble average is identical with the fast time average.

scale separation. The existing wave-mean flow interaction theories are case-dependent, as we have seen in our studies of the viscosity dominated nanometre-scale interaction, and the megametre-scale non-dissipative interactions. The wave-mean flow interaction is a perspective for us to analyse information about our world rather than a rigorous procedure. It is important for, but not restricted to, common fluid systems: it could be applied to different systems such as quantum superfluids [60], also due to the nonlinearilty of General-Gravity equations the mean gravitational field is studied in [34].

Another perspective on the wave-mean flow interaction theory is to make it more general by proposing a universal theory. It seems that case-dependent theories, with approximations by scaling, can never achieve this aim; but theories based on variational principles have this potential because they only require functional relations regardless of scales. Unfortunately, we do not have a Lagrangian or variational formulation for a viscous fluid, which limits the application of the variational approach to non-dissipative interactions. Besides, we know that for wave-mean flow interaction the potential vorticity description is not universal. A counter example is the purely potential mean flow generation by a boundary condition (see e.g. [18]).

Appendix A

Solution of the Basset equation (3.59)

Applying the Laplace transform to (3.59) gives

$$\begin{aligned} & M\left(s^2F(s) - sX^{(0)}(0) - \dot{X}^{(0)}(0)\right) \\ = & -DF(s) - K\left(sF(s) - X^{(0)}(0)\right) - B\left(s^2F(s) - sX^{(0)}(0) - \dot{X}^{(0)}(0)\right)\sqrt{\pi}s^{-1/2}, \end{aligned} \tag{A.1}$$

where $F(s) = \mathcal{L}\{X^{(0)}\}$ is the Laplace transform of $X^{(0)}$. We choose $X^{(0)}(0) = X$ and $\dot{X}^{(0)}(0) = 0$, so that

$$F(s) = X\frac{Ms + \sqrt{\pi}Bs^{1/2} + K}{Ms^2 + \sqrt{\pi}Bs^{3/2} + Ks + D}. \tag{A.2}$$

This function has four poles and a (principal) branch cut associated with $s^{1/2}$. For definiteness, we consider the parameters $M = B = K = D = 1$, for which the poles satisfy $s^{1/2} = -1.19496 \pm \mathrm{i}0.734487$ and $0.308729 \pm \mathrm{i}0.642634$. The second equation leads to two poles, s_1 and s_2 say, with argument in $(-\pi, \pi)$ consistent with the choice of branch cut; the first equation leads to poles on the other Riemann sheet that are irrelevant.

The particle position $X^{(0)}$ is then obtained by inverting the Laplace transform using the contour shown in Figure A.1. This yields

$$\frac{1}{2\pi\mathrm{i}}\left(\int_l + \int_R + \int_r + \int_{L1} + \int_{L2}\right) F(s)\mathrm{e}^{st}\,\mathrm{d}s = \mathrm{Res}_{1,2}\{F(s)\mathrm{e}^{st}\}, \tag{A.3}$$

where $\mathrm{Res}_{1,2}$ denotes the sum of the residues at s_1 and s_2. Taking the limits $R \to \infty$

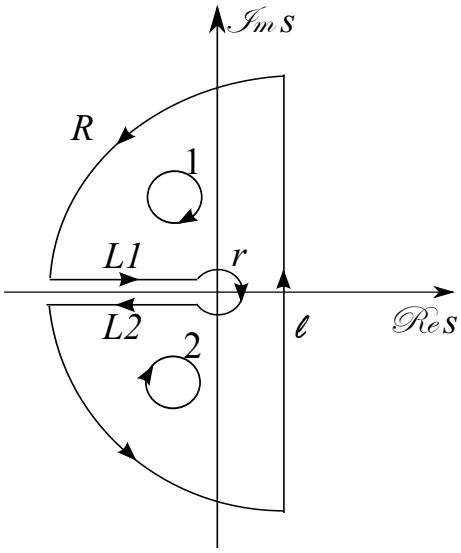

Figure A.1: Contour for the inverse Laplace transform in (A.3). The countour encloses two poles denoted by 1 and 2, and two sides of the branch cut $(-\infty, 0]$ associated with $s^{1/2}$.

and $r \to 0$, $\left(\int\limits_R + \int\limits_r\right) F(s)\mathrm{e}^{st}\,\mathrm{d}s = 0$, leading to

$$X^{(0)} = \frac{1}{2\pi\mathrm{i}} \int\limits_l F(s)\mathrm{e}^{st}\,\mathrm{d}s = \mathrm{Res}_{1,2}\{F(s)\mathrm{e}^{st}\} - \frac{1}{2\pi\mathrm{i}} \left(\int\limits_{L1} + \int\limits_{L2}\right) F(s)\mathrm{e}^{st}\,\mathrm{d}s. \tag{A.4}$$

In (A.4) $\mathrm{Res}_{1,2}\{F(s)\mathrm{e}^{st}\}$ corresponds to two modes of damped oscillations. The remaining term gives a continuous spectrum contribution associated with the branch cut; it can be expressed as

$$X^{(0)}_{\mathrm{cont}} = \frac{-1}{2\pi\mathrm{i}} \left(\int\limits_{L1} + \int\limits_{L2}\right) F(s)\mathrm{e}^{st}\,\mathrm{d}s = \frac{-1}{2\pi\mathrm{i}} \int\limits_0^\infty (f(y) - f(y)^*)\,\mathrm{d}y, \tag{A.5}$$

where

$$f(y) = \frac{-My + \mathrm{i}\sqrt{\pi}By^{1/2} + K}{My^2 - \mathrm{i}\sqrt{\pi}By^{3/2} - Ky + D}\mathrm{e}^{-yt}. \tag{A.6}$$

Appendix B

glm average

In glm, the map from mean to perturbed positions is written in terms of a divergence-free vector field, $\boldsymbol{\nu}(\boldsymbol{X}, t)$ say, as

$$\boldsymbol{X} + \boldsymbol{\xi}(\boldsymbol{X}, t) = \mathrm{e}^{\boldsymbol{\nu}} \boldsymbol{X}. \tag{B.1}$$

Here the exponential denotes the flow map generated by $\boldsymbol{\nu}$; that is, defining $\boldsymbol{x}(s)$ as the solution of

$$\frac{\mathrm{d}}{\mathrm{d}s}\left(\boldsymbol{x}(s)\right) = \boldsymbol{\nu}\left(\boldsymbol{x}(s), t\right), \quad \text{where} \quad \boldsymbol{x}(0) = \boldsymbol{X}, \tag{B.2}$$

and t is regarded as a fixed parameter, $\mathrm{e}^{\boldsymbol{\nu}} \boldsymbol{X} = \boldsymbol{x}(1)$. The glm average is then defined by the condition

$$\langle \boldsymbol{\nu} \rangle = 0, \tag{B.3}$$

which replaces GLM's condition $\langle \boldsymbol{\xi} \rangle = 0$ [115]. The divergence-free property of $\boldsymbol{\nu}$ ensures that (B.1) preserves volume. For small perturbations $\alpha \ll 1$, it is easy to relate $\boldsymbol{\xi}$ to $\boldsymbol{\nu}$ order-by-order in α. Expanding $\boldsymbol{\xi}$ according to (4.26) and, similarly, $\boldsymbol{\nu}$ according to $\boldsymbol{\nu} = \boldsymbol{\nu}^{(1)} + \boldsymbol{\nu}^{(2)} + \cdots$, we can use (B.1) to write

$$\boldsymbol{\xi} = \boldsymbol{\nu} + \boldsymbol{\nu} \cdot \nabla_3 \boldsymbol{\nu} + \cdots = \boldsymbol{\nu}^{(1)} + \left(\frac{1}{2} \boldsymbol{\nu}^{(1)} \cdot \nabla_3 \boldsymbol{\nu}^{(1)} + \boldsymbol{\nu}^{(2)} \right) + \cdots . \tag{B.4}$$

Identifying the first two orders in α yields

$$\boldsymbol{\nu}^{(1)} = \boldsymbol{\xi}^{(1)} \quad \text{and} \quad \boldsymbol{\nu}^{(2)} = \boldsymbol{\xi}^{(2)} - \frac{1}{2} \boldsymbol{\nu}^{(1)} \cdot \nabla_3 \boldsymbol{\nu}^{(1)}. \tag{B.5}$$

The condition (B.3) then becomes

$$\left\langle \boldsymbol{\xi}^{(2)} \right\rangle = \frac{1}{2} \left\langle \boldsymbol{\nu}^{(1)} \cdot \nabla_3 \boldsymbol{\nu}^{(1)} \right\rangle = \frac{1}{2} \left\langle \boldsymbol{\xi}^{(1)} \cdot \nabla_3 \boldsymbol{\xi}^{(1)} \right\rangle . \tag{B.6}$$

Appendix C

Mean dynamics

Following Salmon [108], the equations governing the mean dynamics are derived from the energy-momentum equations

$$\frac{\partial}{\partial X^j}\left(a^i_R \frac{\partial \langle L\rangle}{\partial a^i_{X^j}}\right) = \frac{\partial \langle L\rangle}{\partial R} - \left.\frac{\partial \langle L\rangle}{\partial R}\right|^{\chi}_{\text{expl}} \tag{C.1}$$

applied to the density $\langle L\rangle$ associated with the Lagrangian (4.32) (i.e. $\langle L\rangle$ is the integrand in the expression of $\langle\mathcal{L}\rangle$). In the energy-momentum equations, $(X^0,\ X^1,\ X^2,\ X^3) = (T,\ X,\ Y,\ Z)$, $(a^1, a^2, a^3) = (a, b, \theta)$ and Einstein's summation convention is used; R can be taken to be T, leading to an energy equation, or X, Y or Z, leading to the corresponding momentum equations. The sub- and superscript 'expl' and χ attached to the last term in (C.1) indicate derivatives of the terms that depend explicitly on R, treating the dependence introduced by χ as such an explicit dependence; in other words, the right-hand side of (C.1) collects derivatives associated with the mean flow only.

To keep compact expressions, we make the following definitions:

$$
\begin{aligned}
A \equiv & \frac{1}{J}\frac{\delta\langle\mathcal{L}\rangle}{\delta U} = U - \left(f_0 Y + \frac{1}{2}\beta Y^2\right) + A' \\
= & U - \left(f_0 Y + \frac{1}{2}\beta Y^2\right) - \frac{\mathrm{i}f_0}{4}(\chi_Z \chi^*_{ZX} - \chi^*_Z \chi_{ZX}) - f_0 Y \left\langle \xi^{(2)} \right\rangle_X - f_0 \left\langle \eta^{(2)} \right\rangle, \quad \text{(C.2a)} \\
B \equiv & \frac{1}{J}\frac{\delta\langle\mathcal{L}\rangle}{\delta V} = V + B' \\
= & V - \frac{\mathrm{i}f_0}{4}(\chi_Z \chi^*_{ZY} - \chi^*_Z \chi_{ZY}) - f_0 Y \left\langle \xi^{(2)} \right\rangle_Y, \quad \text{(C.2b)} \\
C \equiv & \frac{1}{J}\frac{\delta\langle\mathcal{L}\rangle}{\delta W} = C' \\
= & -\frac{\mathrm{i}f_0}{4}(\chi_Z \chi^*_{ZZ} - \chi^*_Z \chi_{ZZ}) - f_0 Y \left\langle \xi^{(2)} \right\rangle_Z, \quad \text{(C.2c)} \\
E \equiv & \frac{\delta\langle L\rangle}{\delta J} = \frac{1}{2}(U^2 + V^2) - \left(f_0 Y + \frac{1}{2}\beta Y^2\right) U + \theta Z + P + E' \\
= & \frac{1}{2}(U^2 + V^2) - \left(f_0 Y + \frac{1}{2}\beta Y^2\right) U + \theta Z + P \\
& - \frac{\mathrm{i}f_0}{4}(\chi_Z D_T \chi^*_Z - \chi^*_Z D_T \chi_Z) - \frac{1}{2} f_0 \beta Y |\chi_Z|^2 \\
& - f_0 Y D_T \left\langle \xi^{(2)} \right\rangle - f_0 \left\langle \eta^{(2)} \right\rangle U + \theta \left\langle \zeta^{(2)} \right\rangle, \quad \text{(C.2d)}
\end{aligned}
$$

where A', B', C' and E' group the NIW contributions. Note that (A', B', C') is the wave pseudomomentum. The terms in the energy-momentum tensor (C.1) for $R = T$ can then be written as

$$
\begin{aligned}
a^i_R \frac{\partial\langle L\rangle}{\partial a^i_T} &= a^i_R \frac{\partial U^j}{\partial a^i_T}\frac{\partial\langle L\rangle}{\partial U^j} \\
&= -\frac{1}{J}\frac{\partial\langle L\rangle}{\partial U}\frac{\partial(a,\ b,\ \theta)}{\partial(R,\ Y,\ Z)} - \frac{1}{J}\frac{\partial\langle L\rangle}{\partial V}\frac{\partial(a,\ b,\ \theta)}{\partial(X,\ R,\ Z)} - \frac{1}{J}\frac{\partial\langle L\rangle}{\partial W}\frac{\partial(a,\ b,\ \theta)}{\partial(X,\ Y,\ R)} \\
&= -A\frac{\partial(a,\ b,\ \theta)}{\partial(R,\ Y,\ Z)} - B\frac{\partial(a,\ b,\ \theta)}{\partial(X,\ R,\ Z)} - C\frac{\partial(a,\ b,\ \theta)}{\partial(X,\ Y,\ R)} \qquad \text{(C.3)}
\end{aligned}
$$

when (4.25) is used. Similarly, for $R = X,\ Y,\ Z$, we obtain

$$a_R^i \frac{\partial \langle L \rangle}{\partial a_X^i} = -B\frac{\partial(a,\ b,\ \theta)}{\partial(R,\ T,\ Z)} - C\frac{\partial(a,\ b,\ \theta)}{\partial(R,\ Y,\ T)} + (E - UA - VB - WC)\frac{\partial(a,\ b,\ \theta)}{\partial(R,\ Y,\ Z)}, \tag{C.4a}$$

$$a_R^i \frac{\partial \langle L \rangle}{\partial a_Y^i} = -A\frac{\partial(a,\ b,\ \theta)}{\partial(T,\ R,\ Z)} - C\frac{\partial(a,\ b,\ \theta)}{\partial(X,\ R,\ T)} + (E - UA - VB - WC)\frac{\partial(a,\ b,\ \theta)}{\partial(X,\ R,\ Z)}, \tag{C.4b}$$

$$a_R^i \frac{\partial \langle L \rangle}{\partial a_Z^i} = -A\frac{\partial(a,\ b,\ \theta)}{\partial(T,\ Y,\ R)} - B\frac{\partial(a,\ b,\ \theta)}{\partial(X,\ T,\ R)} + (E - UA - VB - WC)\frac{\partial(a,\ b,\ \theta)}{\partial(X,\ Y,\ R)}. \tag{C.4c}$$

Using (C.3)–(C.4), the momentum equations are derived from (C.1) with $R = X,\ Y,\ Z$ in the form

$$-D_T A + E_X = AU_X + BV_X + CW_X + (Z + \left\langle \zeta^{(2)} \right\rangle)\theta_X, \tag{C.5a}$$

$$-D_T B + E_Y = AU_Y + BV_Y + CW_Y + (Z + \left\langle \zeta^{(2)} \right\rangle)\theta_Y, \tag{C.5b}$$

$$-D_T C + E_Z = AU_Z + BV_Z + CW_Z + (Z + \left\langle \zeta^{(2)} \right\rangle)\theta_Z. \tag{C.5c}$$

Introducing the explicit forms (C.2) of A, B, C and D leads, after simplifications, to (4.36).

Appendix D

Alternative derivation

In this Appendix we show that the QGPV equation (4.8b) can be obtained directly from potential-vorticity conservation. In this procedure GLM, glm and indeed, any definition of the average $\left\langle \boldsymbol{\xi}^{(2)} \right\rangle$ gives the same leading order dynamics because the associated mean flow maps are $O(\alpha^2)$ close. The wave contributions to the mean dynamics come from different sources depending on the definition of the average, but their total effect is the same.

We start from the general Lagrangian (4.27). Taking δP variation we obtain

$$J = 1 + \nabla_3 \cdot \left(\left\langle \boldsymbol{\xi}^{(2)} \right\rangle - \frac{1}{2} \left\langle \boldsymbol{\xi}^{(1)} \cdot \nabla \boldsymbol{\xi}^{(1)} \right\rangle \right). \tag{D.1}$$

The relabeling symmetry of Lagrangian (4.27) gives potential-vorticity conservation

$$D_T \left(\frac{\nabla\theta \cdot \nabla \times \boldsymbol{A}}{J} \right) = 0, \tag{D.2}$$

where $\boldsymbol{A} = (A,\, B,\, C)$ are defined as in (C.2) but with the Lagrangian (4.27) in place of (4.32) [108].

Under quasi-geostrophic scaling and using the buoyancy equation (4.46) to replace W in the above equation, we obtain

$$D_T^0 \left(\frac{N^2(B_X - A_Y) + f_0 \theta'_Z}{J} \right) - \frac{f_0}{N^2} D_T^0 (\theta' (N^2)_Z) = 0, \tag{D.3}$$

where θ follows the definition (4.43). By substituting

$$B_X - A_Y = f_0 + \beta Y + \nabla^2 \psi + \frac{\mathrm{i} f_0}{2} \partial(\chi_Z^*, \chi_Z) + f_0 \left\langle \partial_x \xi^{(2)} + \partial_y \eta^{(2)} \right\rangle, \tag{D.4}$$

and (D.1), we obtain the modified QGPV equation

$$D_T^0\left(f_0+\beta Y+\nabla^2\psi+\partial_Z\left(\frac{f_0^2}{N^2}\partial_Z\psi\right)+\frac{\mathrm{i}f_0}{2}\partial(\chi_Z^*,\chi_Z)+\frac{f_0}{2}\left\langle\boldsymbol{\xi}^{(1)}\cdot\nabla_3\boldsymbol{\xi}^{(1)}\right\rangle\right)=0, \quad \text{(D.5)}$$

identical to (4.8b) since the last term is equal to $fG(\chi^*,\chi)$. Note that the cancellation of the second-order mean displacements (term $\nabla_3\cdot\left\langle\boldsymbol{\xi}^{(2)}\right\rangle$) indicates that this equation is independent of the specific averaging used to define the Lagrangian mean. In contrast, the individual wave contributions to the QGPV, namely the curl of the pseudomomentum (wave terms in (D.4)), the buoyancy term $N^2 f_0\left\langle\partial_Z\zeta^{(2)}\right\rangle$ and the density correction (divergence in (D.1)) depend on the averaging used.

Appendix E

Details of wave solution

In this appendix we show the detail calculation of obtaining the wave approximate solutions. In sections §E.1 and §E.2 approximations of two distinguished regimes are shown, the sublimit regime $\mathrm{II_B}$ corresponding the inertial layer is considered in §E.3.

E.1 Regime I

In this section we consider the position not close to the dominant inertial level, so in the z expansion (5.27) $\alpha = 0$ that

$$\zeta_* = -\frac{k_*\Lambda z}{f} = 1 + Z_\mathrm{I}. \tag{E.1}$$

As we have mentioned that because of the concentration of the wavepacket in spectrum space, k can follow the expansion (5.28). After substituting k and z expressions into (5.24) we obtain

$$w_1 = \frac{\mathrm{i}U_\mathrm{b}hk_*\Delta}{\epsilon\sqrt{2\pi}}\frac{k_*}{\epsilon}\left(\frac{\epsilon}{k_*\Delta}\right)^{\beta}\mathrm{e}^{-\frac{1}{2\Delta^2}\left(y-\frac{J\nu_*}{k_*\sqrt{1+\nu_*^2}}D_1\right)^2}\int_{-\infty}^{\infty}\frac{(1+Z_\mathrm{I})}{k_*\Delta\mathrm{Ro}}\left(\frac{(k_*\Delta)^2\mathrm{Ro}^2-1}{2Z_\mathrm{I}+Z_\mathrm{I}^2}\right)^{1/4} \times \mathrm{e}^{-\epsilon^{2\beta-2}(k_*\Delta)^{2-2\beta}K_\mathrm{I}^2/2+\mathrm{i}\epsilon^{\beta-1}k_*(k_*\Delta)^{-\beta}K(x-X_\mathrm{cI})}\mathrm{d}K_\mathrm{I}, \tag{E.2}$$

where

$$X_\mathrm{cI} = \frac{J}{k_*}\left[\sqrt{1+\nu_*^2}\left(\frac{1+Z_\mathrm{I}}{\sqrt{2Z_\mathrm{I}+Z_\mathrm{I}^2}}-\frac{k_*U_\mathrm{b}}{\sqrt{k_*^2U_\mathrm{b}^2-\epsilon^2f^2}}\right)-\frac{\nu_*^2}{\sqrt{1+\nu_*^2}}D_\mathrm{I}\right] \tag{E.3}$$

with $D_{\mathrm{I}} = \ln(1 + Z_{\mathrm{I}} + \sqrt{2Z_{\mathrm{I}} + Z_{\mathrm{I}}^2}) - \ln(\zeta_{\mathrm{b}*} + \sqrt{\zeta_{\mathrm{b}*}^2 - 1})$. Here the lower limit of the integral is taken as $-\infty$ by omitting exponential small terms, and the expansion of $D(\zeta)$ result in the term $\mathrm{i}\epsilon^{\beta-1}k_*(k_*\Delta)^{-\beta}K(x - X_{\mathrm{cI}})$ in exponential, where the ϵ^β order accord with (5.30).

After balancing the exponential terms in (E.2):

$$-\epsilon^{2\beta-2}(k_*\Delta)^{2-2\beta}K_{\mathrm{I}}^2/2 \sim \mathrm{i}\epsilon^{\beta-1}k_*(k_*\Delta)^{-\beta}K(x - X_{\mathrm{cI}}), \tag{E.4}$$

we obtain a distinguished regime with $\beta = 1$. In fact this finding of β is not necessary as it does not change the dominant effect based on which the expansion is made. And (E.2) can be directly integrated to become

$$w_1 \doteq \mathrm{i}hf(1 + Z_{\mathrm{I}}) \left(\frac{(k_*\Delta)^2\mathrm{Ro}^2 - 1}{2Z_{\mathrm{I}} + Z_{\mathrm{I}}^2}\right)^{1/4} \mathrm{e}^{-\frac{1}{2\Delta^2}\left(y - \frac{J\nu_*}{k_*\sqrt{1+\nu_*^2}}D_1\right)^2} \mathrm{e}^{-\frac{(x-X_{\mathrm{cI}})^2}{2\Delta^2}}, \tag{E.5}$$

which verifies the validity of ray tracing in this regime.

E.2 Regime II

When the wave close to the dominant inertial level the singularity effect become important, so in this section we consider the distinguished regime where singularity effect appear at leading order. Since this region will be closer to the dominant inertial level compared with Regime I, i.e. the region in the vicinity of $\zeta - 1$ with $|\zeta - 1| \ll 1$ so that α is grater than 0 in expression (5.27). Now we should expand $D(\zeta)$ following (5.31), and here the leading order depends on the smaller value between α and β, thus a distinguished regime should be achieved with $\beta = \alpha$. Then the only coefficient to be decided is α, which indicates the vertical region. Now the expansion of $D(\zeta)$ can be explicitly expressed as

$$\begin{aligned} D(\zeta) = &-\ln(\zeta_{\mathrm{b}} + \sqrt{\zeta_{\mathrm{b}}^2 - 1}) + \left(\frac{\epsilon}{k_*\Delta}\right)^{\alpha/2} \sqrt{2(K_{\mathrm{II}} + Z_{\mathrm{II}})} \\ &- \left(\frac{\epsilon}{k_*\Delta}\right)^{\alpha} \frac{k_*\Delta\mathrm{Ro}}{\sqrt{(k_*\Delta)^2\mathrm{Ro}^2 - 1}} K_{\mathrm{II}} + \text{h.o.t.}, \end{aligned} \tag{E.6}$$

where the leading $O(\epsilon^{\alpha/2})$ is different from that of Regime I and it will profoundly change the approximate result.

Substituting the z and k expansions (5.27) and (5.28) into (5.24), and using (E.6),

w_1 can be expressed as

$$\begin{aligned} w_1 \quad = \quad & \frac{\mathrm{i}U_\mathrm{b}hk_*^2\Delta}{2^{1/4}\epsilon^2\sqrt{2\pi}}\left(\frac{\epsilon}{k_*\Delta}\right)^{\alpha-1/4}\frac{(\zeta_\mathrm{b}^2-1)^{1/4}}{\zeta_\mathrm{b}}\mathrm{e}^{-\frac{1}{2\Delta^2}\left(y-\frac{J\nu_*}{k_*\sqrt{1+\nu_*^2}}D_\mathrm{II}\right)^2} \\ & \times\int_{-Z_\mathrm{II}}^{\infty}\frac{1}{(K_\mathrm{II}+Z_\mathrm{II})^{1/4}}\mathrm{e}^{-\epsilon^{2\alpha-2}(k_*\Delta)^{2-2\alpha}K_\mathrm{I}^2/2}\mathrm{e}^{-\mathrm{i}\epsilon^{\alpha/2-1}(k_*\Delta)^{-\alpha/2}J\sqrt{1+\nu_*^2}\sqrt{2(K_\mathrm{II}+Z_\mathrm{II})}} \\ & \times\mathrm{e}^{\mathrm{i}\epsilon^{\alpha-1}K_\mathrm{II}\left(k_*(k_*\Delta)^{-\alpha}x+J(k_*\Delta)^{-\alpha}\left[\sqrt{1+\nu_*^2}\frac{k_*\Delta\mathrm{Ro}}{\sqrt{(k_*\Delta)^2\mathrm{Ro}^2-1}}+\frac{\nu_*^2}{\sqrt{1+\nu_*^2}}D_\mathrm{II}\right]\right)}\mathrm{d}K_\mathrm{II}, \end{aligned} \tag{E.7}$$

where $D_\mathrm{II} = -\ln(\zeta_{\mathrm{b}*}+\sqrt{\zeta_{\mathrm{b}*}^2-1})$. So the distinguished regime is obtained when the exponentials are of the same order:

$$\epsilon^{2\alpha-2}(k_*\Delta)^{2-2\alpha}K_\mathrm{II}^2/2 \sim \mathrm{i}\epsilon^{\alpha/2-1}(k_*\Delta)^{-\alpha/2}J\sqrt{1+\nu_*^2}\sqrt{2(K_\mathrm{II}+Z_\mathrm{II})}, \tag{E.8}$$

from which we get

$$\alpha = 2/3. \tag{E.9}$$

So by substituting $\alpha = 2/3$ into (E.7) we obtain

$$\begin{aligned} w_1 \doteq & \frac{\mathrm{i}U_\mathrm{b}hk_*^2\Delta}{2^{1/4}\sqrt{2\pi}\epsilon^{19/12}(k_*\Delta)^{5/12}}\mathrm{e}^{-\frac{1}{2\Delta^2}\left(y-\frac{J\nu_*}{k_*\sqrt{1+\nu_*^2}}D_\mathrm{II}\right)^2} \\ & \times\int_{-Z_\mathrm{II}}^{\infty}\frac{1}{(K_\mathrm{II}+Z_\mathrm{II})^{1/4}}\mathrm{e}^{\epsilon^{-2/3}(k_*\Delta)^{2/3}\left(-\frac{K_\mathrm{II}^2}{2}-\mathrm{i}J(k_*\Delta)^{-1/3}\sqrt{1+\nu_*^2}\sqrt{2(K_\mathrm{II}+Z_\mathrm{II})}+\mathrm{i}K_\mathrm{II}X_\mathrm{II}\right)}\mathrm{d}K_\mathrm{II}, \end{aligned} \tag{E.10}$$

where

$$X_\mathrm{II} = \epsilon^{1/3}\left(k_*(k_*\Delta)^{-4/3}x+J(k_*\Delta)^{-4/3}\left[\sqrt{1+\nu_*^2}\frac{k_*\Delta\mathrm{Ro}}{\sqrt{(k_*\Delta)^2\mathrm{Ro}^2-1}}+\frac{\nu_*^2}{\sqrt{1+\nu_*^2}}D_\mathrm{II}\right]\right). \tag{E.11}$$

This expression of X_II, where x is rescaled by $(k_*\Delta)^{1/3}\Delta$, shows that the vertical singularity also modify the horizontal scale of the wavepacket.

Taking advantage of the large exponential terms we can using the standard saddle point method to approximate (E.10) as

$$w_1 = \frac{\mathrm{i}U_\mathrm{b}hk_*^2\Delta}{2^{1/4}\epsilon^{5/4}(k_*\Delta)^{3/4}}q(K_\mathrm{IIs})\sqrt{\frac{1}{p''(K_\mathrm{IIs})}}\mathrm{e}^{-\frac{1}{2\Delta^2}\left(y-\frac{J\nu_*}{k_*\sqrt{1+\nu_*^2}}D_\mathrm{II}\right)^2}\mathrm{e}^{(k_*\Delta)^{2/3}P(K_\mathrm{IIs})}, \tag{E.12}$$

where

$$\begin{aligned} q(K_{\rm II}) &= \frac{1}{(K_{\rm II}+Z_{\rm II})^{1/4}}, \\ p(K_{\rm II}) &= -\frac{K_{\rm II}^2}{2} - {\rm i}J(k_*\Delta)^{-1/3}\sqrt{1+\nu_*^2}\sqrt{2(K_{\rm II}+Z_{\rm II})} + {\rm i}K_{\rm II}X_{\rm II}, \end{aligned} \tag{E.13}$$

with $K_{\rm IIs}$ is the saddle point that $p'(K_{\rm IIs}) = 0$ and "$'$" denotes derivative. Here only one out of three saddle points is used in this expression, since the branch cut result in two Riemann surfaces and the contour lies only on one surface, the chosen saddle point is the one that lies on the same Riemann surface and the contour can be diverted into.

Note that in the above expression the boundary effect is not considered because replacing $-Z_{\rm II}$ by $-\infty$ in (E.10) only bring about an exponentially small term. The asymptotics of large $Z_{\rm II}$ limit in (5.34) and small $Z_{\rm I}$ limit in (E.2) match, which indicates that there is no distinguished regime between Regime I and II. This matching is also observed in the subfigure (c) in Figure 5.3.

E.3 Regime $\rm II_B$

In the previous two sections we have visited two distinguished regimes, in order to study wave-mean flow interaction which concentrates in inertial layer with characteristic thickness δ_* as is estimated by (5.13), in this section we study Regime $\rm II_B$ with $\alpha = 1$ such that

$$\zeta_* = 1 + \left(\frac{\epsilon}{k_*\Delta}\right) Z. \tag{E.14}$$

Since Regime $\rm II_B$ is a sublimt of Regime II, we can use the result (5.34) to obtain its approximation, however, for simpler calculation and easier understanding, we directly make approximation in this regime.

Following the argument in the calculation of Regime II in §E.2, for a distinguished regime the wave number should be expanded as

$$k = \epsilon^{-1}k_*\left(1 + \frac{\epsilon}{k_*\Delta}K\right), \tag{E.15}$$

corresponding to (E.14).

Hence, as to the exponential terms

$$(k_*\Delta)^{2-2\alpha}K^2/2 \ll {\rm i}\epsilon^{-1/2}(k_*\Delta)^{-1/2}J\sqrt{1+\nu_*^2}\sqrt{2(K+Z)}, \tag{E.16}$$

which makes the dominant term in exponential of (5.24) is purely imaginary, In addition, considering that when $\alpha = 1$ term $\mathrm{e}^{-(k_*\Delta)^{2-2\alpha}K^2/2} = O(1)$, the stationary phase method can be applied.

Substituting z and k expansion into (5.24) we obtain

$$\begin{aligned} w_1 = & \frac{\mathrm{i}U_\mathrm{b}hk_*(k_*\Delta)^{1/4}}{2^{3/4}\pi^{1/2}\epsilon^{5/4}}\mathrm{e}^{-\frac{1}{2\Delta^2}\left(y-\frac{J\nu_*}{k_*\sqrt{1+\nu_*^2}}D_\mathrm{II}\right)^2} \\ & \times \int_{-Z}^{\infty}\frac{1}{(K+Z)^{1/4}}\mathrm{e}^{-\frac{K^2}{2}}\mathrm{e}^{\epsilon^{-1/2}(k_*\Delta)^{1/2}\left(-\mathrm{i}J(k_*\Delta)^{-1}\sqrt{1+\nu_*^2}\sqrt{2(K+Z)}+\mathrm{i}KX\right)}\mathrm{d}K, \end{aligned} \tag{E.17}$$

which after being approximated by stationary phase results in

$$w_1 \doteq \frac{\mathrm{i}hfJ^{1/2}\left(1+\nu_*^2\right)^{1/4}\left((k_*\Delta)^2\mathrm{Ro}^2-1\right)^{1/4}}{(k_*\Delta)^{1/2}}\mathrm{e}^{-\frac{1}{2\Delta^2}\left(y-\frac{J\nu_*}{k_*\sqrt{1+\nu_*^2}}D_\mathrm{II}\right)^2}\frac{1}{X}\mathrm{e}^{-\frac{1}{2}\left(\frac{J^2\left(1+\nu_*^2\right)}{2(k_*\Delta)^2X^2}-Z\right)^2}. \tag{E.18}$$

where

$$X = \epsilon^{1/2}\left(k_*(k_*\Delta)^{-3/2}x - J(k_*\Delta)^{-3/2}\left[\sqrt{1+\nu_*^2}\frac{(k_*\Delta)\mathrm{Ro}}{\sqrt{(k_*\Delta)^2\mathrm{Ro}^2-1}}+\frac{\nu_*^2}{\sqrt{1+\nu_*^2}}D_\mathrm{II}\right]\right). \tag{E.19}$$

Here the stationary phase is

$$K_\mathrm{s} = \frac{J^2\left(1+\nu_*^2\right)}{2(k_*\Delta)^2X^2} - Z. \tag{E.20}$$

Bibliography

[1] *Digital Library of Mathematical Functions.* National Institute of Standards and Technology from http://dlmf.nist.gov/., 2012-03-23.

[2] M. H. Alford. Improved global maps and 54-year history of wind-work on ocean inertial motions. *Geophys. Res. Lett.*, 30:1424, 2003.

[3] M. Alghane, Y. Q. Fu, B. X. Chen, Y. Li, M. P. Y. Desmulliez, and A. J. Walton. Streaming phenomena in microdroplets induced by Rayleigh surface acoustic wave. *J. Appl. Phys.*, 109(114901):1–8, 2011.

[4] D. G. Andrews and M. E. McIntyre. Planetary waves in horizontal and vertical shear: the generalized Eliassen-Palm relation and the mean zonal acceleratio. *J. Atmos. Sci.*, 33:2031–2048, 1976.

[5] D. G. Andrews and M. E. McIntyre. An exact theory of nonlinear waves on a Lagrangian-mean flow. *J. Fluid Mech.*, 89(4):609–646, 1978.

[6] D. G. Andrews and M. E. McIntyre. Generalised Eliassen-Palm and Charney-Drazin theorems for waves on axisymmetric mean flows in compressible atmospheres. *J. Atmos. Sci.*, 35:175–185, 1978.

[7] S. I. Badulin and V. I. Shrira. On the irreversibility of internal-wave dynamics due to wave trapping by mean flow inhomogeneities. Part 1. Local analysis. *J. Fluid Mech.*, 251:21–53, 1993.

[8] M. P. Baldwin, L J. Gray, T. J. Dunkerton, K. Hamilton, P. H. Haynes, W. J. Randel andJ. R. Holton, M. J. Alexander, I. Hirota, T. Horinouchi, D. B. A. Jones, J. S. Kinnersley, C. Marquardt, K. Sato, and M. Takahashi. The quasi-biennial oscillation. *Revs. Geophys.*, 39:179–229, 2001.

[9] N. J. Balmforth, S. G. Llewellyn Smith, and W. R. Young. Enhanced dissipation of near-inertial waves in an idealized geostrophic flow. *J. Mar. Res.*, 56:1–40, 1998.

[10] M. Barmatz. Overview of containerless processing technologies. *MRS Proceedings*, 9:25–37, 1982.

[11] A. B. Basset. On the motion of a sphere in a viscous liquid. *Phil. Trans. R. Soc. A*, 179:43–63, 1888.

[12] G. K. Batchelor. *An Introduction to Fluid Dynamics*. Cambridge University Press, 1967.

[13] V. B. Berestetskii, E. M. Lifshitz, and L. P. Pitaevskii. *Quantum electrodynamics*. Cambridge University Press, 2nd edition, 1982.

[14] H. Blasius. Grenzschichten in flüssigkeiten mit kleiner reibung. *Z. Math. Phys.*, 56:1–37, 1908.

[15] O. Bokhove, J. Vanneste, and T. Warn. A variational formulation for barotropic quasi-geostrophic flows. *Geophys. Astrophys. Fluid Dynam.*, 88:67–79, 1998.

[16] J. R. Booker and F. P. Bretherton. The critical layer for internal gravity waves in a shear flow. *J. Fluid Mech.*, 27:513–539, 1967.

[17] J. P. Boyd. The noninteraction of waves with the zonally averaged flow on a spherical earth and the interrelationships on eddy fluxes of energy, heat and momentum. *J. Atmos. Sci.*, 33:2285–2291, 1976.

[18] C. E. Bradley. Acoustic streaming field structure: the influence of the radiator. *J. Acoust. Soc. Am.*, 100:13991408, 1996.

[19] F. Bretherton. On the mean motion induced by internal gravity waves. *J. Fluid Mech.*, 36:758–803, 1969.

[20] F. P. Bretherton. The propagation of groups of internal gravity waves in a shear flow. *Quart. J. Roy. Meteor. Soc.*, 92:466–480, 1966.

[21] O. Bühler. On the vorticity transport due to dissipating or breaking waves in shallow-water flow. *J. Fluid Mech.*, 407:235–263, 2000.

[22] O. Bühler. *Waves and mean flows*. Cambridge University Press, 2009.

[23] O. Bühler and M. E. McIntyre. On non-dissipative wavemean interactions in the atmosphere or oceans. *J. Fluid Mech.*, 354:301–343, 1998.

[24] O. Bühler and M. E. McIntyre. Wave capture and wave-vortex duality. *J. Fluid Mech.*, 534:67–95, 2005.

[25] J. G. Charney and P. G. Drazin. Propagation of planetary-scale disturbances from the lower into the upper atmosphere. *J. Geophys. Res.*, 66:83–109, 1961.

[26] S. Chen, G. L. Eyink, M. Wan, and Z. Xiao. Is the Kelvin theorem valid for high Reynolds number turbulence. *Phys. Rev. Lett.*, 97:144505, 2006.

[27] C. J. Cotter and S. Reich. Adiabatic invariance and applications: From molecular dynamics to numerical weather prediction. *BIT Numer. Math.*, 44:439–455, 2004.

[28] C. D. Danilov. Average force acting on a small sphere in a traveling-wave field in a viscous fluid. *Sov. Phys. Acoust.*, 31:26–28, 1985.

[29] C. D. Danilov. The mean force acting on a small body in an axisymmetric sound field in a real medium. *Fluid Dynamics*, 21:812–820, 1986.

[30] C. D. Danilov and M. A. Mironov. Mean force on a small sphere in a sound field in a viscous fluid. *J. Acoust. Soc. Am.*, 107:143–153, 2000.

[31] E. Danioux, J. Vanneste, P. Klein, and H. Sasaki. Spontaneous inertia-gravity-wave generation by surface-intensified turbulence. *J. Fluid Mech.*, 699:153–157, 2012.

[32] E. A. D'Asaro. Turbulence in the upper-ocean mixed layer. *Ann. Rev. Fluid Mech.*, 6:101–115, 2014.

[33] E. A. D'Asaro, C. C. Eriksen, M. D. Levine, C. A. Paulson, P. Niiler, and P. Van Meurs. Upper-ocean inertial currents forced by a strong storm. Part I: Data and comparisons with linear theory. *J. Phys. Oceanogr.*, 25:2909–2936, 1995.

[34] F. Debbasch. What is a mean gravitational field? *Eur. Phys. J. B*, 37(2):257–270, 2004.

[35] S. C. R. Dennis and J. D. A. Walker. Numerical Solutions for Time-dependent Flow Past an Impulsively Strated Sphere. *Phys. Fluids*, 15(4):517–525, 1972.

[36] M. B. Dentry, L. Y. Yeo, and J. R. Friend. Frequency effects on the scale and behavior of acoustic streaming. *Phys. Rev. E*, 89(1):012303, 2014.

[37] A. A. Doinikov. Radiation force due to a spherical sound field on a rigid sphere in a viscous fluid. *J. Acoust. Soc. Am.*, 96(5):3100–3105, 1994.

[38] A. A. Doinikov. Acoustic radiation pressure on a compressible sphere in a viscous-fluid. *J. Fluid Mech.*, 267:1–21, 1994.

[39] A. A. Doinikov. Acoustic radiation pressure on a rigid sphere in a viscous fluid. *Proc. R. Soc. Lond. A*, 447(1931):447–466, 1994.

[40] A. A. Doinikov. theory of acoustic radiation pressure for actural fluids. *Phys. Rev. E*, 54(6):6297–6303, 1996.

[41] A. A. Doinikov. Acoustic radiation force on a sphereical particle in a viscous heat-conducting fluid. I. general formula. *J. Acoust. Soc. Am.*, 101:713–721, 1997.

[42] A. A. Doinikov. Acoustic radiation force on a sphereical particle in a viscous heat-conducting fluid. II. force on a rigid sphere. *J. Acoust. Soc. Am.*, 101(2):722–730, 1997.

[43] T. H. A. Duhaut and D. N. Straub. Wind stress dependence on ocean surface velocity: Implications for mechanical energy input to ocean circulation. *J. Phys. Oceanogr.*, 36:202–211, 2006.

[44] C. Eckart. Vortices and streams caused by sound waves. *Phys. Rev*, 73:68–76, 1948.

[45] H. J. Edmon, Jr., B. J. Hoskins, and M. E. McIntyre. Eliassen-palm cross sections for the troposphere. *J. Atmos. Sci.*, 37:2600–2616, 1980.

[46] A. Eliassen and E. Palm. On the transfer of energy in stationary mountain waves. *Geopy. Publ.*, 22(3):1–23, 1961.

[47] G. Falkovich, E. Kuznetsov, and S. Medvedev. Nonlinear interaction between long inertio-gravity and rossby waves. *Nonlin. Processes Geophys.*, 1:168–171, 1994.

[48] R. Ferrari and C. Wunsch. Ocean circulation kinetic energy: reservoirs, sources, and sinks. *Annu. Rev. Fluid Mech.*, 31:962–971, 2009.

[49] J. Friend and L. Y. Yeo. Microscale acoustofluidics: Microfluidics driven via acoustics and ultrasonics. *Rev. Mod. Phys.*, 83:647–704, 2011.

[50] D. C. Fritts and M. J. Alexander. Gravity wave dynamics and effects in the middle atmosphere. *Rev. Geophys.*, 41:1003, 2003.

[51] T. Frommelt, M. Kostur, M. Wenzel-Schäfer, P. Talkner, P. Hänggi, and A. Wixforth. Microfluidic mixing via acoustically driven chaotic advection. *Phys. Rev. Lett.*, 100:034502, 2008.

[52] L.-L. Fu. Observations and models of inertial waves in the deep ocean. *Rev. Geophys. Space Phys.*, 19:141–170, 1981.

[53] L. L. Fu, T. Keffer, P. P. Niiler, and C. Wunsch. Observations of mesoscale variability in the western North Atlantic: a comparative study. *J. Mar. Res.*, 40 (3):809–848, 1982.

[54] C. Garrett. What is the "near-inertial" band and why is it different from the rest of the internal wave spectrum? *J. Phys. Oceanogr.*, 41:253–282, 2001.

[55] A. Gertz and D. N. Straub. Near-inertial oscillations and the damping of midlatitude gyres: a modeling study. *J. Phys. Oceanogr.*, 39:2338–2350, 2009.

[56] I. Gjaja and D. D. Holm. Self-consistent Hamiltonian dynamics of wave mean-flow interaction for a rotating stratified incompressible fluid. *Physica D*, 98:343–378, 1996.

[57] L. P. Gor'kov. On the forces acting on a small particle in an acoustical field in an ideal fluid. *Soviet Physics*, 6(9):773–775, 1962.

[58] R. Grimshaw. Wave action and wave-mean flow interaction, with application to stratified shear flows. *Ann. Rev. Fluid Mech.*, 16:11–44, 1984.

[59] M. Groschl. Ultrasonic separation of suspended particles - part I: Fundamentals. *Acoustica*, 84:432–447, 1998.

[60] Y. Guo and Oliver Bühler. Wavevortex interactions in the nonlinear Schrödinger equation. *Phys. Fluids*, 26:027105, 2014.

[61] A. Hasha, O. Bühler, and J. Scinocca. Gravity wave refraction by three-dimensionally varying winds and the global transport of angular momentum. *J. Atmos. Sci.*, 65:2892–2906, 2008.

[62] D. Holliday and M. E. McIntyre. On potential energy density in an incompressible stratified fluid. *J. Fluid Mech.*, 107:221–225, 1981.

[63] D. D. Holm, T. Schmah, and C. Stoica. *Geometric mechanics and symmetry.* Oxford University Press, 2009.

[64] J. Hu, J. Yang, and J. Xu. Ultrasonic trapping of small particles by sharp edges vibrating in a flexural mode. *Appl. Phys. Lett.*, 85:6042–6044, 2004.

[65] J. K. Hunter and M. Ifrim. A quasi-linear Schrödinger equation for large amplitude inertial oscillations in a rotating shallow fluid. *IMA J. Appl. Math.*, 78:777–796, 2013.

[66] V. G. Jenson. Viscous flow round a sphere at low Reynolds numbers (<40). *Proc. R. Soc. Lond. A*, 249(1258):346–366, 1959.

[67] W. L. Jones. Propagation of internal gravity waves in fluids with shear flow and rotation. *J. Fluid Mech.*, 30(3):439–448, 1967.

[68] L. V. King. On the acoustic radiation pressure on spheres. *Proc. R. Soc. A*, 147 (861):212–240, 1934.

[69] E. Kunze. Near-inertial wave propagation in geostrophic shear. *J. Phys. Oceanogr.*, 15:544–565, 1985.

[70] H. Lamb. *Hydrodynamics*. Cambridge University Press, 6 edition, 1932.

[71] E. Laugh, M. P. Brenner, and H. A. Stone. Microuidics: The no-slip boundary condition. In C. Tropea J. Foss and A. Yarin, editors, *Handbook of Experimental Fluid Dynamics*, chapter 19, pages 1219–1240. Springer, New-York(2007), 2007.

[72] L. C. St. Laurent, H. L. Simmons, , and S. R. Jayne. Estimating tidally driven mixing in the deep ocean. *Geophys. Res. lett.*, 29:21–1–21–4, 2002.

[73] H. Li, J. R. Friend, and L. Y. Yeo. Surface acoustic wave concentration of particle and bioparticle suspensions. *Biomed Microdevices*, 9(5):647–656, 2007.

[74] J. Lighthill. Acoustic streaming. *J. Sound Vibr.*, 61:391–418, 1978.

[75] M. J. Lighthill. *Waves in Fluids*. Cambridge university press, 1978.

[76] M. S. Longuet-Higgins. Mass transport in water waves. *Phil. Trans. R. Soc. Lond. A*, 245:535–581, 1953.

[77] F. Lott and L. Guez. A stochastic parameterization of the gravity waves due to convection and its impact on the equatorial stratosphere. *J. Geophys. Res.*, 118: 8897–8909, 2013.

[78] F. Lott and M. J. Miller. A new subgrid-scale orographic parametrization: Its formulation and testing. *Quart. J. Roy. Meteor. Soc.*, 123:101–127, 1997.

[79] F. Lott, R. Plougonven, and J. Vanneste. Gravity waves generated by sheared potential vorticity anomalies. *J. Atmos. Sci.*, 67:157–170, 2010.

[80] F. Lott, R. Plougonven, and J. Vanneste. Gravity waves generated by sheared three-dimensional potential vorticity anomalies. *J. Atmos. Sci.*, 69(7):2134–2151, 2012.

[81] F. Lott, C. Millet, and J. Vanneste. Inertia-gravity waves in inertially stable and unstable shear flows. *submitted to J. Fluid Mech.*, 2015.

[82] O. Manor, L. Y. Yeo, and J. R. Friend. The appearance of boundary layers and drift flows due to high-frequency surface waves. *J. Fluid Mech.*, 707:482–495, 2012.

[83] A. Martin and F. Lott. Synoptic responses to mountain gravity waves encountering directional critical levels. *J. Atmos. Sci.*, 64:828–848, 2007.

[84] M. R. Maxey and J. J. Riley. Equation of motion for a small rigid sphere in a nonuniform flow. *Phys. Fluids*, 26(4):883–889, 1983.

[85] M. E. McIntyre. On the 'wave momentum' myth. *J. Fluid Mech.*, 106:331–347, 1981.

[86] M . E. Mclntyre and W. A. Norton. Dissipative wave-mean interactions and the transport of vorticity or potential vorticity. *J. Fluid Mech.*, 212:403–435, 1990.

[87] S.B. Medvedev and V. Zeitlin. Turbulence of near-inertial waves in the continuously stratified fluid. *Physics Letters A*, 371(3):221–227, 1997.

[88] J. W. Miles. On the stability of heterogeneous shear flows. *J. Fluid Mech.*, 10(6): 496–508, 1961.

[89] J. W. Miles. On the stability of heterogeneous shear flows. Part 2. *J. Fluid Mech.*, 16:209–227, 1963.

[90] M. J. Miller, T. N. Palmer, and R. Swinbank. Parametrization and influence of subgridscale orography in general circulation and numerical weather prediction models. *Meteor. Atmos. Phys.*, 40:84–109, 1989.

[91] C. N. K. Mooers. Several effects of a baroclinic current on the cross-stream propagation of inertial-internal waves. *Geophys. Fluid Dyn.*, 6:245–275, 1975.

[92] C. N. K. Mooers. Several effects of baroclinic currents on the three-dimensional propagation of inertial-internal waves. *Geophys. Fluid Dyn.*, 6:277–284, 1975.

[93] C. L. M. H. Navier. Mémoire sur les lois du mouvement des fluides. *Mémoires de l'Académie Royale des Sciences de l'Institut de France*, VI:389–440, 1823.

[94] M. Nikurashin and R. Ferrari. Global energy conversion rate from geostrophic flows into internal lee waves in the deep ocean. *Geophys. Res. Lett.*, 38(8), 2011.

[95] M. Nikurashin, G. K. Vallis, and A. Adcroft. Routes to energy dissipation for geostrophic flows in the Southern Ocean. *Nature Geoscience*, 6:48–51, 2013.

[96] W. L. Nyborg. Acoustic streaming due to attenuated plane waves. *J. Acoust. Soc. Am.*, 25(1):68–75, 1953.

[97] W. L. M. Nyborg. Acoustic streaming. In W. P. Mason, editor, *Physical Acoustics*, volume 2B, pages 265–331. Academic Press, New York, 1965.

[98] S. Oberti, A. Neild, R. Quach, and J. Dual. The use of acoustic radiation forces to position particles within fluid droplets. *Ultrasonics*, 49(1):47–52, 2009.

[99] M. Oliver. Variational asymptotics for rotating shallow water near geostrophy: a transformational approach. *J. Fluid Mech.*, 551:197–234, 2006.

[100] T. N. Palmer, G. J. Shutts, and R. Swinbank. Alleviation of a systematic westerly bias in general circulation and numerical weather prediction models through an orographic gravity wave drag parametrization. *Quart. J. R. Met. Soc.*, 102:1001–1039, 1986.

[101] L. Rayleigh. *Theory of Sound*, volume II, chapter XIX, pages 333 – 342. Dover Pubulications, New York, 1945.

[102] O. Reynolds. On the dynamical theory of incompressible viscous fluids and the determination of the criterion. *Phil. Trans. R. Soc. A*, 186:123–164, 1895.

[103] P B Rhines. Geostrophic turbulence. *Ann. Rev. Fluid Mech.*, 11:401–441, 1979.

[104] N. Riley. Steady streaming. *Annu. Rev. Fluid Mech.*, 33:43–65, 2001.

[105] Y. Rimon and S. Cheng. Numerical solution of a uniform flow over a sphere at intermidiate reynolds numbers. *Phys. Fluids*, 12(5P1):949–959, 1969. ISSN 1070-6631. doi: 10.1063/1.2163685.

[106] P. R. Rogers, J. R. Friend, and L. Y. Yeo. Exploitation of surface acoustic waves to drive size-dependent microparticle concentration within a droplet. *Lab Chip.*, 10(7):2979–2985, 2010.

[107] R. Salmon. Hamiltonian fluid mechanics. *Ann. Rev. Fluid Mech.*, 20:225–256, 1988.

[108] R. Salmon. An alternative view of generalized Lagrangian mean theory. *J. Fluid Mech.*, 719:165–182, 2013.

[109] R. B. Scott, J. A. Goff, A. C. Naveira Garabato, and A. J. G. Nurser. Global rate and spectral characteristics of internal gravity wave generation by geostrophic flow over topography. *J. Geophys. Res.*, 116(C9), 2011.

[110] M. Settnes and H. Bruus. Forces acting on a small particle in an acoustical field in a viscous fluid. *Phys. Rev. E*, 85:016327, Jan 2012.

[111] T. G. Shepherd. Symmetries, conservation laws and Hamiltonian structure in geophysical fluid dynamics. *Adv. Geophys.*, 32:287–338, 1990.

[112] N. L. Shirokova. *Physical Principles of Ultrasonic Technology*, volume 2 of *series*. Plenum, New York, address, edition edition, 1973.

[113] G. Shutts. A linear model of back-sheared flow over an isolated hill in the presence of rotation. *J. Atmos. Sci.*, 58:3293–3311, 2001.

[114] A. M. Soward. A kinematic theory of large magnetic reynolds number dynamos. *Phil. Trans. Roy. Soc. A*, 272:431–462, 1972.

[115] A. M. Soward and P. H. Roberts. The hybrid Euler–Lagrange procedure using an extension of Moffatt's method. *J. Fluid Mech.*, 661:45–72, 2010.

[116] T. M. Squires and S. R. Quake. Microfluidics: fluid physics at the nanoliter scale. *Rev. Mod. Phys.*, 77:977–1026, 2005.

[117] H.A. Stone, A.D. Stroock, and A. Ajdari. Engineering flows in small devices microfluidics toward a lab-on-a-chip. *Annu. Rev. Fluid mech.*, 36:381–411, 2004.

[118] P. Tabeling. *Introduction to Microfluidics*. Oxford University Press, Oxford, 2005.

[119] M. K. Tan, L. Y. Yeo, and J. R. Friend. Rapid fluid flow and mixing induced in microchannels using surface acoustic waves. *EPL*, 87(4), 2009.

[120] M. Uryu. On the transport of energy and momentum in stationary waves in a rotating stratified fluid. *J. Meteor. Soc. Japan*, 51(2):86–92, 1973.

[121] G. K. Vallis. *Atmospheric and oceanic fluid dynamics: fundamentals and large-scale circulation*. Cambridge University Press, 2006.

[122] V. Vandaele, P. Lambert, and A. Delchambre. Non-contact handling in microassembly: Acoustical levitation. *Precision Engineering*, 29:491–505, 2005.

[123] J. Vanneste. Balance and spontaneous generation in geophysical flows. *Annu. Rev. Fluid Mech.*, 45:147–172, 2013.

[124] J. Vanneste. Deriving the Young-Ben Jelloul model of near-inertial waves by Whitham averaging. *arXiv:1410.0253*, 2014.

[125] J. Vanneste and O. Bühler. Streaming by leaky surface acoustic waves. *Proc. R. Soc. A*, 467:1779–1800, 2011.

[126] P. J. Westervelt. The theory of steady forces caused by sound waves. *J. Acoust. Soc. Am.*, 23(3):312–315, 1951.

[127] P. J. Westervelt. The theory of steady rotational flow generated by a sound field. *J. Acoust. Soc. Am.*, 25(1):60–67, 1953.

[128] G. B. Whitham. *Linear and nonlinear waves*. Wiley, 1974. 636 pages.

[129] G. Witt. Height, structure and displacements of noctilucent clouds. *Tellus*, 14:1, 1962.

[130] C. Wunsch. The work done by the wind on the oceanic general circulation. *J. Phys. Oceanogr.*, 28:2332–2340, 1998.

[131] C. Wunsch and R. Ferrari. Vertical mixing, energy, and the eneral circulation of the oceans. *Annu. Rev. Fluid Mech.*, 36:281–314, 2004.

[132] J.-H. Xie and J. Vanneste. Boundary streaming with Navier boundary condition. *Phys. Rev. E*, 88:063304, 2014.

[133] J.-H. Xie and J. Vanneste. Dynamics of a spherical particle in an acoustic field: A multiscale approach. *Phys. Fluids*, 26:102001, 2014.

[134] J.-H. Xie and J. Vanneste. A generalised-Lagrangian-mean model of the interactions between near-inertial waves and mean flow. *submitted to J. Fluid Mech.*, 2014.

[135] M. D. Yamanaka and H. Tanaka. Propagation and breakdown of internal inertio-gravity waves near critical levels in the middle atmosphere. *J. Meteor. Soc. Japan*, 62:1–16, 1984.

[136] L. Y. Yeo and J. R. Friend. Surface acousticwave microfluidics. *Annu. Rev. Fluid Mech.*, 46(379–406), 2013.

[137] W. R. Young and M. Ben Jelloul. Propagation of near-inertial oscillations through a geostrophic flow. *J. Mar. Res.*, 55(4):735–766, 1997.

[138] W. R. Young, Y.-K. Tsang, and N. J. Balmforth. Near-inertial parametric subharmonic instability. *J. Fluid Mech.*, 607:25–49, 2008.

[139] V. Zeitlin, G. M. Reznik, and M. Ben Jelloul. Nonlinear theory of geostrophic adjustment. Part 2. Two-layer and continuously stratified primitive equations. *J. Fluid Mech.*, 491:207–228, 2003.